Evaluation of Metal Ion-Releasing Glass Particles to Enhance Antibiotic Efficacy Against Cystic Fibrosis Infection

by

Maxwell Wolverton

Submitted in partial fulfillment of the requirements
for the degree of Master of Applied Science

at

Dalhousie University
Halifax, Nova Scotia
June 2025

Dalhousie University is located in Mi'kma'ki,
the ancestral and unceded territory of the Mi'kmaq.
We are all Treaty people.

Table of Contents

List of Tables

List of Figures

Abstract

In cystic fibrosis pathophysiology, thickened airway mucus impairs mucociliary clearance and leads to devastating chronic bacterial infections. Respiratory failure and lung damage caused by these chronic infections are the leading causes of mortality in cystic fibrosis patients. While antibiotics remain to be the primary treatment option for cystic fibrosis bacterial airway infections, incomplete bacterial eradication can lead to antibiotic resistance. This project aims to evaluate if conventional antibiotic therapies can be made more effective in treating cystic fibrosis bacterial infections by combining them with antibacterial metal ions delivered via borate bioactive glasses. To evaluate this novel combination therapy, we have designed an *in vitro* airway infection model to mimic the cystic fibrosis microenvironment consisting of bronchial epithelial cells, a mucus-like hydrogel layer, and bacteria deposited using an aqueous two-phase system. The bioactive glass formulations selected for this project showed various levels of additive and synergistic antibacterial properties toward *Pseudomonas aeruginosa* and *Staphylococcus aureus* when combined with conventional antibiotics, while maintaining bronchial epithelial cell viability. The antibiotic-glass combinations produced in this project show promise to improve outcomes for cystic fibrosis patients and those with predispositions to the development of devastating bacterial infections, while limiting the development of widespread antibiotic resistance.

List of Abbreviations and Symbols Used

ALG-MUC	Alginate-mucin
ASL	Airway surface liquid
ASM	Artificial sputum medium
ATPS	Aqueous two-phase system
BHI	Brain Heart Infusion
CF	Cystic fibrosis
CFTR	Cystic fibrosis transmembrane conductance regulator
CFU	Colony-forming unit
DEX	Dextran
DMEM	Dulbecco's Modified Eagle Medium
EdU	5-ethynyl-2'-deoxyuridine
ENaC	Epithelial sodium channel
F-12	Gibco Ham's F-12 Nutrient Mixture
FBS	Fetal bovine serum
HBE	Human bronchial epithelial
LB	Luria-Bertani
MDR	Multi-drug resistant
MRSA	Methicillin-resistant *staphylococcus aureus*
OD_{600}	Optical density (600 nm wavelength)
PBS	Phosphate-buffered saline
PEG	Polyethylene glycol

ROS	Reactive oxygen species
SCFM	Synthetic CF sputum medium
T3SS	Type III secretion system

Acknowledgements

I would like to extend my deepest gratitude to my supervisor Dr. Brendan Leung, for granting me the opportunity to conduct my research within his lab. Your mentorship and support have been instrumental in shaping both my academic growth and personal development throughout this program. I am sincerely thankful for your guidance and encouragement. I would also like to express my appreciation to my committee members, Dr. Zhenyu Cheng and Dr. Daniel Boyd, for their insightful questions and feedback that have significantly contributed to the refinement of my work.

I want to extend my gratitude to all of the members of the Leung Lab, past and present, for making the lab such an energetic and welcoming place to work. Your insightful conversations and camaraderie played a meaningful role in helping me navigate and complete my degree. I also want to extend this gratitude to the rest of the SBME community for their support throughout my degree.

CHAPTER 1. Introduction

1.1 Cystic fibrosis leads to altered airway mucus properties

Cystic fibrosis (CF) is a genetic disease affecting over 100,000 people worldwide with an average life expectancy of 37 years [1], [2]. The leading cause of mortality for CF patients is lung damage and respiratory failure caused by chronic airway infections that occur due to the compromised airway microenvironment characteristic of CF [3], [4]. The main goal of this thesis project is to create a new antibacterial combination therapy that can more effectively manage CF airway infections by targeting bacteria through different routes of action.

The human respiratory system relies upon the airway mucus layer as a first line of defense against pathogens and toxins in inspired air [5], [6]. Mucus is a glycoprotein-rich hydrogel that lines the mucosal surfaces of our body such as the intestines, stomach, urogenital tract, and airway, acting as an interface between human epithelial cells and the outside world [6]. At the epithelial interface, mucus functions as a lubricant, a selectively permeable barrier that allows the passage of nutrients while blocking the entrance of pathogens, a first line of immune defense, and a habitat for the human microbiome, among other functions [6]. In the airway, the mucus layer's function as a first line of immune defense is propagated by the mucociliary clearance mechanism, in which pathogens and toxins get trapped in the airway mucus layer, and the cilia lining the airway are constantly sweeping the mucus up and out of the airway [5]. For the mucociliary clearance mechanism to function effectively, the freedom of movement of

these cilia is of utmost importance, which is facilitated by the viscoelastic properties of mucus [7].

Native mucus is composed of around 97% water and 3% solids [8]. The solids portion of mucus consists of mucin proteins, non-mucin proteins, salts, lipids, and debris [8]. Mucins are large O-linked glycoproteins that have polymeric/colloidal behavior due to their large size and provide the structure framework for mucus [8], [9]. The carbohydrate side chains make up approximately 50% to 90% of the molecular mass of mucins, while the other 10% to 50% is made up of proteins [8], [9]. The gel properties of mucus are primarily caused by the formation of disulfide bonds between the cysteine-rich domains of the mucin proteins [8], [10]. Of the 17 genes encoding mucins in the human genome, MUC5AC and MUC5B are the two major polymeric mucins of airway mucus and are responsible for gel formation [8], [11].

Mucus hydration is controlled primarily by two ion channels in the airway epithelial cells: the cystic fibrosis transmembrane conductance regulator (CFTR) which regulates Cl^- secretion, and the epithelial sodium channel (ENaC), which regulates Na^+ absorption [12], [13]. The regulation of ion concentrations in the airway mucus primarily by these two channels leads to the regulation of mucus hydration by osmosis [8], [12].

In CF pathology, mutations in CFTR gene lead to loss or impairment of CFTR channel function in the airway epithelium [3], [12]. Therefore, loss of CFTR channel function significantly reduces Cl^- secretion and water transport across the airway epithelium, leading to mucus dehydration and resulting in thickened mucus that is more viscous and stickier than healthy mucus [12], [14]. In addition, mucus composition is altered in CF patients, in that CF mucus contains a greater concentration of mucins as

well as DNA and inflammatory cytokines [10], [15], [16]. In CF mucus, the amount of secreted mucins increases by approximately 3-fold compared to that of healthy mucus [17]. This altered CF mucus solids composition further increases mucus adhesion to airway surfaces [12].

1.2 CF mucus properties lead to chronic airway infections

The altered properties of CF airway mucus lead to the development of chronic bacterial airway infections in CF patients by creating an airway microenvironment where bacteria are able to thrive and evade host immune responses [18]. As mentioned earlier, the damage to the lungs then caused by these infections is responsible for a large proportion of the mortality in CF patients [3], [4].

Thickened CF mucus leads to impairment of the mucociliary clearance mechanism, impairment of host immune cell migration, and impairment of antibacterial treatment diffusion through the airway [12]. Mucociliary clearance is impaired because (1) the dehydrated mucus layer is more viscous and therefore more difficult to move, and (2) the periciliary layer volume is decreased due to increased reabsorption of ions and therefore water, both leading to an impaired ability of the cilia to properly beat and propel mucus upward [14], [19], [20]. Coughing, which in healthy humans aids in clearing mucus, is also impaired due to the increased adherence of the dehydrated mucus to the airway surface [12], [21]. In addition, sticky mucus plugs form within airways, further obstructing the airways and leading to impaired airflow, bacterial growth, and neutrophilic airway inflammation [22]. Therefore, these conditions provide an ideal

environment for bacterial growth and recurrent infections as bacteria is not cleared as easily from the airway [12].

This impaired microenvironment of the CF airway allows bacteria to say in place and attach to surfaces, resulting in the formation of bacterial biofilms [23], [24]. When bacteria colonize a surface, flagellum synthesis is inhibited after surface attachment and rapid bacterial growth occurs, leading to the formation of a biofilm [24], [25]. Biofilms create additional challenges for antibiotic therapies as microbial aggregates that build up in biofilms create a blockade that resists antimicrobial agents [26]. Additionally, the bacteria within biofilms can produce exotoxins known as superantigens that allow bacteria to evade the immune system [26], [27]. Biofilm formation is a key characteristic of CF airway infection that contributes to antibiotic inefficacy and subsequent antibiotic resistance.

Common pathological bacterial airway infections in CF patients are characterized mainly by the two bacteria, *Staphylococcus aureus* and *Pseudomonas aeruginosa* [3], [28]. The bacteria involved in CF airway infection varies with the patients age, with infections in children being primarily *S. aureus* and infections in adults being primarily *P. aeruginosa* [3], [28], [29].

P. aeruginosa is a Gram-negative opportunistic pathogen that is commonly involved in nosocomial infections and is difficult to treat due to resistance to multiple antibiotics [3], [30]. CF patients with chronic *P. aeruginosa* infection have been shown to have more severe symptoms and lung degradation over time [3], [28]. *P. aeruginosa* uses a number of mechanisms to adapt and persist in the CF lung, including the ability to

differentiate into a mucoid phenotype that aids in biofilm formation by increasing the production of alginate and other polysaccharides [31], [32].

S. aureus is a Gram-positive opportunistic pathogen found ubiquitously in human populations and environments [33]. *S. aureus* is estimated to have colonized 30% of all humans, but is typically asymptomatic in healthy humans [34]. *S. aureus* is typically the dominant pathogen in young CF patients, but is usually outcompeted eventually by more dominant pathogens, typically *P. aeruginosa* [33], [35]. Methicillin-resistant *S. aureus* (MRSA) is a particular strain of *S. aureus* that has acquired resistance to methicillin and other beta-lactam antibiotics [34], [36]. MRSA is an increasingly common pathogen in community- and hospital-acquired infections, being responsible for 10-fold more infections than all multi-drug resistant (MDR) Gram-negative pathogens combined [34]. The prevalence of MRSA infections in CF is rapidly increasing, highlighting the dangers of antibiotic resistance develop in CF pathogens [37].

P. aeruginosa and *S. aureus* have both been shown to form biofilms within CF mucus [38], [39]. These CF biofilms are characterized by bacterial colonies surrounded by a protective extracellular matrix [38]. Compared to planktonic bacteria, biofilms have reduced antibiotic penetration and increased metabolic adaptation, making them more difficult to eradicate and they show increased antibiotic resistance [40].

In addition to the two major bacteria identified here, other bacterial species have been implicated in CF airway infections such as *Haemophilus influenzae*, *Stenotrophomonas maltophilia*, *Achromobacter*, and *Burkholderia cepacian* complex [4], [28], [29]. Additionally, fungus has been identified as a colonizer of the CF lung [41]. Specifically, the filamentous fungi *Aspergillus fumigatus* and *Scedosporium*

apiospermum as well as *Candida albicans* have been identified as the most prevalent fungi in CF infections [42], [43]. However, it is unknown if these fungal infections are commensal or pathogenic in nature [42], [43].

1.3 Conventional antibiotic therapy leads to antibiotic resistance development in CF pathogens

Antibiotic resistance has emerged as one of the most serious threats to global health, resulting in an estimated 1.2 million deaths annually [44], [45]. The World Health Organization recognizes antimicrobial resistance as a top threat to global public health and development [46]. As antibiotic resistance is constantly evolving, it is projected that global mortality will rise to 10 million deaths annually by 2050 if actions are not taken to control antibiotic resistance [44]. In a healthcare setting, antibiotic-resistant microbes contribute to an increasingly significant proportion of hospital-acquired infections, leading to increased mortality and morbidity [47].

From an economic standpoint, it is projected that antibiotic resistance could cost the global economy up to $100 trillion USD by 2050 due to increased healthcare expenditures and indirect effects on the economy [48]. Looking at this globally, the growing development of antibiotic resistance would have greater economic impacts on low-income countries, leading to increased levels of poverty [49]. These global health and economic challenges presented by antibiotic resistance emphasize the urgent need for alternative antimicrobial strategies.

The primary form of treatment for CF bacterial airway infections is antibiotic therapy [4], [28], [33]. In the treatment of chronic infection, the aim of long-term antibiotic therapy is to reduce microbial load in the lung and therefore reduce chronic lung damage and chronic lung function loss [33]. While antibiotics have been tremendously effective in reducing CF mortality, the widespread use of antibiotics has led to the development of antibiotic resistance in common CF pathogens, making them increasingly difficult to treat [50], [51], [52].

Antibiotic resistance arises when pathogens are exposed to sublethal concentrations of antibiotics, allowing some bacteria to survive rather than being fully eliminated [51], [53]. This incomplete eradication enables naturally resistant strains to persist and multiply, while susceptible strains are eliminated [53], [54]. Over time, resistance traits can spread across microbial populations via horizontal gene transfer [54], [55]. These resistance genes can enable bacteria to evade antibiotics through mechanisms such as cell wall changes that restrict antibiotic access, efflux pumps that pump out the antibiotic, enzymes that modify and/or degrade the antibiotic, and the development of alternative metabolic pathways to those inhibited by the drug [56].

Particularly in CF infections, thickened mucus impairs antibiotic diffusion, leading to a failure to eradicate bacteria and subsequent antibiotic resistance development [51]. Bacterial biofilms have an increased ability to form in CF mucus, and when a biofilm is present, antibiotics that may be able to kill the metabolically active layer of cells on the exterior of the biofilm are often unable to kill the interior bacterial cells, thereby leading to antibiotic resistance development [57], [58].

For chronic *P. aeruginosa* lung infection, long-term inhaled antibiotic therapy, typically with tobramycin, is a cornerstone of medical treatment [28]. Long-term inhaled antibiotic therapy has been shown to slow lung function decline, reduce pulmonary exacerbations, and reduce hospitalizations in CF patients with chronic *P. aeruginosa* infection [28], [59]. Inhaled antibiotic therapy can also be used in early *P. aeruginosa* infection to prevent establishment of a chronic infection [28]. However, long-term inhaled antibiotic therapy can lead to the establishment of MDR *P. aeruginosa* infection due to the many different mechanisms of antibiotic resistance development in *P. aeruginosa* [28], [30].

For *S. aureus*, various anti-staphylococcal antibiotics have been used prophylactically on children with CF to prevent the establishment of a chronic *S. aureus* infection [33]. Antibiotics such as vancomycin and linezolid show potential in being used in the treatment of *S. aureus* infection-induced acute pulmonary exacerbations [28], [60]. However, the widespread use of beta-lactam antibiotics has led to the emergence of MRSA as a major pathogenic strain in CF and other infections [34], [36]. MRSA infections are increasingly difficult to treat in CF and typically require combinations of different antibiotics [61].

While the aggressive use of antibiotics in the treatment of airway infections has overall led to a significant increase in CF life expectancy, this same aggressive use has led to the spread of antibiotic resistance in most bacteria, leading to the development of new strains such as MRSA that are increasingly difficult to treat [30], [33], [62], [63].

1.4 Existing combination therapies to treat CF infections

To prevent the continuing development of antibiotic resistance and better treat MDR bacteria, combination therapies of conventional antibiotics with either other antibiotics or other substances have been investigated in the hopes of targeting bacteria from multiple angles to eradicate bacteria and prevent antibiotic resistance buildup.

Combinations of multiple antibiotics have been investigated in treating CF infections. Specifically, tobramycin, a common treatment for Gram-negative *P. aeruginosa* CF infections, has been combined with other antibiotics to produce promising results. Combining tobramycin, an aminoglycoside antibiotic, with colistin, a polymyxin antibiotic, has been shown to more effectively treat *P. aeruginosa* biofilms, potentially due to the different mechanisms of action of each antibiotic [57], [64]. Tobramycin has also been combined with beta lactam antibiotics in treating *P. aeruginosa*, with the combinations better able to suppress planktonic and biofilm growth [65]. These examples show that combinations of antibiotics that are able to attack bacteria with different mechanisms of action can have synergistic effects in suppressing CF infections [66].

Conventional antibiotics have also been combined with mucolytic agents with the intention of breaking up mucus, allowing for better diffusion of antibiotics through the mucus layer [67], [68]. To further improve CF infection treatment, combining conventional antibiotics with antibiofilm agents such as quercetin that disrupts biofilm formation has been explored [67]. These examples show potential avenues for improving the efficacy of conventional antibiotics on treating CF infections.

Finally, antibiotics have been combined with CFTR modulators to attempt to better clear CF infections [69]. CFTR modulators, such as ivacaftor, are drugs that target the CFTR ion channel with the aim of restoring CFTR function and therefore restoring healthy mucus structure and function [70]. These drugs, only becoming available in the past decade, are now at the forefront of cystic fibrosis research as they target the underlying cause of CF, rather than the symptoms [70], [71]. While the combination of antibiotic therapy with CFTR modulators has been investigated, it appears that chronic CF infections may still be able to resist eradication despite modulator-induced improvements in lung function combined with intense antibiotic treatment [69].

While many combination therapies to improve the efficacy of conventional antibiotics in treating CF infection have been explored, the combination of conventional antibiotics with antibacterial metal ion-based therapies has not been extensively explored.

1.5 Metal ions have antimicrobial effects

Metal ions have been shown to have antimicrobial effects through a variety of mechanisms including damage to microbial cell membranes and cell walls, interactions with microbial DNA, inhibition of enzymes or proteins, and the generation of reactive oxygen species (ROS) [72], [73]. The generation of ROS, highly reactive molecules containing oxygen such as peroxides and superoxide anions, has specifically been identified as a major antibacterial mechanism of metal ions [74]. The ROS generated by metal ions then damage bacterial cell membranes and have antibiofilm activity [74], [75]. As metal ions have been shown to target microorganisms through a variety of

mechanisms simultaneously, there is a decreased risk of antibiotic resistance development [74], [76]. Therefore, by combining metal ions with conventional antibiotics, we can have a large variety of mechanisms that jointly target microorganisms and therefore further reduce the risk of antibiotic resistance development [76].

In the context of CF lung infections, the use of metal ions could have additional benefits, as they (1) are able to traverse through the mucus layer more easily due to their small size and (2) may have some mucolytic effect that could therefore aid bacterial clearance and antibiotic delivery [76]. Some possible mechanisms behind the mucolytic-like effects of metal ions include the disruption of Ca^{2+} crosslinking in mucus and the generation of reactive oxygen species which can degrade mucus structure [77].

In this thesis, we explored the antibacterial effects of zinc and gallium ions. Zinc has been shown to be an effective antimicrobial agent due to its inhibitory effects on various metabolism pathways as well as its ability to generate ROS [74], [78], [79]. Zinc oxide (ZnO) has been shown to be specifically effective against *S. aureus* and *E. coli* [78], [80].

Gallium has had longstanding clinical uses as a diagnostic agent for cancer and infections, a therapeutic agent for cancer, and as a potential anti-inflammatory and immunosuppressive agent [81]. Recently, the antimicrobial properties of gallium have been investigated. It is theorized that gallium acts as a competitive inhibitor in cellular processes involving iron metabolism due to the resemblance between gallium and iron atoms [78], [81]. Through this mechanism, gallium has been shown to be effective in killing planktonic and biofilm *P. aeruginosa* as well as *Mycobacterium tuberculosis* [81].

1.6 Borate bioactive glasses can facilitate the delivery of metal ions to CF airway infections

While metal ions themselves may be useful in treating CF airway infections, a delivery system is required to deliver these metal ions to sites of infection. Metallic nanoparticles have been investigated as a mechanism to deliver antibacterial metal ions to sites of microbial infections [55], [76], [82]. Metallic nanoparticles are able to attach to bacterial membranes via intermolecular forces and then cross the membrane, leading to the accumulation of metal ions inside the bacterium [55], [76], [83]. The accumulation of metal ions inside the bacterium can then lead to the inhibition of enzyme function, deactivation of proteins, inducing of oxidative stress, and modification of gene expression [76], [83].

Borate bioactive glasses have shown potential as degradable matrices for tissue engineering applications and as potential as carriers for metal ions [84], [85], [86]. Borate bioactive glasses have demonstrated effectiveness in enabling the controlled release of molecules to clinical areas of interest within the body in examples such as releasing therapeutic strontium ions for bone regeneration or releasing conventional antibiotic drugs to treat chronic osteomyelitis [87], [88]. Additionally, borate bioactive glasses have been used in wound healing applications [84] and as drug delivery systems for cancer treatment [89], [90]. The highly tunable nature of borate bioactive glasses makes them a favorable candidate for an antibacterial metal ion delivery system in CF infections because degradation rates can be adjusted to ensure proper release of metal ions to the targeted sites of infection and full dissolution of the glass particles in the airways [91].

The novel antibacterial therapy created in this thesis project is centered around the combination of conventional antibiotics with metal ion-releasing borate bioactive glasses.

1.7 Current models of CF airway infection

A representative model of CF infection is required to assess the antibacterial efficacy of novel therapies in a CF-like environment. Therefore, a review of current models of CF lung infection was conducted to select a model to use in this project to assess the novel antibiotic-metal ion combination therapy.

Many *in vivo* animal models have been used to study CF infection as well as CF disease progression, mucociliary clearance deterioration, and CFTR restoration [92]. *In vivo* models have been generated by modifying CFTR orthologs in various animals, resulting in a CF-like pathophysiology in these animals [92], [93]. Pigs [94], [95] and ferrets [96], [97] are the most commonly used animals to study CF infection *in vivo* because both species, when genetically modified to knockout the CFTR ortholog gene, are prone to developing spontaneous lung infections within weeks to months after birth [95], [97], [98]. CF animal models have also been established in smaller animals such as mice [99], [100], zebrafish [101], and tadpoles [102]. While such transgenic CF animal models can provide valuable insights into CF disease and infection progression, there are limitations to the translatability of these animal models to CF in humans [98], [103]. Additionally, animal models require a large amount of time and resources in comparison to smaller and more controllable *in vitro* CF models [98].

Due to the limitations and challenges associated with *in vivo* animal models, there has been extensive investigation into the development of *in vitro* CF airway infection models [104]. Several *in vitro* models have combined host cells with microbial cells successfully, allowing for the study of bacterial-host interactions, biofilm formation, and antibiotic efficacy [104], [105]. However, many models lack key components of the CF airway microenvironment, such as a mucus-mimetic layer [106], [107]. Other *in vitro* models have employed mucus-mimetic materials to better represent the CF airway microenvironment [104]. Specifically, artificial sputum medium (ASM) [108] and synthetic CF sputum medium (SCFM) [109], [110] have been created to supply a nutrient environment reflective of the CF airway. However, these mucus-mimetic media lack the complexity of the *in vivo* mucus layer, and specifically lack the viscoelastic properties of mucus [104].

Therefore, current research has looked into the development of mucus-mimetic materials to better recapitulate the viscoelastic properties of native healthy and CF mucus. Purified mucin proteins alone do not accurately resemble the viscoelastic properties of native mucus, as they lack non-mucin proteins and other components found in mucus that contribute to mucus' physical properties [111]. Therefore, a variety of mucus-mimetic materials have been designed with different backbones such as non-peptide mucin substitutes, mucin-based polypeptide backbones, and hydrogels to mimic the viscoelastic properties of native mucus [112].

An ongoing project in the Leung lab focuses on developing and optimizing an *in vitro* airway infection model to better mimic the structure and microenvironment of the CF airway. To mimic native airway mucus in this model, mucus-mimetic hydrogels have

been engineered and are composed of an alginate-mucin (ALG-MUC) interpenetrating hydrogel network using calcium chloride ($CaCl_2$) as a crosslinker [113], [114]. Two formulations of ALG-MUC hydrogels were designed to mimic the properties of healthy and CF airway mucus by increasing crosslinker and mucin content in the CF hydrogel to mimic the thickened CF mucus properties [114].

Using these mucus-mimetic hydrogels, a novel *in vitro* airway infection model was designed, incorporating human bronchial epithelial cells with common CF bacteria in a CF-like airway microenvironment [114]. In this model, human bronchial epithelial cells are seeded on a flat-bottom well plate, the mucus-mimetic hydrogels are deposited over top, and bacteria are deposited over top of the mucus-mimetic hydrogels using an aqueous two-phase system (ATPS) (Figure 1A) [114]. The ATPS uses two incompatible polymers that partition into separate aqueous phases in order to confine bacteria to one of the phases, allowing for the repeatable and controlled deposition of bacteria into the model [114], [115].

In this thesis project, the existing *in vitro* airway infection model developed by O'Brien et al. [114] was translated into a transwell insert system, where cell culture media is delivered to the mammalian cells basolaterally, while the mucus layer containing bacteria is deposited on the apical side of the mammalian cells (Figure 1B). The purpose of this change was to improve the structural relevance of the model by introducing a different route from the hydrogel layer for nutrient delivery to the

mammalian cells. This newly developed model was then used to assess the antibacterial efficacy of the antibiotic-metal ion combination therapy.

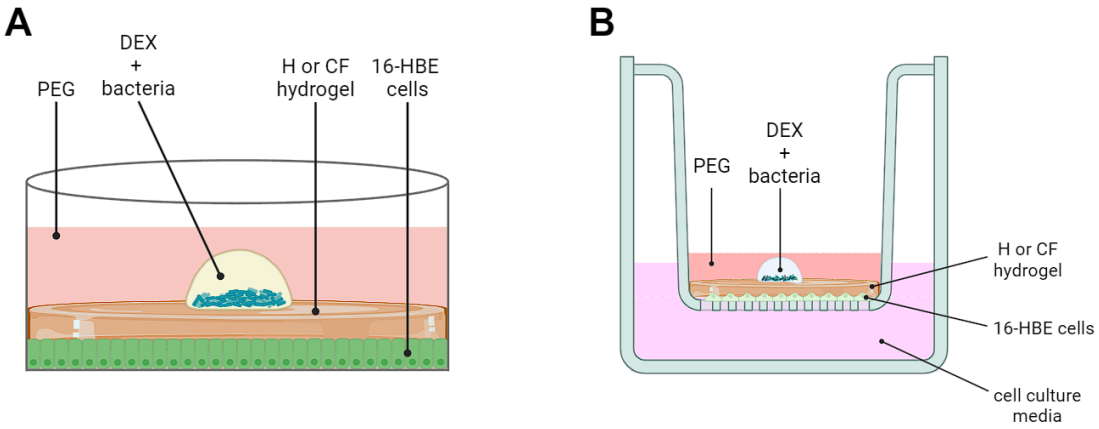

Figure 1: Comparison of previously designed CF airway infection model to new proposed CF airway infection model. A. The previously designed *in vitro* airway infection model, within a flat-bottom well plate, contains a bronchial epithelial cell monolayer, mucus-mimetic hydrogel, and an ATPS to confine bacteria [106]. **B.** The newly proposed *in vitro* airway infection model, using a transwell insert, contains an apical compartment with the same composition as the previous model but now with a basolateral compartment containing cell culture media. Diagram created with BioRender.com.

1.8 Rationale, hypothesis, and objectives

The major goal of this thesis project was to assess if the addition of metal ion-releasing bioactive glass could augment conventional antibiotics to better eradicate bacterial infection in a CF-like airway microenvironment.

In CF patients, lung damage and respiratory failure caused by chronic microbial infections are the leading causes of mortality [3], [4]. CF patients are highly susceptible to the development of chronic airway infections due to thickened mucus characteristic of the CF airway, which leads to increased bacterial colonization as well as impaired

diffusion of antibiotic drugs [12], [22]. Because of this compromised airway environment, conventional antibiotics often fail to eradicate bacteria in CF infections, thereby allowing the surviving population of bacteria to develop antibiotic resistance [51]. Therefore, the development of new therapies to fully eradicate bacterial infections in the CF airway is needed to prevent the development of antibiotic resistance. By combining conventional antibiotics with metal-ion releasing bioactive glass, we aim to create a therapy that will more effectively treat CF bacterial infections and prevent antibiotic resistance development by targeting bacteria using multiple mechanisms of action.

We hypothesized that the addition of metal-ion releasing bioactive glass will augment conventional antibiotics to more effectively suppress bacterial growth in a CF-like airway microenvironment. To test this hypothesis, there were two main objectives:

Objective 1: Create an *in vitro* airway infection model containing human bronchial epithelial cells, mucus-mimetic hydrogels, and a bacterial culture established using an ATPS. Convert the previously created airway infection model to a transwell insert-based model to better mimic airway structure and allow for an additional route of cell culture media delivery independent of the hydrogels/bacteria. Induce a quiescent-like state on the bronchial epithelial cells to better represent native airway cells.

Objective 2: Assess the efficacy and safety of antibiotic-glass combinations using the previously designed *in vitro* airway infection model. Antibacterial efficacy of the antibiotic-glass combinations was assessed using a CFU/ml assay and cytotoxicity of the antibiotic-glass combinations on the mammalian bronchial epithelial cells was assessed

using a live/dead cell viability assay. A schematic of the overall experimental design can be found in Figure 2 below.

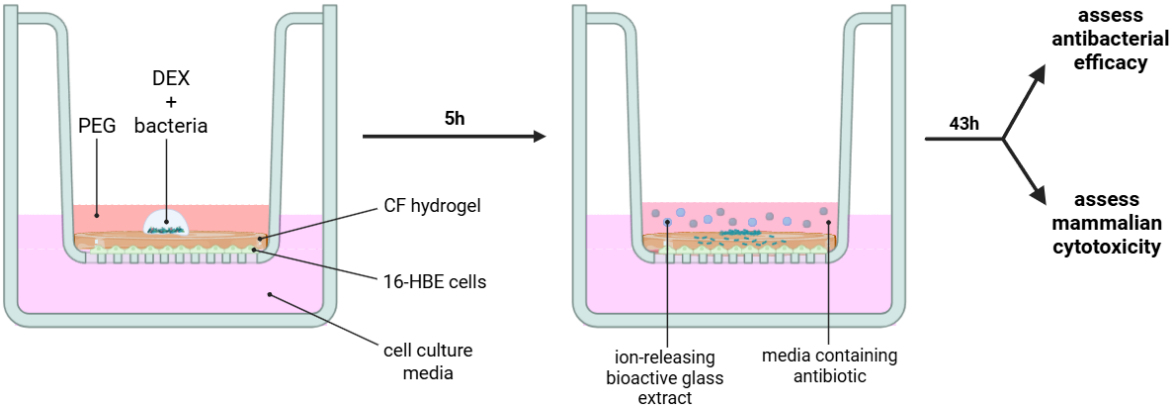

Figure 2. Schematic of overall experiment to test efficacy and safety of metal ion-releasing bioactive glasses combined with conventional antibiotics. The CF airway infection model is created with 16-HBE cells, a CF-mimetic hydrogel layer, and bacteria deposited using an ATPS. 5 hours after bacteria deposition, the ATPS is replaced with media containing antibiotic and glass extract. The model is cultured for another 43 hours to a total time of 48 hours, after which antibacterial efficacy and mammalian cytotoxicity of the antibiotic-glass combinations are assessed. Diagram created with BioRender.com.

CHAPTER 2. Materials and Methods

2.1 Cell culture conditions

For this project, the 16-HBE cell line (16HBE14o-) was used to mimic the bronchial epithelial cell layer. For continuous culture, 16-HBE cells were cultured in a 1:1 ratio of Dulbecco's Modified Eagle Medium (DMEM), high glucose (Thermo Fisher Scientific, Gibco. Cat. No. 11965092), and Gibco Ham's F-12 Nutrient Mixture (Thermo Fisher Scientific, Gibco. Cat. No. 11765054) supplemented with 10% fetal bovine serum (FBS; Thermo Fisher Scientific, Gibco. Cat. No. A5256701) and 1% antibiotic-antimycotic (AA; Thermo Fisher Scientific, Gibco. Cat. No. 15240062). 16-HBE cells were incubated at 37 ºC and 5% CO_2. During continuous culture, 16-HBE were passaged upon reaching 60% to 80% confluency and media was changed every 3 days to minimize over confluency and accumulation of metabolites.

In the airway infection model, 16-HBE cells were cultured with a 1:1 ratio of DMEM, low glucose (Thermo Fisher Scientific, Gibco. Cat. No. 11885084), and F-12 supplemented with 1% FBS. The lower FBS and glucose concentrations were used to induce the 16-HBE cells into a quiescent-like state more representative of bronchial epithelial cells and to prevent over confluency. Note that no AA was added to media for experiments involving bacteria, to prevent interference with bacteria growth.

In the airway infection model, 16-HBE cells were seeded at a cell density of approximately 30000 cells/well on transwell inserts (VWR, Avantor. Cat. No. 734-3263) in a 24-well plate. The inserts were coated with collagen (Advanced BioMatrix, BICO. PureCol® Bovine Collagen Solution, Type I, Cat. No. 5005) before cell seeding to

encourage cell adhesion and promote a uniform distribution of cells on the inserts. The collagen solution was added to the inserts at a concentration of 0.05 mg/ml for 2 hours before the collagen solution was aspirated and the inserts were left to air-dry in the biosafety cabinet for 45 minutes. Before adding the hydrogel and bacteria component of the airway infection model, 16-HBE cells were grown for 48 hours in DMEM, high glucose/F-12 + 10% FBS to reach full confluency, and then were grown for an additional 48 hours in DMEM, low glucose/F-12 + 1% FBS to induce a quiescent-like state.

2.2 Bacteria culture conditions

Within the airway infection model, two strains of bacteria were used: *Pseudomonas aeruginosa* CF18 and *Staphylococcus aureus* ATCC 6538. The strain of *P. aeruginosa* that was used in this project was isolated from the airways of a child with CF.

Frozen stocks of the two bacteria strains were prepared in their respective broths with 25% (v/v) glycerol and were stored at -80 ºC. *P. aeruginosa* was cultured using Luria-Bertani (LB; Sigma-Aldrich. Cat. No. 1.10285) broth while *S. aureus* was cultured using Brain Heart Infusion (BHI; Sigma-Aldrich. Cat. No. 1.10493) broth. To culture the bacteria in preparation for use in experiments, the frozen stocks were streaked on 1.5% (w/v) agar (Sigma-Aldrich. Cat. No. A1296) plates of their respective broth, and then the plates were incubated for 16 to 18 hours at 37 ºC and 5% CO_2. Then, liquid cultures were prepared by inoculating 3 ml of the respective broth with a single colony from each of the streaked agar plates. The liquid culture was then cultured for 16 to 18 hours in a shaking incubator at 200 rpm and 37 ºC prior to use for experiments.

2.3 ATPS preparation

An ATPS composed of polyethylene glycol (PEG) and dextran (DEX) was used to contain the bacteria within a DEX droplet above the mucus-mimetic hydrogel layer of the model. To prepare the ATPS, 5% (w/v) PEG (35 kDa, Sigma-Aldrich. Cat. No. 8.18892) and 5% (w/v) DEX (500 kDa, Pharmacosmos. Cat. No. 5510 0070 9006) were dissolved in DMEM/F-12 + 10% FBS and in LB broth using a rocking platform shaker. Previous lab members have optimized the containment of *P. aeruginosa* and *S. aureus* using a 5% PEG/5% DEX ATPS and have found that LB broth is suitable for containment and growth of *S. aureus* in addition to *P. aeruginosa* [114].

After mixing, the solutions were filter sterilized using a 0.22 μm vacuum filtration system and then centrifuged at 3000 g for 90 minutes to allow the two phases to separate. Then, the separated PEG-rich and DEX-rich phase from each of the two ATPS were collected by careful pipetting and stored at 4 ºC. The preparation of these two ATPS solutions was performed in order to harvest the PEG-rich phase from the 5% PEG/5% DEX ATPS in DMEM/F-12 + 10% FBS to support cell growth, while also harvesting the DEX-rich phase from the 5% PEG/5% DEX ATPS in LB broth to support bacteria growth and confinement.

2.4 Preparation of hydrogel stock solutions

The mucus-mimetic hydrogels in the airway infection model were composed of an alginate-mucin (ALG-MUC) hydrogel crosslinked by calcium chloride ($CaCl_2$), and therefore require alginate, mucin, and $CaCl_2$ stock solutions to be prepared.

To prepare alginate stock solutions, alginic acid sodium salt powder (low viscosity, MP Biomedicals. Cat. No. 154725) was sterilized by ultraviolet (UV) light by placing the powder horizontally in a Falcon tube and then placing the tube in a UV sterilizer for 60 minutes, rotating the tube every 20 minutes to maximize the sterilized surface area. The alginic acid sodium salt was then dissolved in PBS and HEPES buffer (Sigma-Aldrich. Cat. No. H3375) was added to prepare a stock solution of 30 mg/ml alginate and 75 Mm HEPES buffer that was stored at 4 ºC.

To prepare $CaCl_2$ stock solutions, $CaCl_2$ (Sigma-Aldrich. Cat. No. 746495) was dissolved in deionized (DI) water and then filter sterilized using a 0.22 μm syringe filter to a concentration of 2 mg/ml.

To prepare mucin stock solutions, Mucin Type II powder (from porcine stomach, Sigma-Aldrich, Cat. No. M2378) was spread on a petri dish, then saturated with 95% ethanol, and then heated in a 70 ºC oven for 24 hours. Subsequently, the sterilized mucin powder was collected and dissolved in PBS to produce a 200 mg/ml mucin stock solution that was stored at 4 ºC.

2.5 Preparation of hydrogels for use in the airway infection model

Formulations for a CF mucus-mimetic hydrogel, healthy mucus-mimetic hydrogel, and alginate cushion were optimized and characterized previously in the lab [114] and these formulations will be used in the healthy and CF airway infection models (Table 1). The alginate cushion, containing no mucin, was incorporated into the model to

prevent direct contact between the 16-HBE cells and the mucin, which was shown to have a cytotoxic effect previously in the lab [114].

Table 1: Composition of mucus-mimetic hydrogels. ALG-MUC hydrogels were previously optimized to mimic the airway mucus composition of CF patients and healthy individuals **[114]**. An alginate cushion was also optimized to use as a non-mucin containing barrier between the mucin-containing hydrogels and the 16-HBE cells.

	Cushion	Healthy	CF
Alginate	1.50%	1.50%	1.50%
Mucin	0%	1%	4%
CaCl2	0.5 mg/ml	0.5 mg/ml	0.6 mg/ml

To assemble the hydrogels for use in the airway infection model, alginate and mucin stock solutions were first mixed together and diluted with PBS to the desired concentrations. $CaCl_2$ was then be added and mixed rapidly to allow for crosslinking of the ALG-MUC hydrogel. After the hydrogel had begun to crosslink, the hydrogels were deposited on top of the 16-HBE monolayer and given time to solidify. Following this process, the alginate cushion was deposited at a thickness of 0.4 mm and incubated for 10 minutes to solidify. Then, the healthy or CF hydrogel was deposited on top of the alginate cushion at a thickness of 1.1 mm and incubated for 30 minutes to solidify.

To promote uniformity of the hydrogel phase, the plate containing the airway infection model was centrifuged at 100 g for 5 min to allow the gel to spread out. While centrifuging the hydrogels, PBS was added to the basolateral compartment of the transwell to prevent the insert membrane flexing and hydrogel aggregation in the center of the insert. This centrifugation step was done prior to incubating the hydrogels to allow them to solidify.

2.6 Assembling the airway infection model

To assemble the airway infection model, 16-HBE cells were first seeded on transwell inserts within a 24-well plate at a cell density of 30000 cells/well. Before seeding the 16-HBE cells, the transwell inserts were coated with collagen to enhance cell attachment. Then, the 16-HBE cells were grown for 48 hours with DMEM/F-12 + 10% FBS in the apical and basolateral compartment until they reached 100% confluency. At confluency, the growth media was removed from both compartments, washed with PBS, and replaced with DMEM low glucose/F-12 + 1% FBS and cultured for an additional 48 hours to induce a quiescent-like state in the 16-HBE cells. Then, the media in the apical compartment was removed, and the hydrogels were added on top of the 16-HBE monolayer as described in Section 2.5. The alginate cushion was added first at a height of 0.4 mm, incubated for 10 minutes at 37 ºC and 5% CO_2 to solidify, and then either the healthy or CF mucus-mimetic hydrogel was added at a height of 1.1 mm and incubated for 30 minutes at 37 ºC and 5% CO_2 to solidify, for a total hydrogel height of 1.5 mm to mimic airway mucus thickness. After the gels had solidified in the incubator, the PEG-rich phase from a 5% PEG/5% DEX ATPS in DMEM/F-12 + 10% FBS was added atop the hydrogels in the apical compartment. Then, using the BioMek 4000 Automated Liquid Handler (Beckman Coulter), a 0.5 Ml droplet of the DEX-rich phase from a 5% PEG/5% DEX ATPS in LB broth containing the chosen bacteria at an OD_{600} of 0.01 was added directly above the hydrogel layer, within the PEG-rich phase. The model was then cultured at 37 ºC and 5% CO_2 for 5 hours to allow the bacteria to settle into the hydrogel phase in a controlled manner.

After 5 hours of bacterial containment within the ATPS, the liquid ATPS phase was removed from the model and replaced with media containing bioactive glass extract and/or antibiotics. It was previously shown in the lab that *P. aeruginosa* failed to be confined by the PEG/DEX ATPS after 5 hours, and therefore the ATPS phase is removed after 5 hours, since the bacteria has diffused into the hydrogel layers by then. After removing the ATPS phase, glass extract-antibiotic combinations dissolved in DMEM low glucose/F-12 + 1% FBS were added to the apical compartment. The model was then cultured at 37 ºC and 5% CO_2 for an additional 43 hours to reach a total culture time of 48 hours, after which, bacterial growth and cell viability were assessed. A summary of the airway infection model assembly is shown in Figure 3.

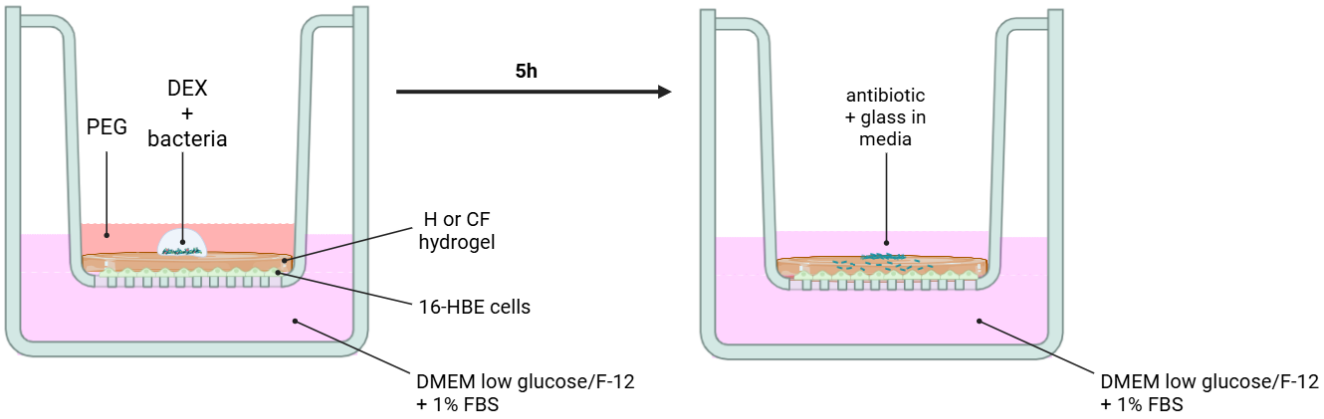

Figure 3: Schematic of airway infection model assembly. The airway infection model contains a 16-HBE monolayer on the surface of the apical compartment, followed by a healthy or CF hydrogel layer. On top of that, an ATPS is added to contain bacteria to the DEX droplet. The basal compartment is be supplied DMEM low glucose/F-12 + 1% FBS. After 5 hours of bacterial confinement, the ATPS liquid phase is removed from the apical compartment and bioactive glass extracts and antibiotics dissolved in DMEM, low glucose/F-12 + 1% FBS are added. Diagram created with BioRender.com.

2.7 Assessment of bacteria growth in the airway infection model

For experiments using one strain of bacteria, bacterial growth in the liquid and hydrogel phases of the airway infection model were assessed using spot plating techniques to determine CFU/ml. Firstly, 20 µl of the liquid phase of the apical compartment was extracted. The rest of the liquid phase was then discarded, and the hydrogel phases were pipetted into microcentrifuge tubes, which were then centrifuged at 10000 g for 10 minutes to pellet bacteria. The bacteria pellet was then resuspended in 50 Ml PBS to match the volume of the hydrogels. The centrifuging was done in order to get the bacteria out of the hydrogels and into a liquid medium.

Then, a 96-well plate was used to serially dilute the liquid and hydrogel phase samples from 10^1 to 10^6. 20 Ml from each dilution was then spot plated onto LB agar plates divided into six sections, one for each dilution (Figure 4). The LB agar plates were then incubated at 37 ºC and 5% CO_2 for 16 to 18 hours, after which, the number of colonies was recorded for dilutions where there was a countable range of colonies between 30 and 300.

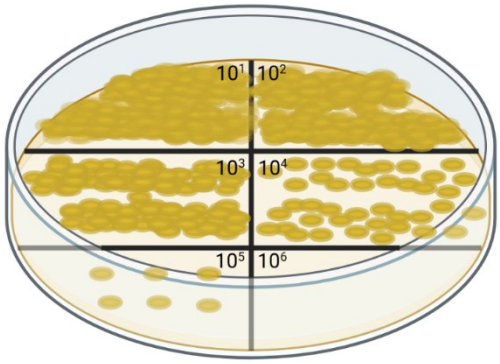

Figure 4: Spot plating to determine CFU/ml. A sample from the liquid or hydrogel phase of the airway infection model is serially diluted from 10^1 to 10^6. These dilutions are then plated on LB agar, allowing for colonies to be counted at certain dilutions. In this example, the 10^4 dilution is the countable dilution with a number of colonies between 30 and 300. Diagram created with BioRender.com.

Equation 1 was then used to calculate the CFU/ml of the liquid and hydrogel phases for each condition:

$$N = \frac{C}{(V)(D)} \quad (1)$$

In Equation 1, N is the concentration of viable bacteria in CFU/ml, C is the colony count, V is the volume of sample plated in ml, and D is the dilution factor.

For experiments using both *P. aeruginosa* and *S. aureus* cultured together, spot plating could not be used to assess bacterial growth as the two types of bacterial colonies would be indistinguishable in small droplets. Therefore, spread plating techniques were used to determine the CFU/ml of each of the two bacteria when co-cultured together in the model.

For spread plating, the liquid and hydrogel phase samples were prepared and serially diluted in the same manner as for spot plating. Instead of plating multiple dilutions onto one LB agar plate, 100 µl of one dilution was plated onto one LB agar plate and then spread around the plate using a spreader. By using a greater volume of sample and spreading it out, we were able to distinguish the *P. aeruginosa* colonies (blue, fuzzy) from the *S. aureus* colonies (yellow, sharp) by color and morphology, thereby allowing us to assess the growth of each bacteria species in the model. CFU/ml can be calculated from these colony counts also using Equation 1. An example end product of spread plating is shown in Figure 5.

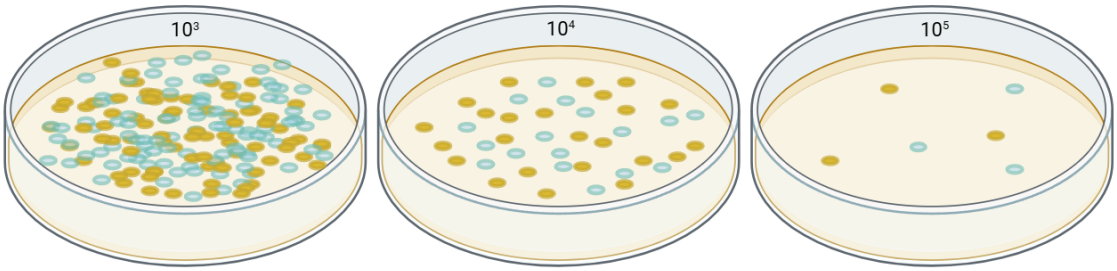

Figure 5: Spread plating to determine CFU/ml of two bacteria species. A sample from the liquid or hydrogel phase of the airway infection model is serially diluted from 10^1 to 10^6. Each dilution is then plated and spread on one LB agar plate, allowing for colonies each of species to be counted based on color and morphology. Diagram created with BioRender.com.

2.8 Determination of antibiotic minimum inhibitory concentrations for bacteria in the airway infection model

Prior to determining the potential antibacterial efficacy of the antibiotic-glass combinations, the minimum inhibitory concentration (MIC) of each antibiotic for its respective bacteria was determined in the healthy and CF airway infection models. The antibiotics tobramycin (Sigma-Aldrich. Cat. No. 32986-56-4) and vancomycin (Sigma-Aldrich. Cat. No. SBR00001) were selected for *P. aeruginosa* and *S. aureus* respectively as they are common antibiotics used to treat their respective bacteria.

For the MIC experiments, the airway infection model was assembled as described in Section 2.6 with either *P. aeruginosa* or *S. aureus* at an OD_{600} of 0.01, and with either the healthy or CF hydrogel. 5 hours after the addition of the bacteria to the model, the ATPS liquid phase was replaced with DMEM, low glucose/F-12 + 1% FBS containing a range of concentrations of either tobramycin for *P. aeruginosa* or vancomycin for *S. aureus*. The tobramycin concentrations tested were: 0, 4, 8, 16, 32, and 64 µg/ml. The

vancomycin concentrations tested were: 0, 8, 12, 16, 24, and 32 µg/ml. The airway infection model was then cultured for 43 hours with these antibiotics, after which bacteria growth was assessed.

Bacterial growth in the liquid and hydrogel phases of the airway infection model were assessed using spot plating techniques as described in Section 2.7. Both the experiment to determine the MIC of tobramycin on *P. aeruginosa* in the model and the experiment to determine the MIC of vancomycin on *S. aureus* in the model were repeated with three biological replicates. The MIC_{90} of each antibiotic for its respective bacteria was determined as the lowest concentration of antibiotic at which there is less than 10% bacteria growth compared to the no treatment control.

2.9 Assessment of cell viability in the airway infection model

Cell viability was assessed using a live/dead assay consisting of calcein AM (Thermo Fisher Scientific, Gibco. Cat. No. C1430) and ethidium homodimer-1 (Thermo Fisher Scientific, Gibco. Cat. No. E1169), and Hoechst 33342 stain (Thermo Fisher Scientific, Gibco. Cat. No. H3570). The calcein AM and ethidium homodimer-1 solutions were first mixed together and diluted to 4 mM and 16 mM respectively in PBS, and the Hoechst stain was diluted to 32.4 Mm in PBS.

The live/dead assay was performed keeping the apical compartment intact so as not to disturb the structure of the model or wash out the unattached dead cells. Therefore, the calcein AM/ethidium homodimer-1 working solution was first added to the basolateral compartment and then the model was incubated at 37 ºC and 5% CO_2 for 20

minutes. The basolateral compartment was then rinsed and then the model was incubated with the Hoechst stain in the basolateral compartment for 10 minutes at room temperature protected from light. The basolateral compartment was then rinsed, and PBS was added to image.

The EVOS™ FL Auto 2 Imaging System (Thermo Fisher Scientific, Gibco. Cat. No. AMAFD2000) was used to image the live cells (GFP channel), dead cells (RFP channel), and DNA (DAPI channel). ImageJ was then used to count the number dead-stained and Hoechst-stained cells in each 10x or 20x magnification image. Cell viability was then calculated using the number of dead cells and total cells from the Hoechst stain using Equation 2.

$$\text{Cell Viability} = \left(1 - \frac{D}{H}\right) \text{X } 100\% \tag{2}$$

In Equation 2, D is the number of dead cells and H is the number of Hoechst-stained cells.

2.10 Preparation of bioactive glass extracts

16 borate bioactive glass formulations containing zinc and gallium ions were created by the Boyd lab. The antibacterial efficacy of all 16 glasses on planktonic *P. aeruginosa* and *S. aureus* was evaluated previously in the lab. From these 16 candidates, we selected the top 3 candidates based on this planktonic antibacterial efficacy data to be tested using the airway infection model. The ionic compositions of these 3 selected

candidates (#11, #13, #16) are shown in Table 2. To identify the glasses for the rest of the thesis, they were named based on their composition of either Ga^{3+} and/or Zn^{2+} ions.

Table 2: Compositions of the three bioactive glass formulations used in this project.

Glass #	Identifier	B_2O_3 *mol %*	Na_2O *mol %*	ZnO *mol %*	Ga_2O_3 *mol %*
11	**Ga^{3+} Glass**	56.28	30	0	13.72
13	**Zn^{2+} Glass**	62.78	30	7.22	0
16	**Ga^{3+}/Zn^{2+} Glass**	50	25.90	4.10	20

To prepare the glass extracts, 0.1 g of each glass was weighed and added to 10 ml of cell culture media in a 50 ml Falcon tube, which was placed on a shaking incubator at 200 rpm for 48 hours at 37 °C to dissolve the glass and release the metal ions into the media. The resulting mixture was then centrifuged, and the extracted supernatant was collected and labelled as "dilution 1". These extracts were then diluted down to the proper dilutions for each experiment.

2.11 Assessment of antibacterial efficacy and cytotoxicity of antibiotic-glass combinations in CF airway infection model with bacteria in monoculture

The antibiotic-glass combinations were tested on either *P. aeruginosa* or *S. aureus* using the CF airway infection model. Tobramycin-glass combinations were tested on the CF model with *P. aeruginosa* while vancomycin-glass combinations were tested on the CF model with *S. aureus*. The CF airway infection model was first assembled as described in Section 2.6 with either *P. aeruginosa* or *S. aureus* at an OD_{600} of 0.01.

Five hours after the addition of the bacteria to the model, the ATPS liquid phase was replaced with DMEM, low glucose/F-12 + 1% FBS containing the antibiotic-glass

combinations. For the tobramycin-glass on *P. aeruginosa* experiments, either 0 or 16 µg/ml tobramycin was used with each of the three glass extracts at a dilution of 0, 1/32, or 1/16. For the vancomycin-glass on *S. aureus* experiments, either 0 or 16 µg/ml vancomycin was used with each of the three glass extracts at a dilution of 0, 1/4, or 1/2. The range of glass dilutions selected for each experiment was based upon previous work done in the lab that assessed the antibacterial efficacy of the glasses on planktonic *P. aeruginosa* or *S. aureus*.

The model was then cultured with the antibiotic-glass combinations to reach a total culture time of 48 hours, after which bacteria growth in the liquid and hydrogel phases was assessed using spot plating as described in Section 2.7 and 16-HBE cell viability was assessed as described in Section 2.9. Both the experiment testing the tobramycin-glass combinations on *P. aeruginosa* and the experiment testing the vancomycin-glass combinations on *S. aureus* were repeated with three biological replicates.

2.12 Assessment of antibacterial efficacy and cytotoxicity of antibiotic-glass combinations in CF airway co-infection model with bacteria in co-culture

The antibiotic-glass combinations were tested on *P. aeruginosa* and *S. aureus* cultured together using the CF airway infection model. For the first experiment, the same parameters as the tobramycin-glass on *P. aeruginosa* in monoculture experiment were used but *S. aureus* was now added to see if adding *S. aureus* would change how the tobramycin-glass combinations affected *P. aeruginosa* growth. For the second

experiment, the opposite was done meaning the same parameters as the vancomycin-glass on *S. aureus* in monoculture experiment were used but *P. aeruginosa* was now added. A summary of the specific antibiotic-glass combinations used in these polymicrobial experiments as well as in the previously described monomicrobial experiments are listed in Table 3 below.

Table 3: Summary of antibiotic-glass combinations used in each experiment. For each experiment assessing antibiotic-glass efficacy in the monomicrobial or polymicrobial airway infection model, the bacteria *P. aeruginosa* (PA) and/or *S. aureus* (SA), the type and concentration of antibiotic, and the glass dilutions used in each experiment are listed. The corresponding results sections for the monomicrobial and polymicrobial experiments are identified as well.

	Monomicrobial (3.4)		**Polymicrobial (3.5)**	
Bacteria	PA	SA	PA+SA	PA+SA
Treatment	tob-glass	van-glass	tob-glass	van-glass
Ab Concentration	16 µg/ml	16 µg/ml	16 µg/ml	16 µg/ml
Glass Dilutions	1/32, 1/16	1/4, 1/2	1/32, 1/16	1/4, 1/2

For both polymicrobial experiments, the CF airway infection model was first assembled as described in Section 2.6 with a combination of *P. aeruginosa* at an OD_{600} of 0.005 and *S. aureus* at an OD_{600} of 0.005 to reach a combined OD_{600} of 0.01. Five hours after the addition of the bacteria to the model, the ATPS liquid phase was replaced with DMEM, low glucose/F-12 + 1% FBS containing the antibiotic-glass combinations. For the tobramycin-glass on co-cultured bacteria experiments, either 0 or 16 µg/ml tobramycin was used with each of the three glass extracts at a dilution of 0, 1/32, or 1/16.

For the vancomycin-glass on co-cultured bacteria experiments, either 0 or 16 µg/ml vancomycin was used with each of the three glass extracts at a dilution of 0, 1/4, or 1/2.

The model was then cultured with the antibiotic-glass combinations to reach a total culture time of 48 hours, after which bacteria growth in the liquid and hydrogel phases was assessed using spread plating as described in Section 2.7 and 16-HBE cell viability was assessed as described in Section 2.9. Note that to reduce the total number of LB agar plates used in these experiments, only the 10^4, 10^5, and 10^6 dilutions were plated as these dilutions consistently contained colonies in the countable range. Both the experiment testing the tobramycin-glass combinations on co-cultured bacteria and the experiment testing the vancomycin-glass combinations on co-cultured bacteria were repeated with two biological replicates.

2.13 Statistical analysis

All statistical analyses were performed using GraphPad Prism (Version 10.3.1). An Ordinary Two-Way Analysis of Variance (ANOVA) with Šidák's Multiple Comparison's Test with p values represented as * $p < 0.05$, ** $p < 0.01$, *** $p < 0.001$, **** $p < 0.0001$ was used to determine statistical significance for the antibacterial efficacy data of the antibiotic-glass combinations. The Šidák's Multiple Comparison's Test was used because it is well-suited for situations where multiple independent comparisons are being made, rather than situations where full pairwise comparisons or comparisons to a single control are being made [116]. This is the same type of situation where the Bonferroni method is used, but the Šidák method was chosen as it offers

slightly greater sensitivity than the Bonferroni method while still effectively controlling the risk of false positives [116]. The two factors analyzed were: glass dilution, with three levels depending on the experiment; and antibiotic concentration, with two levels, 0 and 16 μg/ml. This allowed us to identify statistical significance in the effects of glass alone and glass + antibiotic on bacterial growth in the airway infection model.

Thes statistical significance of the cell proliferation data using different media compositions was determined using an Ordinary Two-Way ANOVA with Šidák's Multiple Comparison's Test with p values represented as * $p < 0.05$, ** $p < 0.01$, *** $p < 0.001$, **** $p < 0.0001$. The two factors analyzed were: FBS concentration, with three levels: 0%, 1%, and 10%; and glucose concentration, with two levels: 1.4 mg/dl and 3.2 mg/dl. This allowed us to identify statistically significant effects of FBS and glucose concentration on 16-HBE proliferation.

CHAPTER 3. Results

3.1 Establishing an ATPS to confine bacteria on top of the hydrogel phase of the airway infection model

In developing the airway infection model, a repeatable method to produce an ATPS on top of the mucus-mimetic hydrogels was developed. This was necessary as a method to deposit bacteria into the airway infection model in a controlled manner.

3.1.1 Determining the height of DEX droplet deposition on the transwell insert

In the airway infection model, the BioMek 4000 Automated Liquid Handler was used to deposit the DEX droplet within the PEG phase above the hydrogels as the DEX droplet has a small volume of 0.5 µl that is difficult to successfully pipette by hand in a repeatable manner. Therefore, the first step of developing this method was to calibrate the BioMek and determine a distance from the bottom of the well for the BioMek to deposit into the transwell insert. When determining this distance, it is important that when the DEX droplet leaves the pipette tip, it is touching the pipette tip and the insert surface at the same time so that the DEX droplet doesn't split into multiple droplets. A range of distances from 1.0 mm to 1.4 mm was determined to produce a sufficient droplet on the insert surface (Figure 6).

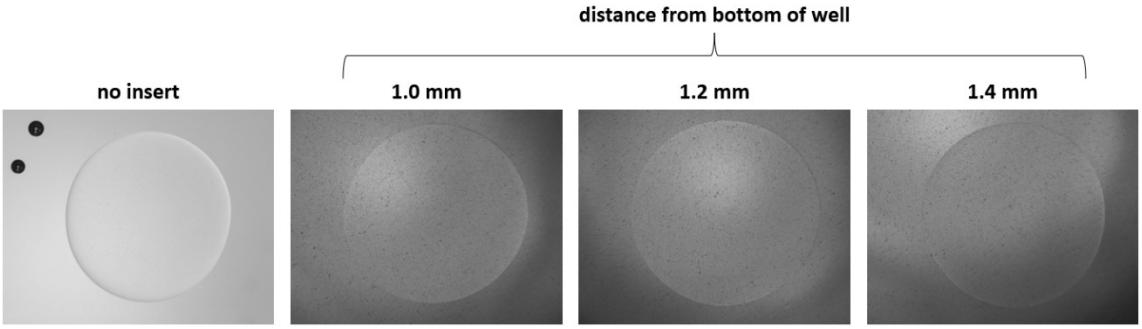

Figure 6: DEX droplets deposited on the surface of PET membrane inserts in a 24-well plate. Phase contrast images were taken immediately after deposition using the BioMek 4000 Automated Liquid Handler. DEX droplets were deposited at different heights measured from the bottom of the well to account for the distance between the insert surface and the well surface.

3.1.2 Visualizing bacteria confinement in the airway infection model

Next, an alginate-$CaCl_2$ hydrogel without mucins was deposited on the transwell insert at a volume of 50 ul to mimic the thickness of the hydrogel phase in the airway infection model. It was necessary to not use mucins for this hydrogel so we could image the bacteria dispersion using brightfield microscopy. Then, the BioMek was used to deposit a DEX droplet containing either no bacteria, *P. aeruginosa*, *S. aureus*, or both bacteria on top of the hydrogel using a deposition height of 2.4 mm to account for the hydrogel thickness of 1.4 mm. To ensure that the DEX droplet was being deposited properly, there were groups with no insert and/or no hydrogel at according deposition heights. Images were taken at 0h, 6h, and 24h to assess bacteria growth in the DEX droplet. After 6 hours, there appears to be a defined area of bacterial growth visible on top of the hydrogels, with no DEX droplet outline visible (Figure 7).

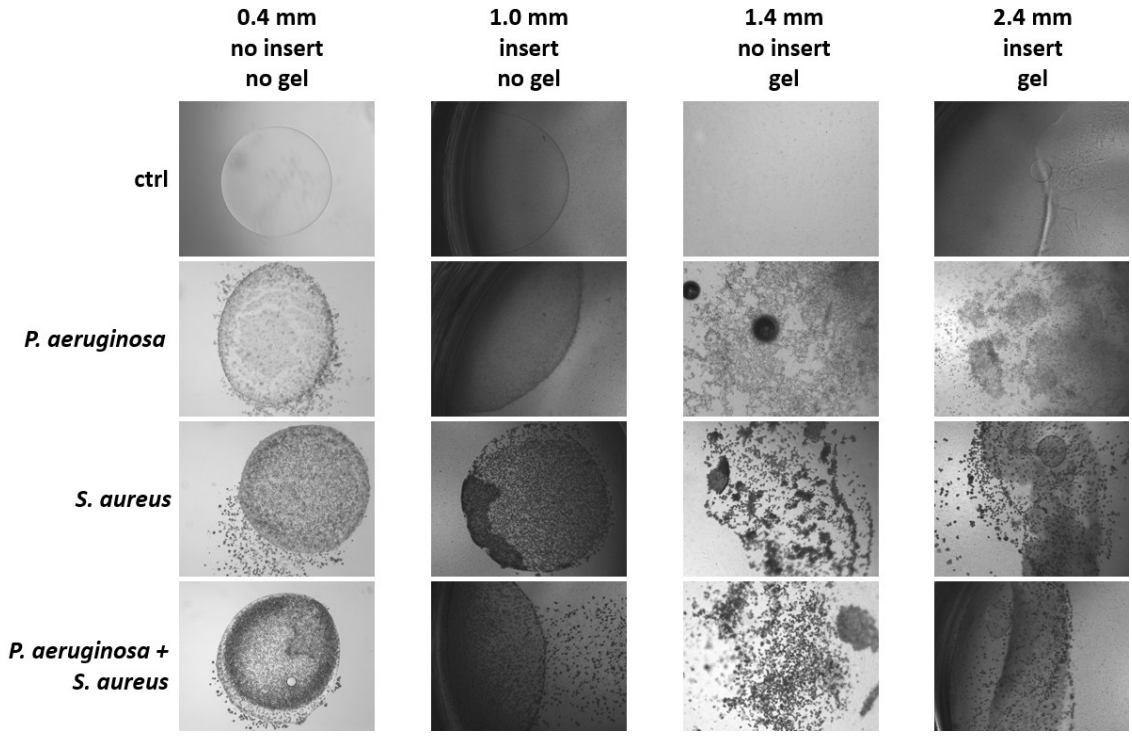

Figure 7: 6 hour phase contrast images of bacteria-containing DEX droplets deposited on top of transwell inserts and/or mucus-mimetic hydrogels. The DEX droplets were deposited at distances from the bottom of the well corresponding to the height of the transwell insert and/or hydrogel with an additional 0.4 mm to account for the distance between the pipette tip and the surface to deposit the DEX droplet on to. In the hydrogel groups, we do not see a defined DEX droplet, rather a localized area of bacterial growth.

3.1.3 Determining the height of DEX droplet deposition on the airway infection model

For the next experiments to assess the ATPS confinement of bacteria on top of the hydrogel phase of the airway infection model, only *S. aureus* was used as *S. aureus* is better confined by the PEG/DEX ATPS after 5 hours, and therefore easier to visualize if it is confined or not. The distance from the bottom of the well was varied from 2.0 mm to 2.8 mm to assess if DEX droplet deposition height has an effect on how well the bacteria is confined in the airway infection model. It was found that changing the DEX deposition

height did not have an effect on how well the bacteria was confined, with all heights having a confined area of bacteria near the edge of the well (Figure 8).

At this time, it was noted that there appeared to be a trail of bacteria from the center of the insert, where the DEX droplet was deposited, to the side of the insert, where the final area of bacteria was. This sliding could have caused the bacteria to escape confinement. This was due to the incubator not being level, and this was corrected in the next experiments. Also, the BioMek was depositing the DEX droplets towards the top and right of the inserts and therefore the BioMek was reprogrammed with a calibrated X,Z position so that in the next experiments, DEX droplets were deposited in the center of the insert.

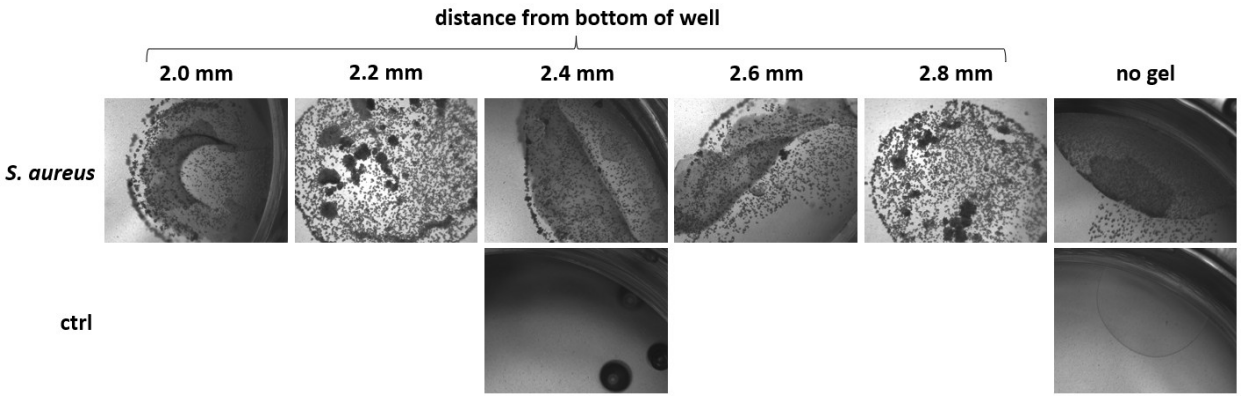

Figure 8: 6 hour phase contrast images of *S. aureus*-containing DEX droplets deposited on top of mucus-mimetic hydrogels within a transwell insert. The DEX droplets were deposited at varying distances from the bottom of the well to attempt to optimize the proper distance for a DEX droplet to form. In the hydrogel groups, we do not see a defined DEX droplet, rather a localized area of bacterial growth.

The range of DEX droplet deposition heights was increased to 2.4 mm to 4.0 mm to see if higher heights would produce a droplet without puncturing the hydrogel. For this experiment, the incubator was levelled and the BioMek was centered. There did not appear to be any differences in bacteria confinement between deposition heights (Figure 9). However, it was noticed that the bacteria appeared to migrate to imperfections in the hydrogel and therefore hydrogel uniformity in the insert needed to be improved (Figure 9).

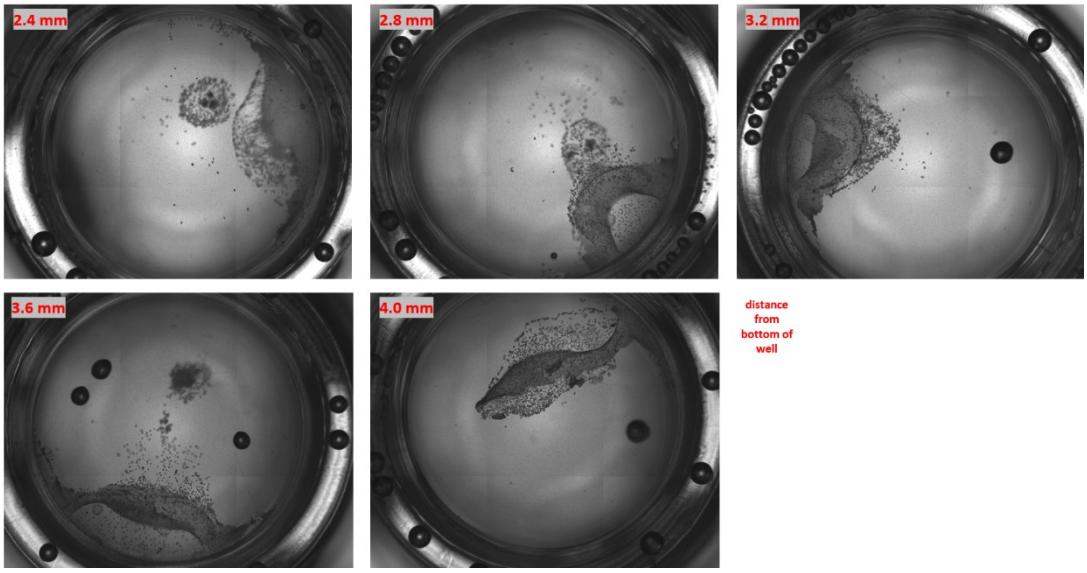

Figure 9: Bacteria confinement on hydrogel. Using the BioMek 4000 Liquid Handler, DEX droplets containing *S. aureus* (OD = 0.01) were deposited on an alginate hydrogel within a transwell insert at different heights from 2.4 mm to 4.0 mm. Note that the bacteria appears to migrate towards imperfections in the gel. 5 hour images.

3.1.4 Improving hydrogel uniformity

To improve hydrogel uniformity in the insert, the hydrogel was first manually moved around after pipetting onto the insert to get it to fully cover the insert and eliminate gaps in the hydrogel. Secondly, after hydrogel deposition, the entire plate was centrifuged for 5 min at 100 g to get it to spread out uniformly. With this new

centrifuging technique, it appeared that the area of bacterial confinement was much more centered, defined, and consistent (Figure 10). However, when centrifuging, the basolateral compartment was left empty, and therefore it appeared that the insert membrane flexed inwards and therefore the hydrogel aggregated towards the center, which is visible in the images as an empty outer ring of no hydrogel in the insert (Figure 10). Once again, the DEX droplet deposition height was manipulated, but there appeared to be no difference in bacteria confinement in the range of 2.0 mm to 4.0 mm (Figure 10). And therefore 2.5 mm was used going forward which is calculated based on height for tip to not touch surface (0.4 mm) + height of insert relative to well surface (0.6 mm) + gel thickness (1.5 mm).

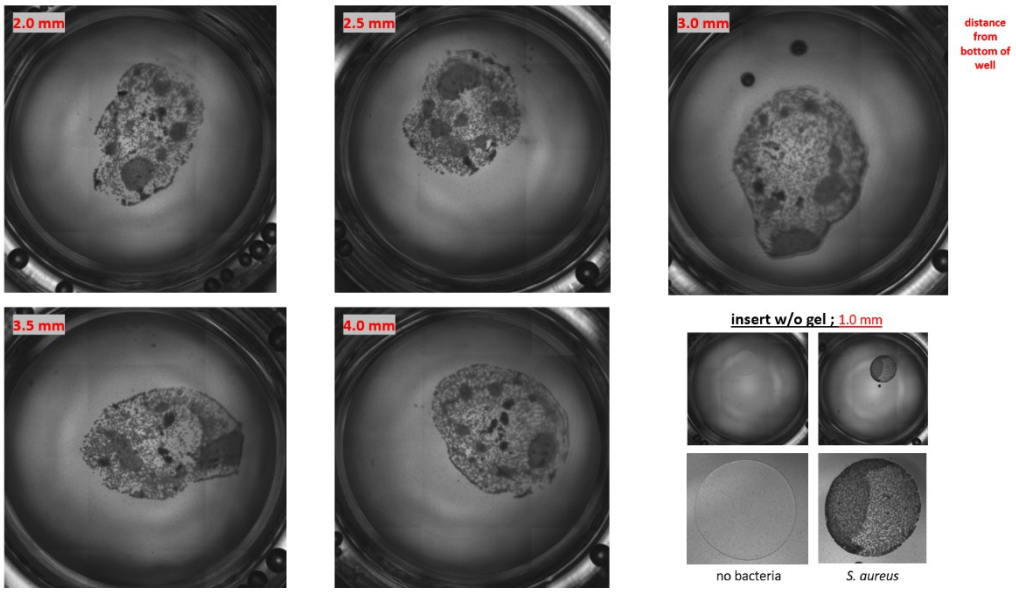

Figure 10: Bacteria confinement on hydrogel after centrifuging hydrogel. Using the BioMek 4000 Liquid Handler, DEX droplets containing *S. aureus* (OD = 0.01) were deposited on an alginate hydrogel within a transwell insert at different heights from 2.0 mm to 4.0 mm. For this experiment, the hydrogel was manually spread, and the plate was centrifuged at 200 g for 5 min after gel deposition with an empty basolateral compartment. 5 hour images.

Following up on the last experiment, PBS was added to the basolateral compartment while centrifuging to prevent the insert membrane flexing inwards. With this change, there now appears to be no empty outer ring indicating that the gel is covering the entire insert surface, and we see a more uniform droplet that doesn't migrate to the gel edge (Figure 11).

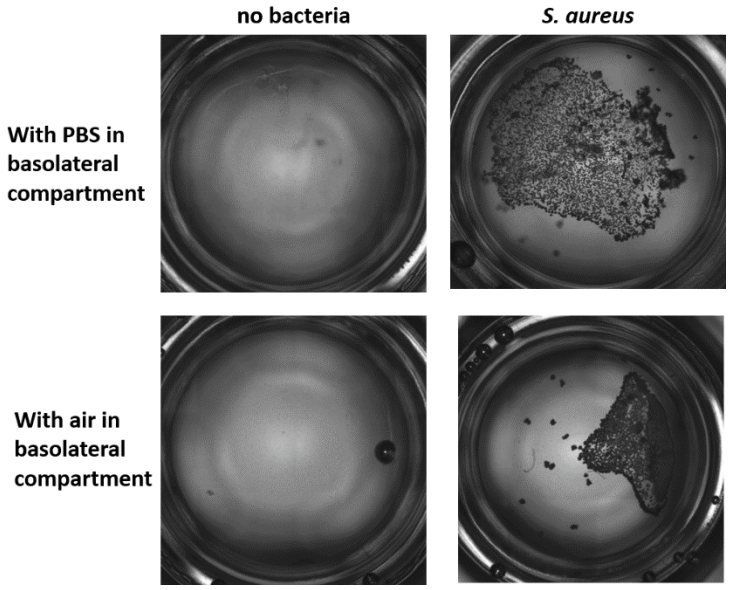

Figure 11: Bacteria confinement on hydrogel after centrifuging hydrogel with PBS in basolateral compartment. Using the BioMek 4000 Liquid Handler, DEX droplets containing *S. aureus* (OD = 0.01) and no bacteria were deposited on an alginate hydrogel within a transwell insert at a 2.5 mm deposition height from bottom of well. For this experiment, the plate was centrifuged at 100 g for 5 min after hydrogel deposition with PBS in the basolateral compartment to prevent insert flexing. 5 hour images.

3.2 Inducing quiescence in 16-HBE cells in the airway infection model

Inducing quiescence on 16-HBE cells via altering the FBS and glucose concentration of the cell culture media was investigated to more accurately represent the state of bronchial epithelial cells in the airway and prevent 16-HBE overgrowth.

3.2.1 16-HBE viability and clumping with different FBS concentrations

16-HBE cells were grown for 5 days after reaching 100% confluency with different FBS concentrations in the cell culture media. Phase contrast images were taken and a live/dead assay was performed to assess cell health and viability with lowered FBS concentrations. From the live/dead assay, it appears that all FBS conditions show a monolayer of live cells (Figure 12). However, the higher FBS conditions (8%, 10%) had more empty patches and clusters of overgrown cells visible under phase contrast microscopy (Figure 12). Therefore, since 16-HBE survived under serum starvation, decreasing 16-HBE proliferation by serum starvation was further investigated.

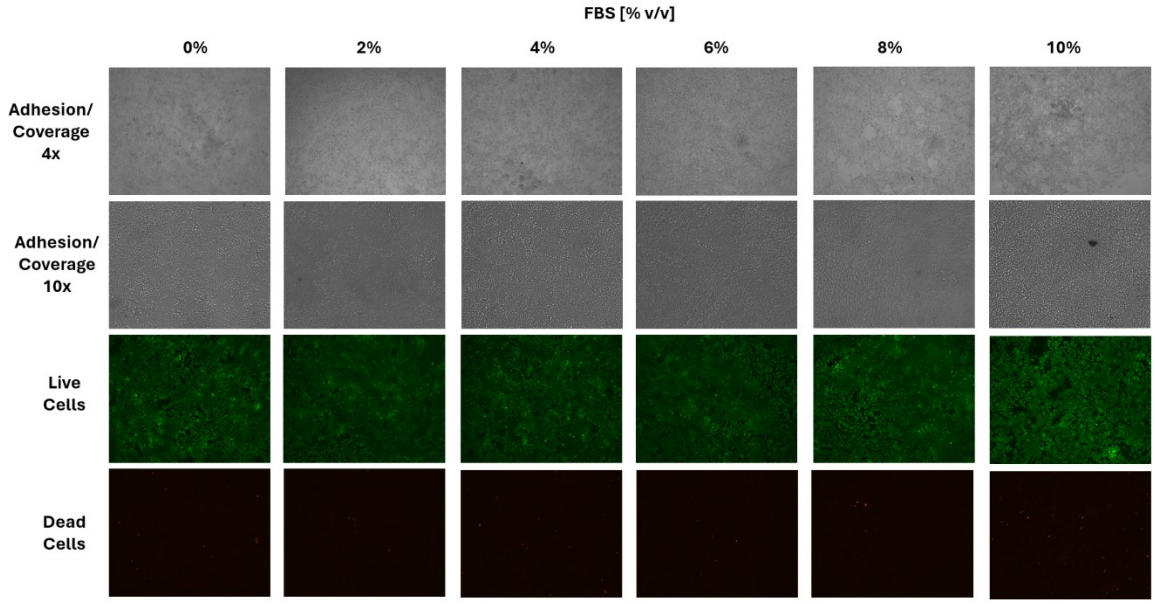

Figure 12: Cell images and live/dead assay after 5 days growth post 100% confluency with varying levels of FBS. Images were taken at 4x magnification to assess cell confluency and cell survival 5 days after reaching 100% confluency when grown with different FBS concentrations.

3.2.2 Determining optimal stain time of EdU proliferation assay

The EdU cell proliferation assay was selected to quantify 16-HBE proliferation when adjusting media composition, which assesses proliferation by staining cells that have proliferated during a chosen stain time. First, the stain time of the EdU reagent had to be optimized to best capture differences in 16-HBE proliferation. Initially, a stain time of 72 hours was chosen based on previous lab protocols. Using the 72 hour stain time, almost all of the cells present stained by Hoechst were also stained by EdU, indicating that almost all the cells had proliferated during the 72 hours (Figure 13).

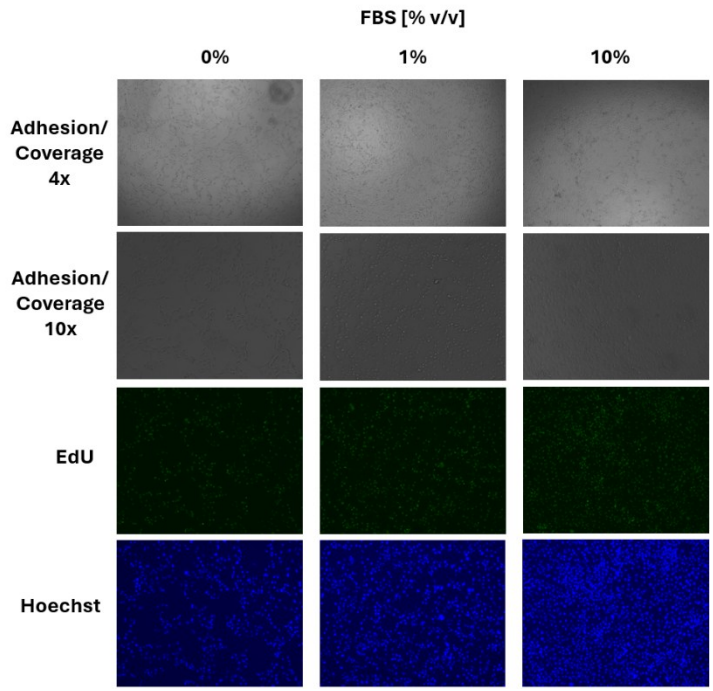

Figure 13: Representative cell images and EdU assay after 72 hours growth post 100% confluency with varying levels of FBS with a 72 hour EdU stain time. Images were taken using an EVOS microscope to assess 16-HBE proliferation 72 hours after reaching 100% confluency when grown with different FBS concentrations. EdU stains cells that have proliferated over the 72 hours stained with EdU. Hoechst stains DNA, thereby representing the total cell count.

Next, the EdU stain time was reduced to 24 hours to attempt to capture differences in cell proliferation. With a 24 hour EdU stain time, we again see that almost all of the Hoechst-stained cells were also EdU stained, and therefore the EdU stain time needed to be further reduced (Figure 14). Interestingly, the 16-HBEs cultured with DMEM/F-12 + 10% FBS for 4 days appeared to have less cells overall and cells appearing bigger in size, potentially due to cell death due to excess over confluency (Figure 14).

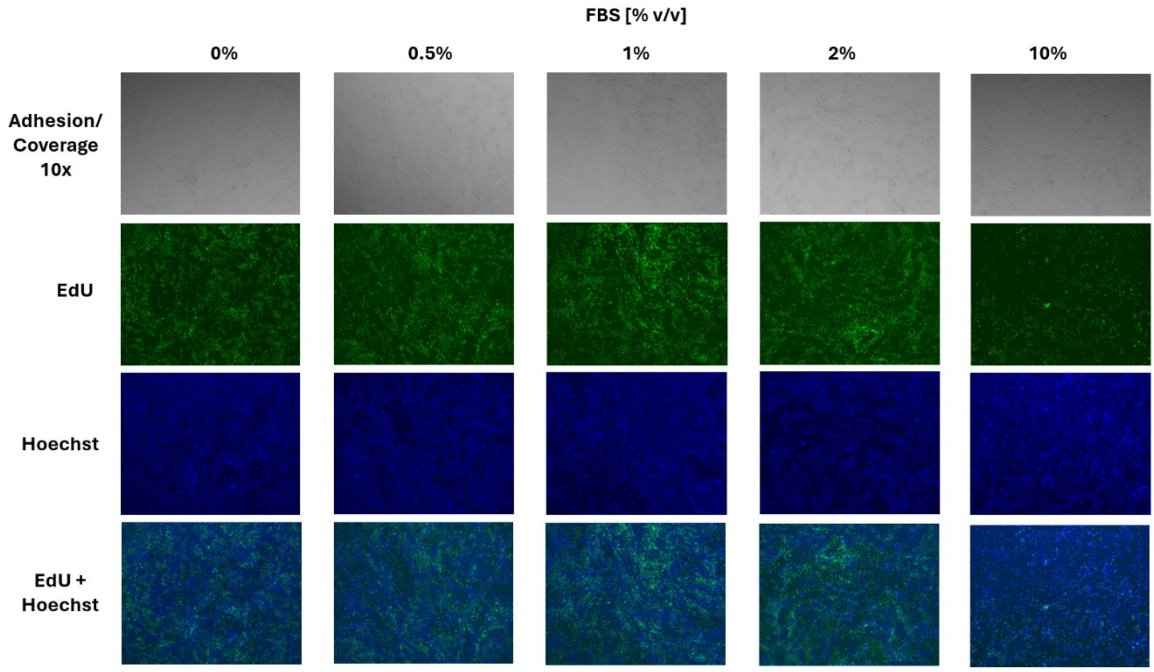

Figure 14: Representative cell images and EdU assay after 4 days growth post 80% confluency with varying levels of FBS with a 24 hour EdU stain time. Images were taken using an EVOS microscope to assess 16-HBE proliferation 4 days after reaching 80% confluency when grown with different FBS concentrations. EdU stains cells that have proliferated over the 24 hours stained with EdU. Hoechst stains DNA, thereby representing the total cell count.

Next, an EdU assay was performed with EdU stain times of 1h, 2h, 6h, and 24h to find a stain time where differences in proliferation were visible. 16-HBE were cultured

with cell culture media containing varying levels of FBS (0%, 1%, 10%) and glucose (3.2 mg/dl or 1.4 mg/dl) for 4 days, after which the EdU assay was performed. From the representative merged EdU and Hoechst images, it appears that the 1h, 2h, and 6h stain times were better able to show differences in proliferation compared to the 24h stain time, in which all cells appeared to be EdU stained (Figure 15). Note again that in the high glucose + 10% FBS group, the cells appear larger in morphology and less cells overall, suggesting that over confluency leading to cell damage occurred (Figure 15).

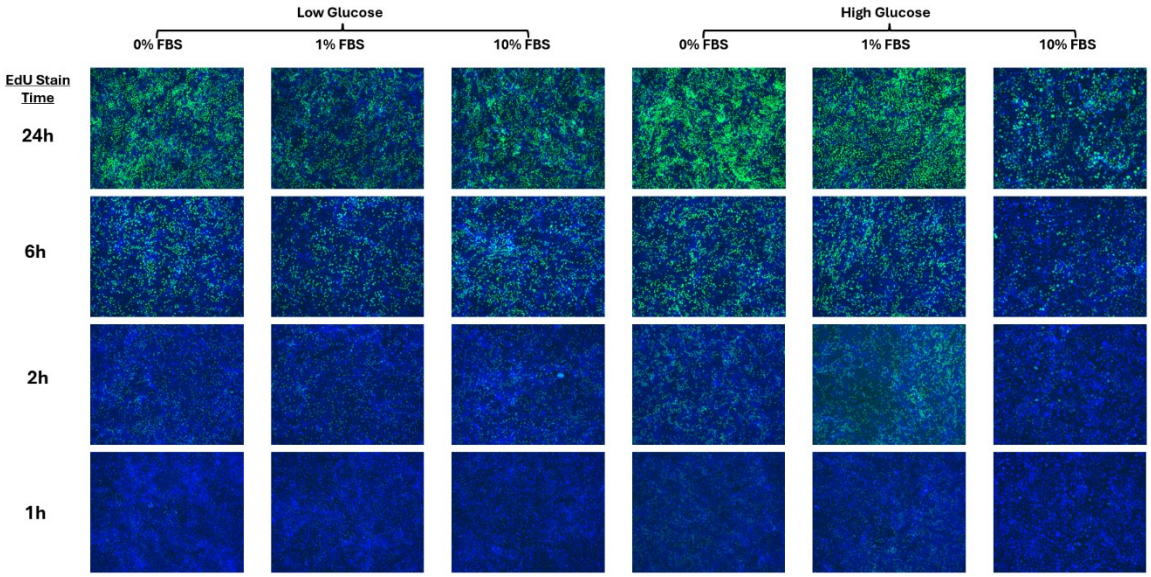

Figure 15: Comparison of EdU assay images with different EdU stain times. Representative 10x magnification merged images of EdU stain and Hoechst stain after 4 days growth post 80% confluency with different concentrations of FBS and glucose in cell culture media. EdU stain time was varied to optimize the EdU proliferation assay.

Looking closer at the cell proliferation differences between high and low glucose, we see that the difference in cell proliferation is apparent under the 1h, 2h, and 6h stain times (Figure 16). For all future EdU proliferation experiments, a stain time of 2 hours was selected as we can see a noticeable difference in proliferation and the EdU stain is bright enough to be visible (Figure 16).

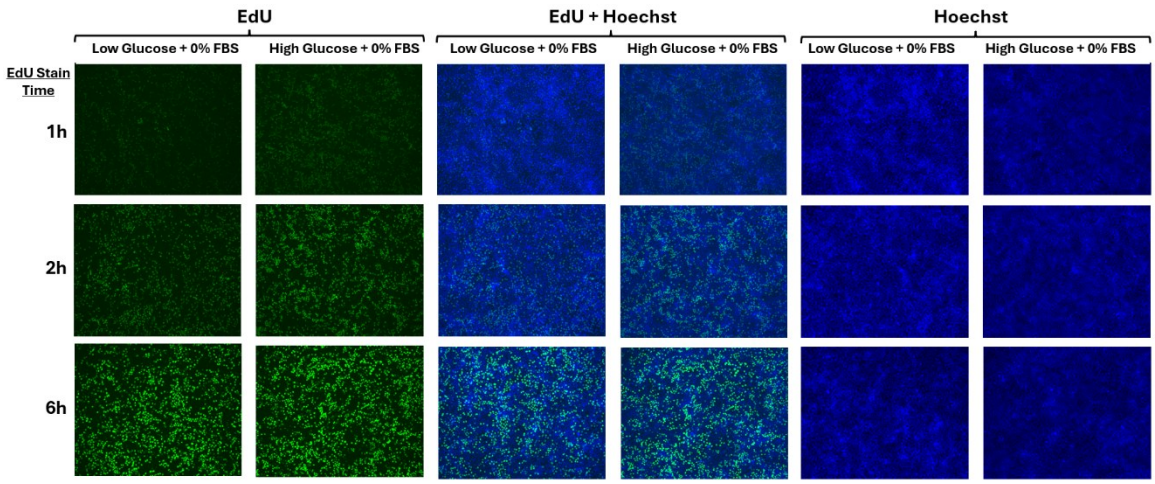

Figure 16: Comparison of differences seen in 16-HBE proliferation with different EdU stain times. 16-HBE were grown in either high or low glucose cell culture media containing 0% FBS for 4 days. Representative 10x images of EdU stain, Hoechst stain, and merge are shown. EdU stain time was varied to optimize the EdU proliferation assay.

3.2.3 Effect of FBS and glucose on 16-HBE proliferation

The EdU assay was used with a 2 hour EdU stain time to quantify 16-HBE proliferation when grown over 2 days and 4 days with cell culture media containing different concentrations of FBS (0%, 1%, 10%) and glucose (3.2 mg/dl, 1.4 mg/dl). Cell proliferation was quantified by dividing the number of EdU-stained cells to the number of Hoechst-stained cells. After 2 days, there does not appear to be a difference in cell proliferation in 16-HBEs cultured with different concentrations of FBS and/or glucose (Figure 17). After 4 days, we see a decrease in cell proliferation in the low glucose groups compared to high glucose (Figure 17). For the 10% FBS groups, we see a low proliferation in high glucose 10% FBS, which is most likely due to over confluency-related cell damage (Figure 17). There does not appear to be a difference in proliferation between 0% and 1% FBS, and therefore 1% FBS was chosen for the cell culture media in the airway infection model to prevent unnecessary serum starvation. The low glucose +

10% FBS group had higher proliferation than the low glucose + 1% FBS group, therefore 1% FBS was chosen to decrease 16-HBE proliferation.

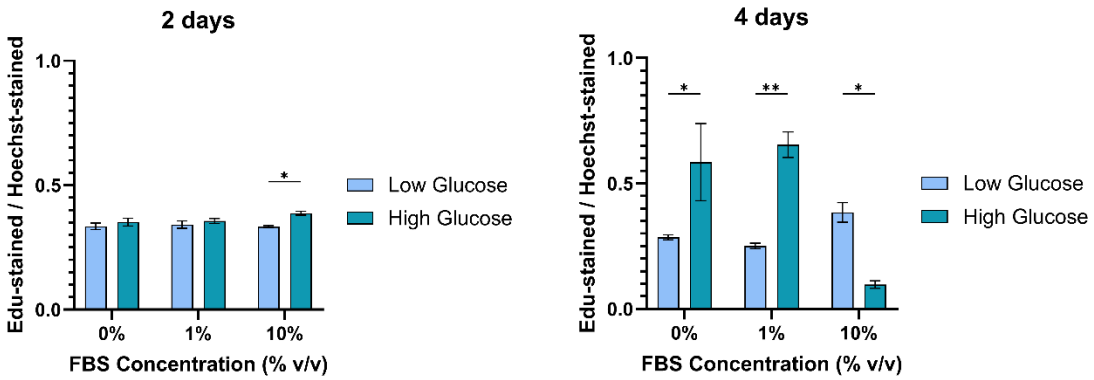

Figure 17: EdU assay cell proliferation data after 2 days and 4 days of 16-HBE cultured with different media compositions. 16-HBE were cultured for either 2 days or 4 days with cell culture media containing different concentrations of glucose and FBS, after which an EdU assay was performed to assess cell proliferation. Error bars are mean ± SEM. N=1. Ordinary Two-Way ANOVA with Šidák's Multiple Comparisons Test; * $p < 0.05$, ** $p < 0.01$, *** $p < 0.001$, **** $p < 0.0001$.

From the representative EdU and Hoechst images, we see a decreased 16-HBE proliferation when cultured with low glucose (1.4 mg/dl) to high glucose (3.2 mg/dl) for 4 days (Figure 18). Based on this data, 16-HBE were cultured for a total of 4 days in the airway infection model with cell culture media containing 1.4 mg/dl glucose and 1% FBS to induce quiescence.

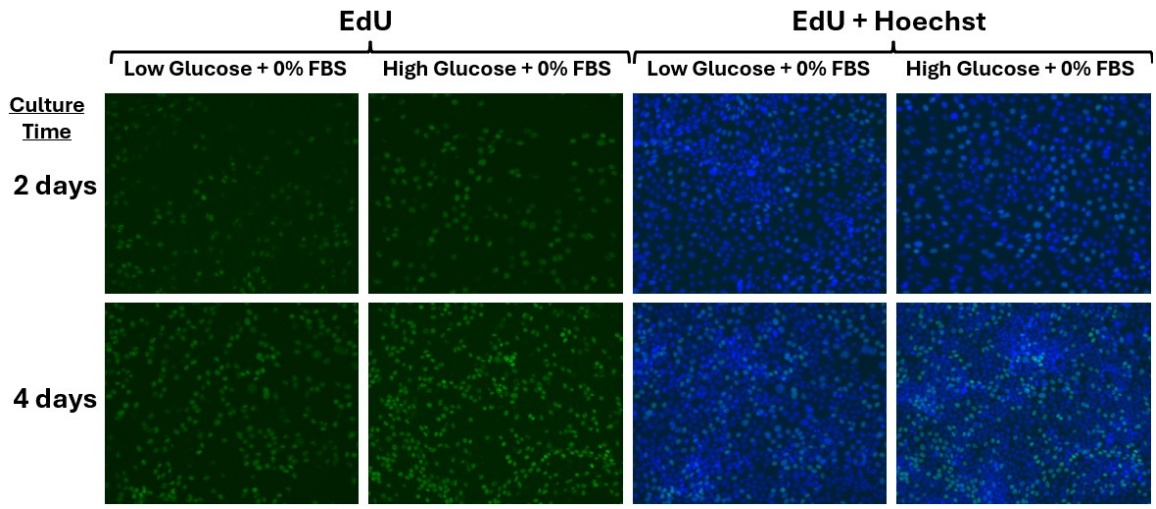

Figure 18: Representative 20x magnification images of the EdU-stained and Hoechst-stained cells for the low glucose + 0% FBS and high glucose + 0% FBS groups. 16-HBE were cultured for either 2 days or 4 days with cell culture media containing different concentrations of glucose and FBS, after which an EdU assay was performed to assess cell proliferation.

3.2.4 16-HBE viability with different media compositions

To ensure that changing the media composition would not decrease cell viability below 90%, a live/dead assay was performed to assess cell viability of 16-HBE cells in the airway infection model cultured with the two different media compositions for 4 days after reaching confluency. The "quiescence media", determined previously to slow down 16-HBE proliferation, contains 1.4 mg/dl glucose and 1% FBS while the "growth media", typically used to culture 16-HBEs, contains 3.2 mg/dl glucose and 10% FBS. When cultured in either medium, the mammalian cells in the healthy and CF airway infection model had cell viabilities greater than 90% and therefore potential cytotoxicity associated with lowered nutrient supply is not a significant concern for the airway infection model (Figure 19).

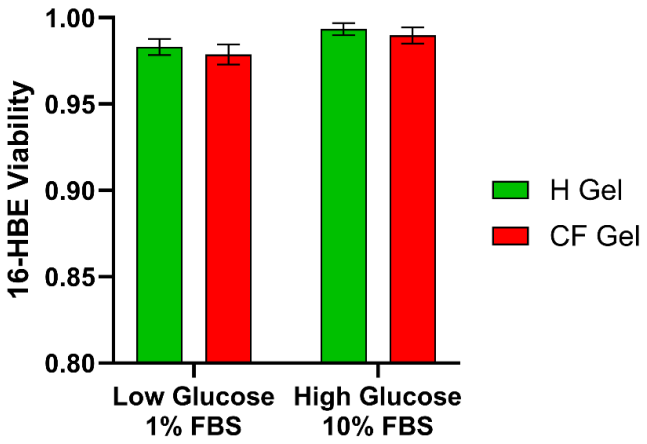

Figure 19: 16-HBE viability in the healthy and CF airway infection model when cultured with lower glucose and FBS. 16-HBE were cultured in the airway infection model with either media containing 1.4 mg/dl glucose and 1% FBS (quiescence medium) or media containing 3.2 mg/dl glucose and 10% FBS (growth medium) for 4 days, after which 16-HBE viability was determined using a live/dead assay. N=1. Mean ± SD.

3.3 Determining relevant MIC_{90} of chosen antibiotics in the airway infection model

After designing the *in vitro* airway infection model with a transwell insert system and quiescence-induced bronchial epithelial cells, the antibacterial efficacies of the two antibiotics selected for this project were examined in the airway infection model. This was done to determine the effective MIC_{90} of tobramycin for *P. aeruginosa* and vancomycin for *S. aureus* to determine an antibiotic concentration to use with the bioactive glasses that will allow us to see if more bacterial growth is inhibited with the addition of the bioactive glasses.

3.3.1 Determining MIC_{90} of tobramycin on *P. aeruginosa* in the airway infection model

The antibacterial efficacy of tobramycin on *P. aeruginosa* was determined in the healthy and CF airway infection models by adding a range of tobramycin concentrations to the airway infection model and measuring *P. aeruginosa* growth (Figure 20). The airway infection model was grown for a total of 48 hours with tobramycin and *P. aeruginosa*, and then spot plating was performed to assess *P. aeruginosa* growth. *P. aeruginosa* growth data was obtained for both the healthy and CF models and the liquid and hydrogel phases of each model. Based on this data, the MIC_{90} of tobramycin on *P. aeruginosa* was determined to be 32 µg/ml for the CF hydrogel phase since this was the lowest concentration at which *P. aeruginosa* growth decreased by more than 90% (Figure 20). Therefore, for the tobramycin-glass combination experiments, 16 µg/ml (MIC_{90}/2) was chosen as the single tobramycin concentration so that some bacteria growth in the hydrogel phase would be inhibited by tobramycin, but not so much that the augmentative effect of the bioactive glass couldn't be seen.

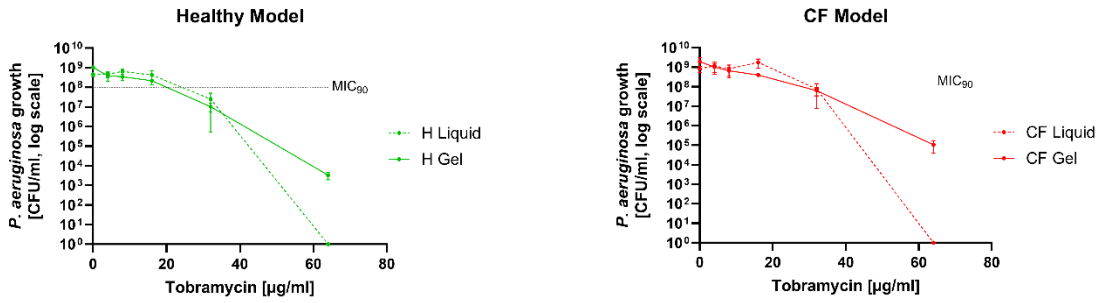

Figure 20: Treatment of *P. aeruginosa* with different tobramycin concentrations to determine minimum inhibitory concentration within the airway infection model. CFU/ml was obtained after 48 hours of culture of *P. aeruginosa* in the model with varying tobramycin concentrations dissolved in cell media, added to the apical compartment. The MIC_{90} line marks the CFU/ml at which bacteria growth is 10% of the no treatment control. Mean ± SEM. N=3.

3.3.2 Determining MIC_{90} of vancomycin on *S. aureus* in the airway infection model

The antibacterial efficacy of vancomycin on *S. aureus* was determined in the healthy and CF airway infection models by adding a range of vancomycin concentrations to the airway infection model and measuring *S. aureus* growth. The airway infection model was grown for a total of 48 hours with vancomycin and *S. aureus*, and then spot plating was performed to assess *S. aureus* growth. *S. aureus* growth data was obtained for both the healthy and CF models and the liquid and hydrogel phases of each model. Initially, the range of vancomycin concentrations chosen was from 0.125 µg/ml to 2 µg/ml as 0.125 µg/ml was determined previously in the lab to be the MIC of vancomycin on *S. aureus* when grown planktonically. When using this range of vancomycin concentrations in the airway infection model, no significant antibacterial effect was observed (Figure 21A). In the next trial, the range of concentrations was expanded to 0.125 µg/ml to 32 µg/ml in order to better capture the antibacterial range of vancomycin in the airway infection model. While an antibacterial effect was observed at 32 µg/ml vancomycin, there appeared to be a jump from no effect to an effect from 8 µg/ml to 32 µg/ml (Figure 21B). Therefore, a narrower range of concentrations from 8 µg/ml to 32 µg/ml was selected for the final experiment to determine the MIC_{90} of vancomycin for *S. aureus* in the airway infection model.

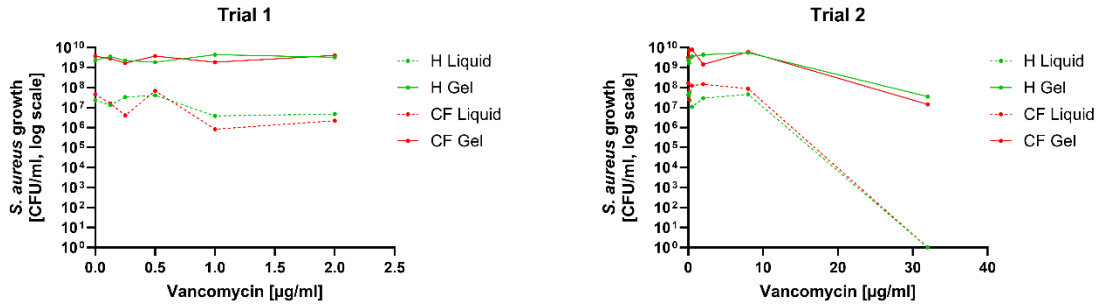

Figure 21: Treatment of *S. aureus* with different vancomycin concentrations in the airway infection model to determine a range of antibacterial concentrations. CFU/ml were determined after 48 hours of culture of *S. aureus* in the model with varying vancomycin concentrations dissolved in cell media, added to the apical compartment. N=1.

Using the new range of vancomycin concentrations, the MIC_{90} of vancomycin on *S. aureus* was determined to be 32 µg/ml for the CF hydrogel phase since this was the lowest concentration at which *S. aureus* growth decreased by more than 90% (Figure 22). Therefore, for the vancomycin-glass combination experiments, 16 µg/ml ($MIC_{90}/2$) was chosen as the single vancomycin concentration so that some bacteria growth in the hydrogel phase would be inhibited by vancomycin, but not so much that the augmentative effect of the bioactive glass couldn't be seen.

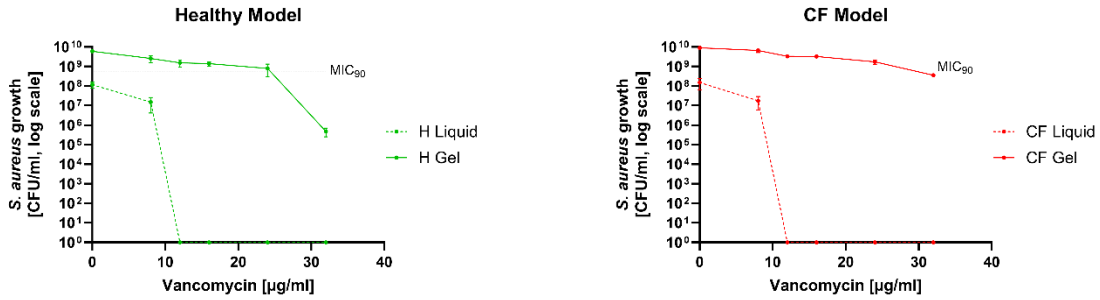

Figure 22: Treatment of *S. aureus* with different vancomycin concentrations to determine minimum inhibitory concentration within the airway infection model. CFU/ml were determined after 48 hours of culture of *S. aureus* in the model with varying vancomycin concentrations dissolved in cell media, added to the apical compartment. The MIC_{90} line marks the CFU/ml at which bacteria growth is 10% of the no treatment control. Mean ± SEM. N=3.

3.4 The effect of antibiotic-glass combinations on monomicrobial *P. aeruginosa* and *S. aureus* growth and mammalian cell viability in the CF airway infection model

Combinations of one of the three bioactive glass extracts (Ga^{3+}, Zn^{2+}, Ga^{3+}/Zn^{2+}) and one of the two antibiotics were added to the CF airway infection model for a total of 48 hours, after which bacteria growth and mammalian cell viability were assessed. Tobramycin-glass combinations were added to the CF airway infection model with *P. aeruginosa* (initial OD_{600} = 0.01) in monoculture, while vancomycin-glass combinations were added to the CF airway infection model with *S. aureus* (initial OD_{600} = 0.01) in monoculture. A summary of the antibiotic-glass combinations used in these monomicrobial experiments can be found in Table 3.

3.4.1 Effect of tobramycin-glass combinations on *P. aeruginosa* growth

The antibacterial efficacy of the bioactive glass extracts combined with tobramycin on *P. aeruginosa* growth was examined in the CF airway infection model after culturing the model for a total of 48 hours.

For the initial experiment on the tobramycin-glass combinations, glass extract dilutions of 1/256 and 1/512 were used since these dilutions had been shown to have an antibacterial effect on planktonic *P. aeruginosa* from work done by previous lab members. These glass dilutions were combined with either 0 or 16 μg/ml tobramycin based on the determined $MIC_{90}/2$ from Section 3.3.1.

All three glass extracts at dilutions of 1/256 and 1/512 did not appear to have an effect on *P. aeruginosa* growth in the hydrogel phase or liquid phase of the CF airway infection model (Figure 23). Therefore, these dilutions were deemed too high to have an antibacterial effect in the CF airway infection model, and therefore lower dilutions of glass extracts were investigated.

As for tobramycin efficacy on *P. aeruginosa* in the CF airway infection model, we see that 16 μg/ml tobramycin decreased *P. aeruginosa* growth to around 50% in the hydrogel phase and to around 5% in the liquid phase (Figure 23).

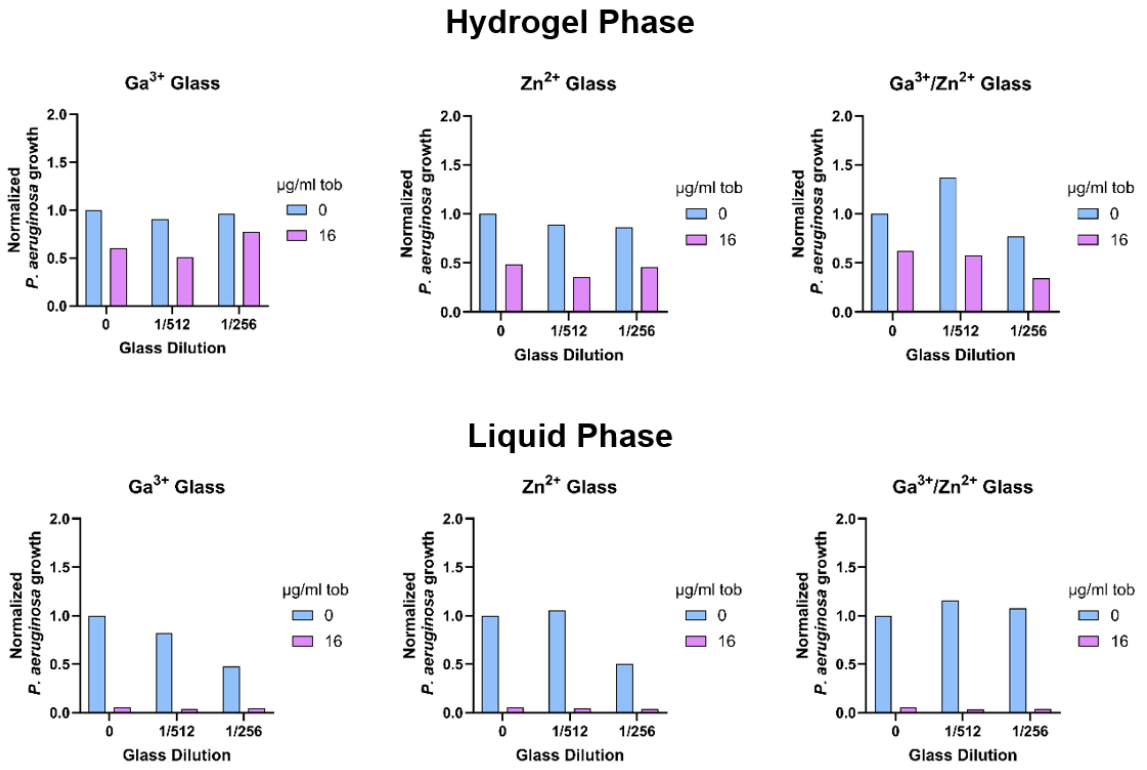

Figure 23: *P. aeruginosa* growth in the monomicrobial CF airway infection model with different tobramycin-glass combinations with low glass concentrations. The CF airway infection model, containing *P. aeruginosa*, was cultured with glass extracts containing Ga^{3+} and/or Zn^{2+} ions at two different dilutions (1/512, 1/256) with or without 16 µg/ml tobramycin for 48 hours. *P. aeruginosa* growth in the hydrogel phase and liquid phase was normalized to the no treatment control of each phase. N=1.

Since the glass extracts at a dilution as low as 1/256 were shown not to have an antibacterial effect in the CF airway infection model, the glass extract dilutions needed to be decreased. We chose to decrease the glass extract dilutions by 8-fold to 1/32 and 1/16 to reflect the 8-fold increase we found in the MIC_{90} of tobramycin for *P. aeruginosa* in the CF airway infection model compared the MIC_{90} of tobramycin on planktonic *P. aeruginosa* (Table 3).

At glass extract dilutions of 1/32 and 1/16, the Ga^{3+} glass and Ga^{3+}/Zn^{2+} glass both significantly decreased *P. aeruginosa* growth compared to the no treatment control in the hydrogel phase of the CF airway infection model (Figure 24). The Zn^{2+} glass, however, did not significantly reduce *P. aeruginosa* growth in the hydrogel phase (Figure 24).

When the Ga^{3+} glass was combined with 16 µg/ml tobramycin, *P. aeruginosa* hydrogel phase growth decreased in comparison to tobramycin alone and glass alone, thereby showing some augmentative effect of the Ga^{3+} glass on tobramycin on suppressing *P. aeruginosa* growth (Figure 24). However, the tobramycin-Ga^{3+}/Zn^{2+} glass combinations had similar *P. aeruginosa* hydrogel phase growth to the Ga^{3+}/Zn^{2+} glass alone, thereby not showing any augmentative effect on suppressing *P. aeruginosa* growth (Figure 24).

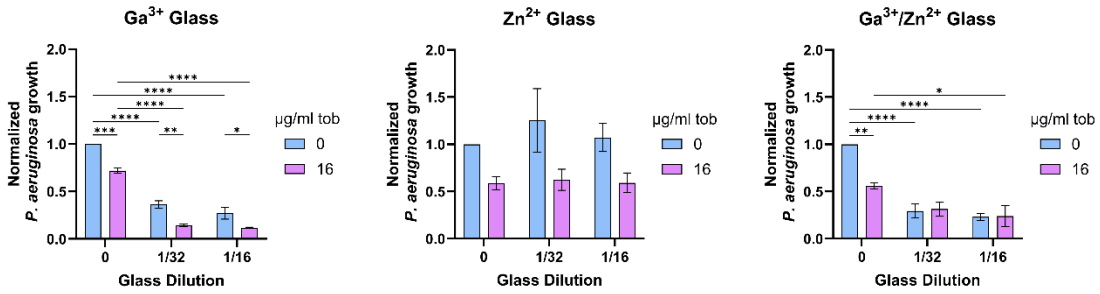

Figure 24: *P. aeruginosa* growth in the hydrogel phase of the monomicrobial CF airway infection model with different tobramycin-glass combinations. The CF airway infection model, containing *P. aeruginosa*, was cultured with glass extracts containing Ga^{3+} and/or Zn^{2+} ions at two different dilutions (1/32, 1/16) with or without 16 µg/ml tobramycin for 48 hours. *P. aeruginosa* growth was normalized to the no treatment control. Mean ± SEM. N=3. Ordinary Two-Way ANOVA with Šidák's Multiple Comparisons Test; * $p < 0.05$, ** $p < 0.01$, *** $p < 0.001$, **** $p < 0.0001$. Raw data with CFU/ml values are available in Figure 36 (Appendix A).

In the liquid phase of the CF airway infection model, we see similar trends in *P. aeruginosa* growth in comparison to the hydrogel phase but magnified (Figure 25). Similarly to the hydrogel phase, the Ga^{3+} glass and Ga^{3+}/Zn^{2+} glass both decrease *P. aeruginosa* growth in the liquid phase, and the Zn^{2+} glass did not have a significant effect on *P. aeruginosa* liquid phase growth (Figure 25). It is difficult to discern augmentative trends between the Ga^{3+}-containing glasses and tobramycin in suppressing *P. aeruginosa* growth in the liquid phase because *P. aeruginosa* growth is decreased to near zero by both Ga^{3+}-containing glasses (Figure 25).

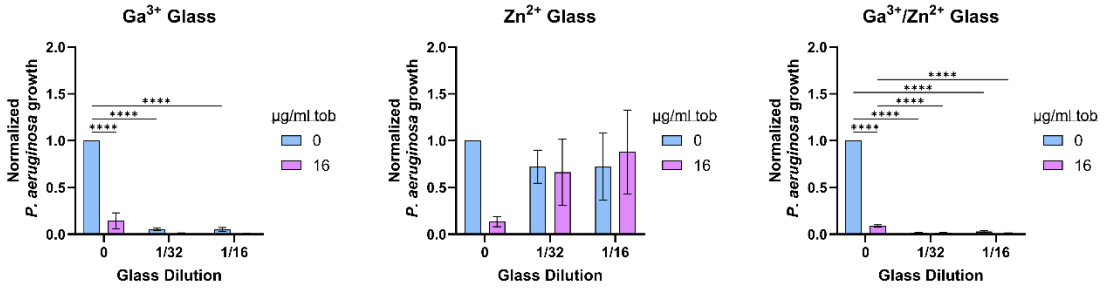

Figure 25: *P. aeruginosa* growth in the liquid phase of the monomicrobial CF airway infection model with different tobramycin-glass combinations. The CF airway infection model, containing *P. aeruginosa*, was cultured with glass extracts containing Ga^{3+} and/or Zn^{2+} ions at two different dilutions (1/32, 1/16) with or without 16 µg/ml tobramycin for 48 hours. *P. aeruginosa* growth was normalized to the no treatment control. Mean ± SEM. N=3. Ordinary Two-Way ANOVA with Šidák's Multiple Comparisons Test; * $p < 0.05$, ** $p < 0.01$, *** $p < 0.001$, **** $p < 0.0001$. Raw data with CFU/ml values are available in Figure 37 (Appendix A).

3.4.2 Effect of vancomycin-glass combinations on *S. aureus* growth

The antibacterial efficacy of the bioactive glass extracts combined with vancomycin on *S. aureus* growth was examined in the CF airway infection model after culturing the model for a total of 48 hours.

Glass extract dilutions of 1/4 and 1/2 were used in these vancomycin-glass combinations (Table 3). These dilutions were selected to reflect the 8-fold decrease in glass extract dilution adjustment that was made for the tobramycin-glass combinations in Section 3.4.1 as the 1/32 dilution for these glasses was shown to be effective at suppressing planktonic *S. aureus* growth previously in the lab. These glass dilutions were combined with either 0 or 16 µg/ml vancomycin based on the determined $MIC_{90}/2$ from Section 3.3.2.

At the selected glass extract dilutions of 1/4 and 1/2, the Ga^{3+} glass and Zn^{2+} glass both significantly decreased *S. aureus* growth compared to the no treatment control in the hydrogel phase of the CF airway infection model (Figure 26). The Ga^{3+}/Zn^{2+} glass, however, did not significantly reduce *S. aureus* growth in the hydrogel phase (Figure 26).

When the Zn^{2+} glass at the 1/4 dilution was combined with 16 µg/ml vancomycin, *S. aureus* hydrogel phase growth decreased in comparison to vancomycin alone and glass alone, thereby showing some augmentative effect of the Zn^{2+} glass on vancomycin on suppressing *S. aureus* growth (Figure 26). However, the vancomycin-Ga^{3+} glass combinations had similar *S. aureus* growth to the Ga^{3+} glass alone, thereby not showing any augmentative effect on suppressing *S. aureus* growth (Figure 26).

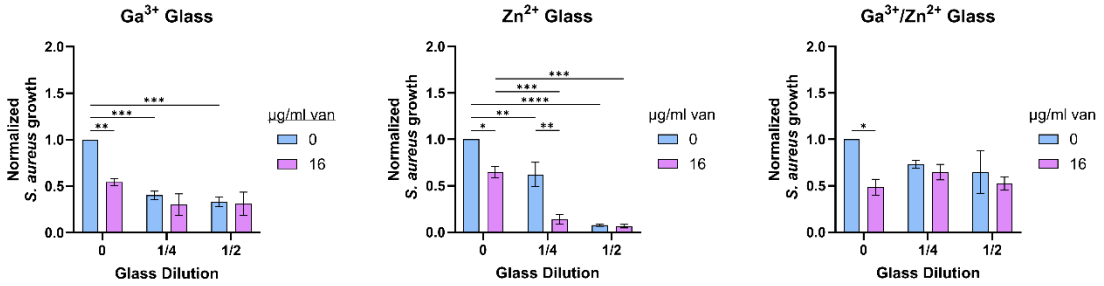

Figure 26: *S. aureus* growth in the hydrogel phase of the monomicrobial CF airway infection model with different vancomycin-glass combinations. The CF airway infection model, containing *S. aureus*, was cultured with glass extracts containing Ga^{3+} and/or Zn^{2+} ions at two different dilutions (1/4, 1/2) with or without 16 µg/ml vancomycin for 48 hours. *S. aureus* growth was normalized to the no treatment control. Mean ± SEM. N=3. Ordinary Two-Way ANOVA with Šidák's Multiple Comparisons Test; * $p < 0.05$, ** $p < 0.01$, *** $p < 0.001$, **** $p < 0.0001$. Raw data with CFU/ml values are available in Figure 38 (Appendix A).

In the liquid phase of the CF airway infection model, *S. aureus* growth was near zero in all groups containing 16 µg/ml vancomycin (Figure 27). *S. aureus* liquid phase growth was decreased when cultured with the Ga^{3+} and Zn^{2+} glasses, only at the 1/2 dilution (Figure 27). However, due to variability in the liquid phase growth data between trials, these results were not statistically significant.

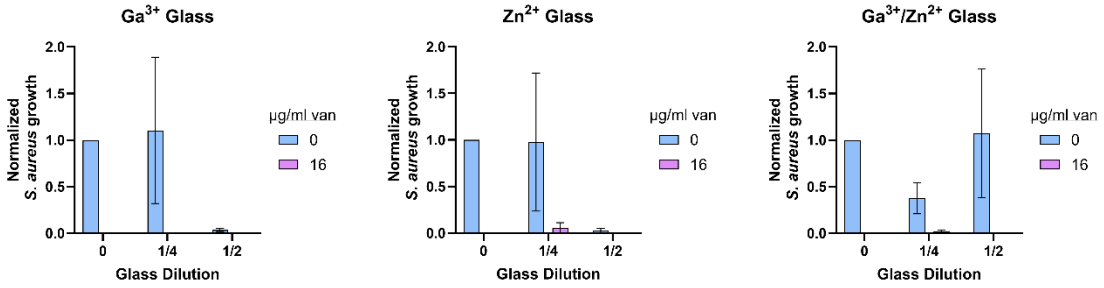

Figure 27: *S. aureus* growth in the liquid phase of the monomicrobial CF airway infection model with different vancomycin-glass combinations. The CF airway infection model, containing *S. aureus*, was cultured with glass extracts containing Ga^{3+} and/or Zn^{2+} ions at two different dilutions (1/4, 1/2) with or without 16 µg/ml vancomycin for 48 hours. *S. aureus* growth was normalized to the no treatment control. Mean ± SEM. N=3. Ordinary Two-Way ANOVA with Šidák's Multiple Comparisons Test; * $p < 0.05$, ** $p < 0.01$, *** $p < 0.001$, **** $p < 0.0001$. Raw data with CFU/ml values are available in Figure 39 (Appendix A).

3.4.3 Mammalian cell viability in the monomicrobial CF airway infection model with different antibiotic-glass combinations

16-HBE viability was determined using a live/dead assay after the CF airway infection model was cultured with antibiotic-glass combinations for 48 hours and bacterial growth was assessed. During these experiments, *P. aeruginosa* or *S. aureus* was present in monoculture for the 48 hours.

For the model cultured with *P. aeruginosa* exposed to tobramycin-glass combinations for 48 hours, all groups containing 16 µg/ml tobramycin had a 16-HBE viability > 90% (Figure 28). However, the groups with 0 µg/ml tobramycin and no glass extracts did not have any cells that remained attached to insert surface, and therefore cell

viability was marked down as 0% (Figure 28). In instances when we see no cells remaining, it is likely that bacterial overgrowth resulted in mass 16-HBE death.

The groups cultured with the Ga^{3+} glass and the Ga^{3+}/Zn^{2+} glass with or without 16 µg/ml tobramycin had a 16-HBE viability > 90% (Figure 28). However, the groups cultured with the Zn^{2+} glass and 0 µg/ml tobramycin had no cells remaining in a similar manner to when no glass or tobramycin was present (Figure 28).

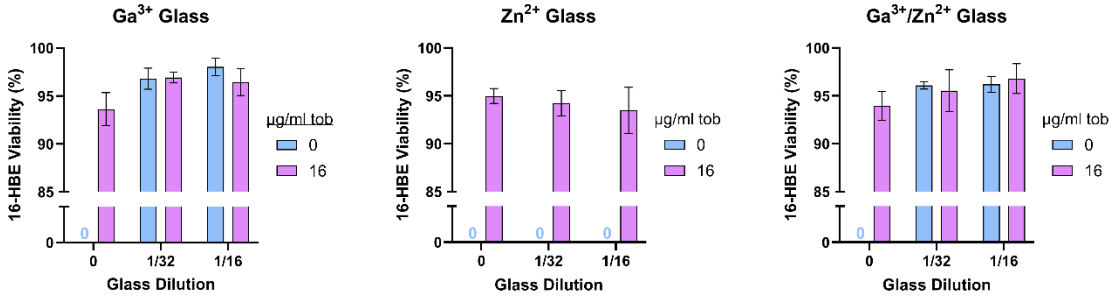

Figure 28: 16-HBE viability in the monomicrobial CF airway infection model with different tobramycin-glass combinations. The CF airway infection model, containing *P. aeruginosa*, was cultured with glass extracts containing Ga^{3+} and/or Zn^{2+} ions at two different dilutions (1/32, 1/16) with or without 16 µg/ml tobramycin for 48 hours, after which 16-HBE viability was determined using a live/dead assay. Mean ± SEM. N=3.

For the model cultured with *S. aureus* exposed to vancomycin-glass combinations for 48 hours, the groups without glass and either 0 µg/ml or 16 µg/ml vancomycin all had a 16-HBE viability > 90% (Figure 29). When cultured with all three glass extracts and either 0 µg/ml or 16 µg/ml vancomycin, 16-HBE viability remained greater than 90% (Figure 29).

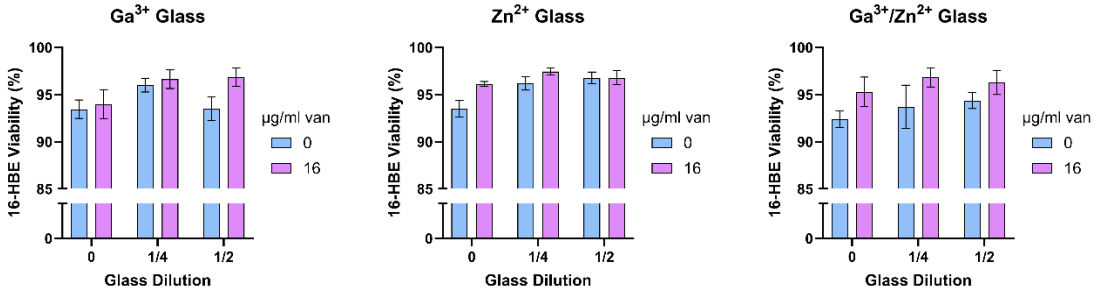

Figure 29: 16-HBE viability in the monomicrobial CF airway infection model with different vancomycin-glass combinations. The CF airway infection model, containing *S. aureus*, was cultured with glass extracts containing Ga^{3+} and/or Zn^{2+} ions at two different dilutions (1/4, 1/2) with or without 16 µg/ml vancomycin for 48 hours, after which 16-HBE viability was determined using a live/dead assay. Mean ± SEM. N=3.

3.5 The effect of antibiotic-glass combinations on co-cultured *P. aeruginosa* and *S. aureus* growth and mammalian cell viability in the CF airway co-infection model

Combinations of one of the three bioactive glass extracts (Ga^{3+}, Zn^{2+}, Ga^{3+}/Zn^{2+}) and one of the two antibiotics were added to the CF airway co-infection model for a total of 48 hours, after which bacteria growth and mammalian cell viability were assessed. Either tobramycin-glass or vancomycin-glass combinations were added to the CF airway co-infection model with *P. aeruginosa* (initial OD_{600} = 0.005) and *S. aureus* (initial OD_{600} = 0.005) cultured together to assess how bacterial growth responses differ in a polymicrobial environment. The specific antibiotic-glass combinations used in these polymicrobial experiments as well as in the previous monomicrobial experiments can be found in Table 3.

3.5.1 Effect of tobramycin-glass combinations on *P. aeruginosa* and *S. aureus* growth

The antibacterial efficacy of the bioactive glass extracts combined with tobramycin on *P. aeruginosa* and *S. aureus* growth was examined in the polymicrobial CF airway co-infection model after culturing the model for a total of 48 hours. Glass extract dilutions of 1/32 and 1/16 were combined with either 0 or 16 μg/ml tobramycin, the same combinations used on the *P. aeruginosa* model in Section 3.4.1.

There was significantly decreased *P. aeruginosa* hydrogel phase growth compared to the no treatment control for the groups containing either the Ga^{3+} glass or the Ga^{3+}/Zn^{2+} glass (Figure 30). For the Zn^{2+} glass, however, there was no significant change in *P. aeruginosa* hydrogel phase growth (Figure 30). Similar trends are seen in the *P. aeruginosa* liquid phase growth data (Figure 31).

In the polymicrobial model, the presence of Ga^{3+} glass and Ga^{3+}/Zn^{2+} glass resulted in an increase in *S. aureus* hydrogel phase growth compared to the no treatment control to around 450% and 300% growth respectively (Figure 30). The presence of the Zn^{2+} glass did not appear to impact *S. aureus* growth in the polymicrobial model (Figure 30). Remember that for this experiment, the glass extracts were at much higher dilutions (1/32, 1/16) compared to the vancomycin-glass experiments (1/4, 1/2) and therefore may not be as effective in suppressing *S. aureus* growth which was seen in the monomicrobial vancomycin-glass experiments (Figure 26). Increased *S. aureus* growth in the presence of Ga^{3+} and Ga^{3+}/Zn^{2+} glass was not seen in the liquid phase (Figure 31).

The presence of 16 µg/ml tobramycin did not appear to have an impact on *S. aureus* hydrogel phase growth in the model, except for the Ga^{3+}/Zn^{2+} glass and 16 µg/ml tobramycin group in which *S. aureus* growth was decreased in comparison to Ga^{3+}/Zn^{2+} glass alone (Figure 30).

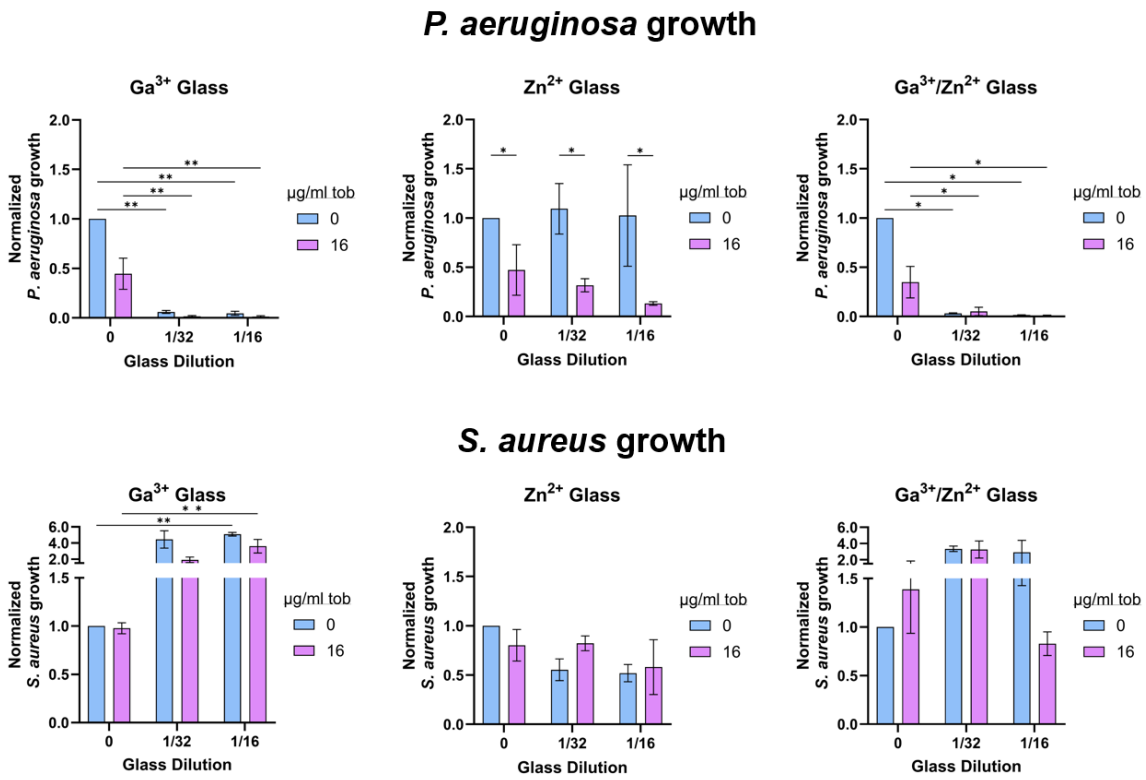

Figure 30: *P. aeruginosa* growth and *S. aureus* growth in the hydrogel phase of the polymicrobial CF airway co-infection model with different tobramycin-glass combinations. The CF airway co-infection model, containing *P. aeruginosa* and *S. aureus*, was cultured with glass extracts containing Ga^{3+} and/or Zn^{2+} ions at two different dilutions (1/32, 1/16) with or without 16 µg/ml tobramycin for 48 hours. Bacterial growth was normalized to the no treatment control. Mean ± SEM. N=2. Ordinary Two-Way ANOVA with Šidák's Multiple Comparisons Test; * $p < 0.05$, ** $p < 0.01$, *** $p < 0.001$, **** $p < 0.0001$. Raw data with CFU/ml values are available in Figure 40 (Appendix B).

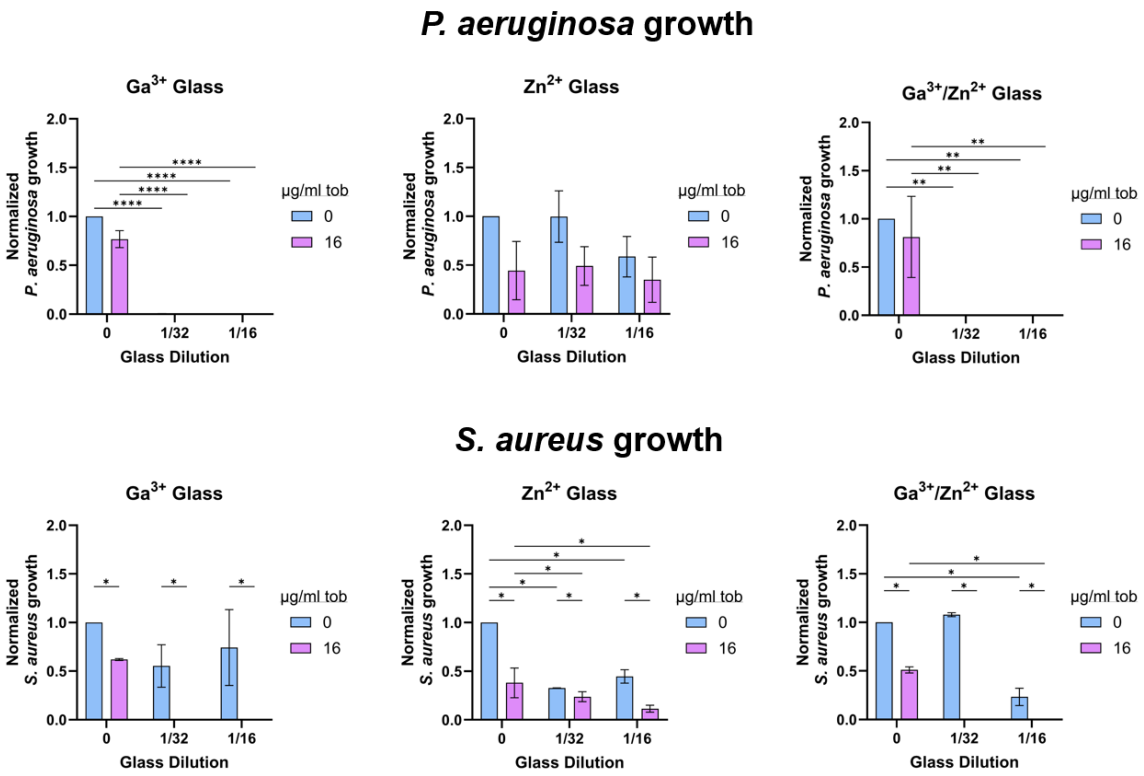

Figure 31: *P. aeruginosa* growth and *S. aureus* growth in the liquid phase of the polymicrobial CF airway co-infection model with different tobramycin-glass combinations. The CF airway co-infection model, containing *P. aeruginosa* and *S. aureus*, was cultured with glass extracts containing Ga^{3+} and/or Zn^{2+} ions at two different dilutions (1/32, 1/16) with or without 16 µg/ml tobramycin for 48 hours. Bacterial growth was normalized to the no treatment control. Mean ± SEM. N=2. Ordinary Two-Way ANOVA with Šidák's Multiple Comparisons Test; * $p < 0.05$, ** $p < 0.01$, *** $p < 0.001$, **** $p < 0.0001$. Raw data with CFU/ml values are available in Figure 41 (Appendix B).

3.5.2 Effect of vancomycin-glass combinations on *P. aeruginosa* and *S. aureus* growth

The antibacterial efficacy of the bioactive glass extracts combined with vancomycin on *P. aeruginosa* and *S. aureus* growth was examined in the polymicrobial CF airway co-infection model after culturing the model for a total of 48 hours. Glass extract dilutions of 1/4 and 1/2 were combined with either 0 or 16 µg/ml vancomycin, the same combinations used on the *S. aureus* model in Section 3.4.2.

There was significantly decreased *P. aeruginosa* hydrogel phase growth compared to the no treatment control for the groups containing either the Ga^{3+} glass or the Ga^{3+}/Zn^{2+} glass (Figure 32). For the Zn^{2+} glass, however, there was no significant change in *P. aeruginosa* hydrogel phase growth, but there appears to be a trend of decreased *P. aeruginosa* growth at the 1/2 glass dilution (Figure 32). Similar trends are seen in the *P. aeruginosa* liquid phase growth data (Figure 33).

In the polymicrobial model, the presence of the Ga^{3+}/Zn^{2+} glass resulted in an increase in *S. aureus* hydrogel phase growth compared to the no treatment control to around 300% growth (Figure 32). For the Ga^{3+} glass, there was a lesser increase in *S. aureus* growth to 195% and 133% for the 1/4 and 1/2 dilutions respectively (Figure 32). The presence of the Zn^{2+} glass did not have a consistent effect on *S. aureus* growth (Figure 32). In the liquid phase however, the presence of all three glasses at the 1/2 dilution resulted in *S. aureus* growth decreasing (Figure 33).

The presence of 16 µg/ml vancomycin, by itself, greatly decreased *S. aureus* growth in the hydrogel phase which was consistent when combined with the Zn^{2+} glass (Figure 32). However, when combined with the Ga^{3+} glass, the inhibitory effect of

vancomycin was not present, and when combined with the Ga^{3+}/Zn^{2+} glass, *S. aureus* growth was increased in comparison to the no treatment control (Figure 32).

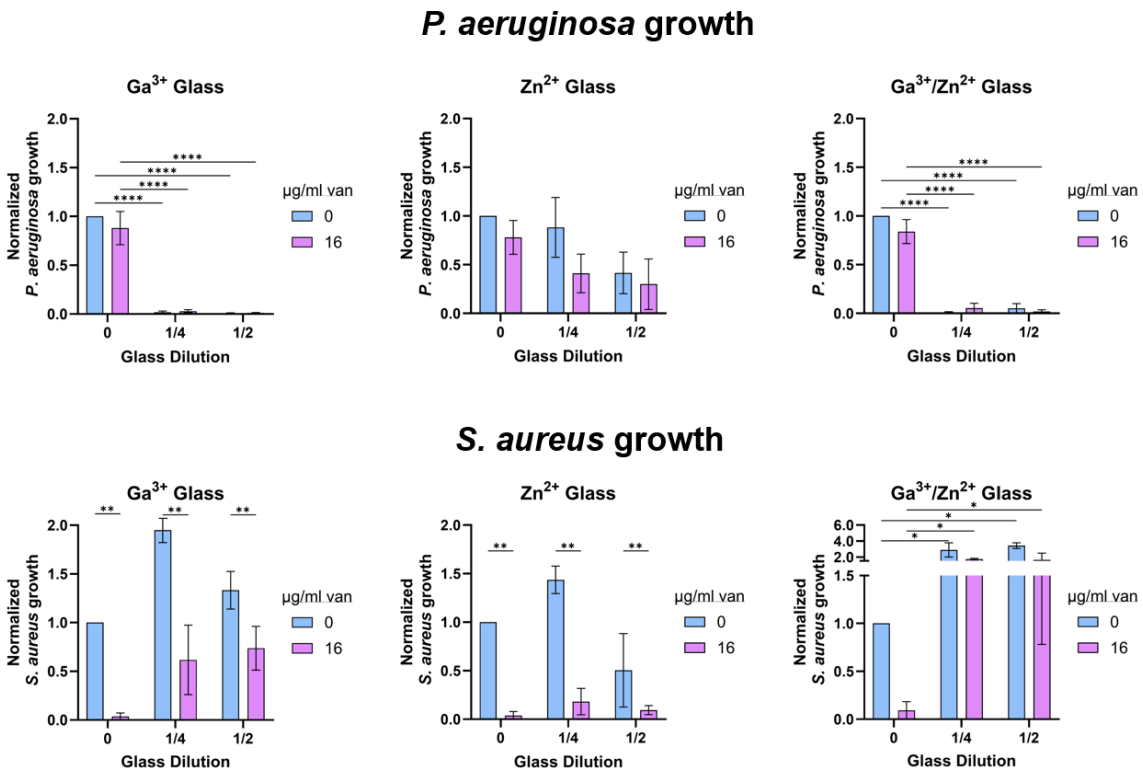

Figure 32: *P. aeruginosa* growth and *S. aureus* growth in the hydrogel phase of the polymicrobial CF airway co-infection model with different vancomycin-glass combinations. The CF airway co-infection model, containing *P. aeruginosa* and *S. aureus*, was cultured with glass extracts containing Ga^{3+} and/or Zn^{2+} ions at two different dilutions (1/4, 1/2) with or without 16 µg/ml vancomycin for 48 hours. Bacterial growth was normalized to the no treatment control. Mean ± SEM. N=2. Ordinary Two-Way ANOVA with Šidák's Multiple Comparisons Test; * $p < 0.05$, ** $p < 0.01$, *** $p < 0.001$, **** $p < 0.0001$. Raw data with CFU/ml values are available in Figure 42 (Appendix B).

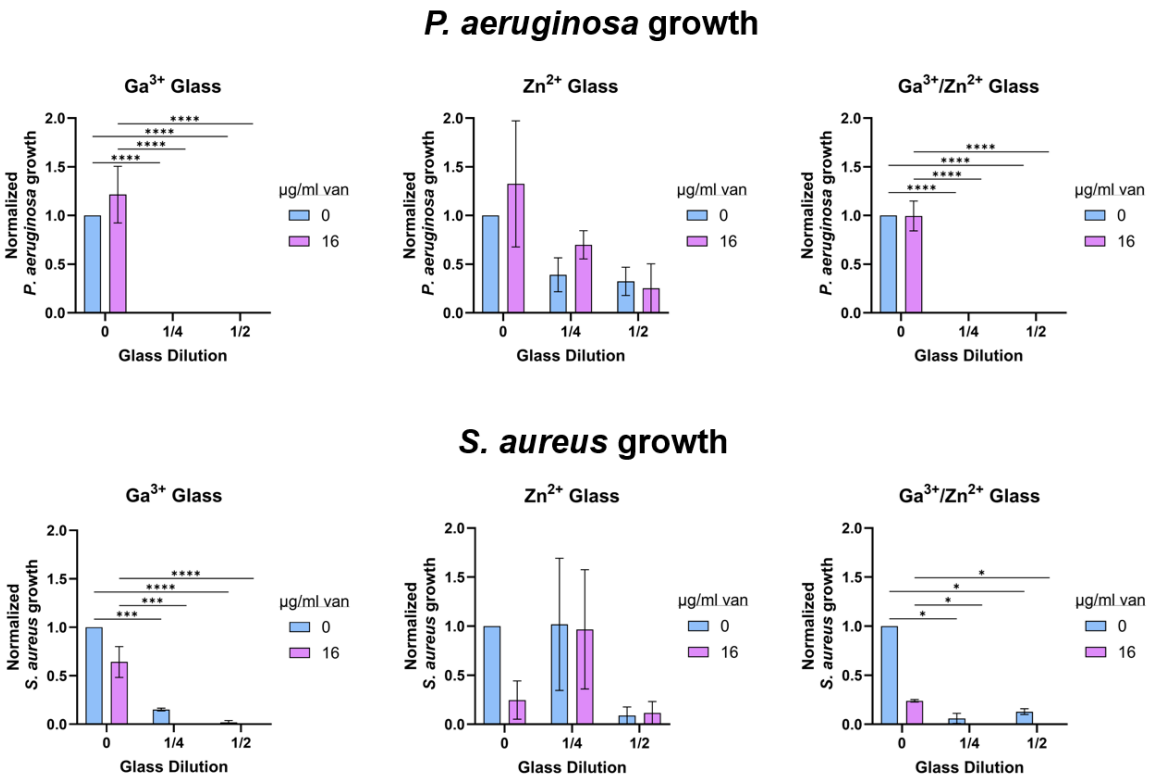

Figure 33: *P. aeruginosa* growth and *S. aureus* growth in the liquid phase of the polymicrobial CF airway co-infection model with different vancomycin-glass combinations. The CF airway co-infection model, containing *P. aeruginosa* and *S. aureus*, was cultured with glass extracts containing Ga^{3+} and/or Zn^{2+} ions at two different dilutions (1/4, 1/2) with or without 16 µg/ml vancomycin for 48 hours. Bacterial growth was normalized to the no treatment control. Mean ± SEM. N=2. Ordinary Two-Way ANOVA with Šidák's Multiple Comparisons Test; * $p < 0.05$, ** $p < 0.01$, *** $p < 0.001$, **** $p < 0.0001$. Raw data with CFU/ml values are available in Figure 43 (Appendix B).

3.5.3 Mammalian cell viability in the polymicrobial CF airway co-infection model with different antibiotic-glass combinations

16-HBE viability was determined using a live/dead assay after the CF airway co-infection model was cultured with antibiotic-glass combinations for 48 hours and

bacterial growth was assessed. During these experiments, *P. aeruginosa* and *S. aureus* both were present in co-culture for the 48 hours.

For the polymicrobial model exposed to tobramycin-glass combinations for 48 hours, all groups containing 16 µg/ml tobramycin had a 16-HBE viability > 90% (Figure 34). However, the groups with 0 µg/ml tobramycin and no glass extracts did not have any cells that remained attached to insert surface, and therefore cell viability was marked down as 0% (Figure 34).

The groups cultured with the Ga^{3+} glass and the Ga^{3+}/Zn^{2+} glass with or without 16 µg/ml tobramycin had a 16-HBE viability > 90% (Figure 34). However, the groups cultured with the Zn^{2+} glass and 0 µg/ml tobramycin had no cells remaining in a similar manner to when no glass or tobramycin was present (Figure 34). All of the trends seen here were also seen in the monomicrobial *P. aeruginosa* model exposed to tobramycin-glass combinations (Figure 28).

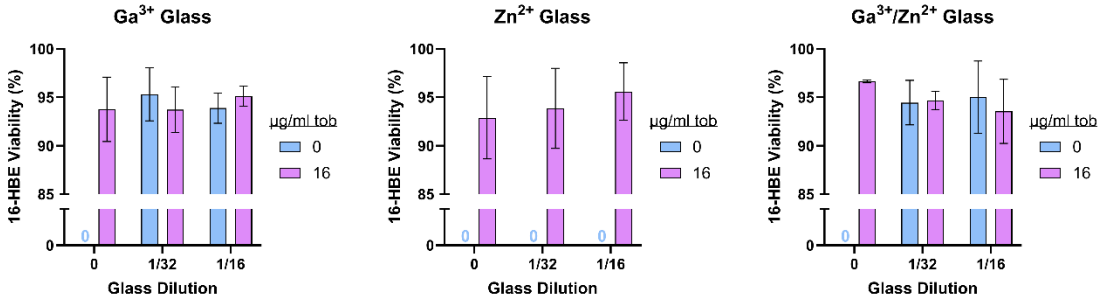

Figure 34: 16-HBE viability in the polymicrobial CF airway co-infection model with different tobramycin-glass combinations. The CF airway co-infection model, containing *P. aeruginosa* and *S. aureus*, was cultured with glass extracts containing Ga^{3+} and/or Zn^{2+} ions at two different dilutions (1/32, 1/16) with or without 16 µg/ml tobramycin for 48 hours, after which 16-HBE viability was determined using a live/dead assay. Mean ± SEM. N=2.

For the polymicrobial model exposed to vancomycin-glass combinations for 48 hours, all groups containing no glass extract and either 0 µg/ml or 16 µg/ml vancomycin did not have any cells that remained attached to the insert surface (Figure 35). When all three glass extracts were added to the model with or without vancomycin, 16-HBE viability was greater than 90% (Figure 35).

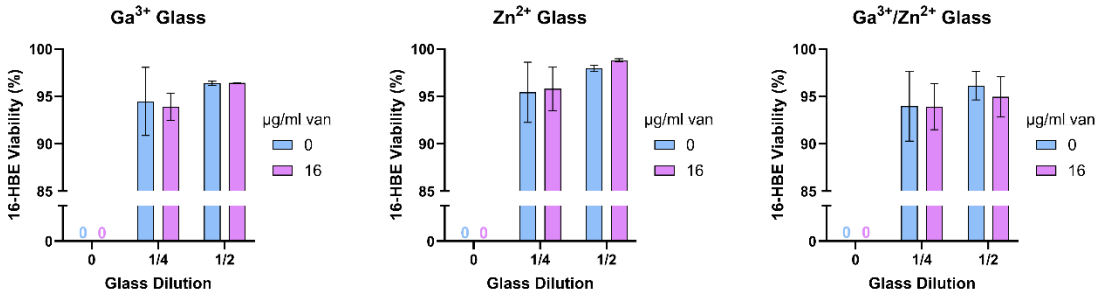

Figure 35: 16-HBE viability in the polymicrobial CF airway co-infection model with different vancomycin-glass combinations. The CF airway co-infection model, containing *P. aeruginosa* and *S. aureus*, was cultured with glass extracts containing Ga^{3+} and/or Zn^{2+} ions at two different dilutions (1/4, 1/2) with or without 16 µg/ml vancomycin for 48 hours, after which 16-HBE viability was determined using a live/dead assay. Mean ± SEM. N=2.

CHAPTER 4. Discussion

Lung damage and respiratory failure caused by chronic microbial infections are the leading causes of mortality in CF patients [3], [4]. The CF airway is a favourable microenvironment for the development of chronic airway infections due to the unique properties of CF mucus [18]. In CF pathophysiology, a genetic mutation results in impaired airway epithelium ion transport, leading to a dehydrated, thickened mucus layer [12], [14]. This thickened mucus layer then leads to impaired mucociliary clearance and cough clearance, allowing bacteria to more easily colonize the CF airway [19], [21]. Additionally, thickened mucus impairs diffusion of antibiotic drugs through the CF airway [22]. All of these factors provide difficulties for conventional antibiotics, leading to failures to eradicate CF infections, thereby allowing the surviving bacteria to develop antibiotic resistance [51], [53]. This emphasizes the need for the development of novel antibacterial therapies to suppress CF infections while preventing antibiotic resistance development.

The research outlined in this thesis involved the development of a novel combination therapy to treat CF airway infections by targeting pathogens from multiple mechanisms of action. By utilizing multiple routes to suppress pathogen growth, this novel therapy has the potential to reduce the development of resistance to conventional antibiotics. In this thesis project, conventional antibiotics were combined with metal ion-releasing bioactive glasses, and then the antibacterial efficacy of these combinations was assessed in an *in vitro* model of CF airway infection to determine if the addition of metal ion-releasing bioactive glasses could augment conventional antibiotic efficacy.

The antibacterial efficacy of the antibiotic-glass combinations was first assessed on *P. aeruginosa* and *S. aureus* cultured separately, with tobramycin and vancomycin used for *P. aeruginosa* and *S. aureus* respectively. The antibacterial efficacy of the antibiotic-glass combinations was then assessed on *P. aeruginosa* and *S. aureus* cultured together in the airway infection model.

4.1 The *in vitro* airway infection model mimics the healthy and CF airway microenvironment

The *in vitro* airway infection model developed in this project allows the co-culture of common CF bacteria with human bronchial epithelial cells in an airway-like microenvironment. The manipulation of the composition of the mucus-like component of the model allows for a simple method to produce the physical and biological characteristics of a healthy-like and a CF-like airway model. By adjusting the mucin and crosslinker concentration, we can mimic the differences in viscoelastic properties in healthy and CF mucus [17]. We can also mimic the increased mucin content which is seen in native CF mucus [17].

In this thesis project, the existing airway infection model previously developed in the lab was translated to a transwell insert system to more accurately mimic the airway structure, providing a distinct route for nutrient transport to the 16-HBE cells, separate from the mucus layer. In a native airway, nutrient transport occurs through the basolateral side of epithelial cells [117]. In the previous airway infection model, nutrient delivery was occurring through the apical side of the 16-HBE cells and nutrients would have to

pass through the mucus layer to get to the cells [114]. With this new modification to the model, nutrient delivery occurs through the basolateral side to be consistent with native airway structure and to prevent interference from the mucus layer on the nutrient supply.

Additionally in the model developed in this project, a quiescent-like state was induced on the 16-HBE cells by lowering their nutrient supply to produce a slower proliferation state, more representative of the native bronchial epithelium [118]. This was done successfully by lowering the FBS and glucose content of the 16-HBE media (Figure 17) which resulted in no significant additional cytotoxicity (Figure 19).

In interpreting the results from the airway infection model, it is important to consider the potential effects of confounding variables that may influence the outcome independently of the experimental treatment. While several core variables (e.g. hydrogel composition, incubation conditions, inoculum size) were tightly controlled to ensure experimental consistency, other factors that are more difficult to control may contribute to inter-replicate variability and should be considered when interpreting the model's reproducibility and predictive accuracy. The table below summarizes key confounding variables that may have impacted the outputs of the model, indicating which were controlled for and which were not (Table 4).

Table 4: Summary of confounding variables in the airway infection model. Key confounding variables that may influence the model outputs are listed with a description and potential impact on results.

Confounding Variable	Description	Controlled?	Potential Impact on Results
Temperature and CO_2	Standard incubation conditions (37 °C, 5% CO_2)	Yes	Affects bacterial growth kinetics
Incubation time before treatment	Time bacteria were allowed to adhere/grow before antibiotic-glass treatment	Yes	Influences biofilm maturity and resistance to treatment
Initial bacteria concentration	The bacterial OD_{600} added at time zero	Yes	Influences biofilm maturity and resistance to treatment
Hydrogel composition	Mucus-mimetic hydrogel properties (concentration, components)	Yes	Alters bacterial adherence and biofilm formation, diffusion of treatment
Operator technique variability	Manual steps in hydrogel preparation and deposition, spot plating, etc	No	Minor inconsistencies may affect reproducibility of outputs
Heterogeneity in bacterial subpopulations	Natural phenotypic variation within the same strain	No	Could lead to variability in susceptibility to treatment
pH shifts during incubation	Localized pH changes from bacterial or mammalian cell metabolism	No	Could alter bacterial/mammalian cell viabiltiy and treatment ion release kinetics
Hydrogel dehydration or shrinkage	Minor drying during incubation or handling	No	Could impact hydrogel properties and therefore nutrient and treatment diffusion
Limited oxygen diffusion in hydrogel	Potential oxygen gradients in deeper hydrogel regions	No	Could cause heterogeneous bacterial growth and affect mammalian cells
Ion sequestration by hydrogel components	Hydrogel may bind or buffer the released treatment metal ions	No	Could reduce free ion concentration, lowering antibacterial efficacy

4.2 Antibacterial efficacy of tobramycin and vancomycin was determined in the healthy and CF airway infection model

The MIC_{90} of tobramycin and vancomycin for *P. aeruginosa* and *S. aureus*, respectively, were determined in the healthy and CF airway infection model to determine reasonable antibiotic concentrations to combine with the bioactive glass extracts. In doing

this, we generated data that shows us differences in antibiotic efficacy in the healthy vs CF models and in the hydrogel vs liquid phase.

We see that the MIC_{90} of both antibiotics in the CF airway infection model is higher than in the healthy CF model for *P. aeruginosa* (Figure 20) and *S. aureus* (Figure 22). This was expected because in human CF infections, the increased CF mucus thickness leads to a reduction in antibiotic transport and efficacy [12], [51]. Therefore, this difference in antibiotic efficacy in the healthy vs. CF models supports the validity of the airway infection model in modelling healthy and CF airway environments.

For *P. aeruginosa*, there was a similar amount of bacteria growth in the liquid phase compared to the hydrogel phase with and without tobramycin (Figure 20). However, *P. aeruginosa* growth in the liquid phase was reduced to zero at the highest tobramycin concentration, while some bacteria remained in the hydrogel phase (Figure 20). Conversely, there was around a 100-fold decrease in *S. aureus* growth in the liquid phase compared to the hydrogel phase without vancomycin (Figure 22). With increasing concentrations of vancomycin, *S. aureus* growth in the liquid phase quickly dropped to zero, while *S. aureus* growth in the hydrogel phase decreased at a much slower rate (Figure 22). One potential explanation for the comparative decrease in liquid phase growth only for *S. aureus* is that *S. aureus* is non-motile while *P. aeruginosa*, possessing pili and flagella, is motile [119]. Therefore, *S. aureus* may have stayed in the hydrogel phase and not migrated to the liquid phase as much as a motile bacteria like *P. aeruginosa*.

4.3 *P. aeruginosa* and *S. aureus* growth were decreased in the presence of specific glass extracts in monomicrobial CF infections

P. aeruginosa and *S. aureus* growth in the monomicrobial CF airway infection model over 48 hours were assessed in the presence of each of the three bioactive glass extracts (Ga^{3+}, Zn^{2+}, Ga^{3+}/Zn^{2+}) and the antibiotics, tobramycin and vancomycin, respectively.

At the 1/32 dilution, both Ga^{3+}-containing glasses significantly suppressed *P. aeruginosa* growth while the Zn^{2+}-only glass did not suppress *P. aeruginosa* growth (Figure 24). The antibacterial efficacy of the Ga^{3+}-containing glasses on *P. aeruginosa* was expected because Ga^{3+} is known to be effective specifically against bacteria dependent on iron metabolism, and has been shown to be effective against *P. aeruginosa* by interfering with iron-mediated metabolic pathways [81], [120]. Iron uptake in *P. aeruginosa* has been shown to be important in regulating quorum sensing and activating several virulence genes [121]. Specifically in CF infection, *P. aeruginosa* has been shown to upregulate pathways to acquire iron during chronic infection in order to grow and proliferate [122]. The Ga^{3+} ion, due to many similarities in its ionic properties to the Fe^{3+} ion, can act as an iron-mimetic in biological systems as it will bind with high affinity to iron-binding sites, leading to the disruption of biological pathways where Fe^{3+} is required [123], [124]. Specifically, Ga^{3+} and Fe^{3+} have similar octahedral ionic radii and tetrahedral ionic radii [125]. Therefore, since *P. aeruginosa* requires Fe^{3+} uptake to grow during CF infection, Ga^{3+} ions, acting as a competitive inhibitor of Fe^{3+}, are taken up instead, leading to the disruption of metabolic pathways in *P. aeruginosa* and subsequent bacterial death. This outlines a potential mechanism explaining why the Ga^{3+}-containing

glass extracts were effective at suppressing *P. aeruginosa* growth in the airway infection model. Additionally, gallium has been shown to have antibiofilm activity against Gram-negative biofilms, specifically *Acinetobacter baumannii* and *P. aeruginosa* [126], [127]. Therefore, gallium's efficacy against *P. aeruginosa* may be due not only to its role as a competitive iron inhibitor, but also due to its role as an antibiofilm agent.

Conversely, the Zn^{2+}-only glass did not suppress *P. aeruginosa* growth in the CF airway infection model. This was surprising as zinc is known to have antibacterial efficacy against a variety of bacterial species through various antibacterial mechanisms [128]. Zn^{2+} ions can inhibit glycolysis in bacteria and increase membrane permeability to protons, leading to the further disruption of metabolic pathways [129], [130]. Additionally, Zn^{2+} ions are able to generate ROS that can damage bacterial cell membranes and have antibiofilm activity [79], [131]. It is possible that the concentration of Zn^{2+} ions added to the model was too low to have an effect on *P. aeruginosa* growth and with a higher concentration, Zn^{2+} ions would suppress *P. aeruginosa* growth through one or multiple of the aforementioned antibacterial pathways. However, it is important to mention that zinc itself is an essential mineral for *P. aeruginosa* and the uptake of zinc is necessary for many of the growth, colonization, and virulence functions of *P. aeruginosa* [132], [133]. Therefore, it may be possible that at the low concentration of Zn^{2+} ions that were supplied to *P. aeruginosa* in the airway infection model by the 1/32 and 1/16 Zn^{2+} glass extract dilutions, the Zn^{2+} ion concentration was too low to function as an antibacterial agent, and rather the Zn^{2+} ions were taken up by *P. aeruginosa* to be used in its own supportive pathways.

Looking at *S. aureus* growth when cultured with the bioactive glass extracts at the 1/4 dilution, the Ga^{3+} glass and the Zn^{2+} glass significantly suppressed *S. aureus* growth while the Ga^{3+}/Zn^{2+} glass did not suppress *S. aureus* growth significantly (Figure 26). The antibacterial efficacy of the Ga^{3+}-only glass on *S. aureus* was expected because Ga^{3+} is known to have antibacterial efficacy by interfering with iron metabolism and having some antibiofilm activity [123], [131]. *S. aureus*, similarly to *P. aeruginosa*, relies upon iron as an essential mineral for growth, proliferation, and colonization [134], [135]. Therefore, we expected the Ga^{3+}-containing glasses to suppress *S. aureus* growth similarly to *P. aeruginosa*, potentially by interfering with iron metabolism.

The antibacterial efficacy of the Zn^{2+}-only glass on *S. aureus* was also expected because Zn^{2+} ions have a number of potential antibacterial mechanisms, including bacterial glycolysis inhibition, ROS generation, and bacterial membrane disruption [79], [130]. Additionally, zinc-based particles have previously been shown to be effective against Gram-positive bacteria in particular [78], [80].

However, the lack of efficacy of the Ga^{3+}/Zn^{2+} glass on suppressing *S. aureus* growth was not expected. Since both Ga^{3+} and Zn^{2+} ions would be present, this may suggest that there is some antagonistic effect between the two ions that leads to no net suppression of *S. aureus* growth. One potential explanation is that the presence of Zn^{2+} ions could interfere with the ability of Ga^{3+} ions to be mistakenly imported by *S. aureus* in place of Fe^{3+} ions, and therefore this would reduce the antibacterial efficacy of Ga^{3+} ions. Another potential explanation is that the Ga^{3+} and Zn^{2+} ions together could form metal complexes that are poorly bioavailable, thereby reducing the concentration of free ions. Nonetheless, this is an interesting finding that warrants further investigation.

4.4 Specific glass extracts augmented antibiotics to suppress *P. aeruginosa* and *S. aureus* growth in monomicrobial CF infections

P. aeruginosa and *S. aureus* growth in the monomicrobial CF airway infection model over 48 hours were assessed in the presence of each of the three bioactive glass extracts (Ga^{3+}, Zn^{2+}, Ga^{3+}/Zn^{2+}) and the antibiotics, tobramycin and vancomycin, respectively. From this data, we evaluated if the antibiotic-glass combinations were able to suppress bacterial growth more than antibiotic alone or glass alone, allowing us to evaluate if the glass extracts were able to augment antibiotic efficacy.

For the *P. aeruginosa* model cultured with tobramycin-glass combinations, the results show that the Ga^{3+}-only glass at the 1/32 and 1/16 dilution combined with tobramycin had a significantly lower *P. aeruginosa* growth than for tobramycin alone and for the Ga^{3+}-only glass alone (Figure 24). Therefore, the Ga^{3+}-only glass was shown to augment tobramycin to better suppress *P. aeruginosa* growth in the CF airway infection model. This observed augmentation could be explained by the targeting of *P. aeruginosa* through different mechanisms, as Ga^{3+} ions may act primarily by disrupting iron metabolism [124] while tobramycin acts primarily by disrupting protein synthesis and outer membrane function [136].

For the Ga^{3+}/Zn^{2+} glass, *P. aeruginosa* growth was similar when cultured with and without tobramycin (Figure 24) and therefore we concluded that there was no augmentation of the antibiotic efficacy of tobramycin on *P. aeruginosa* in the presence of the Ga^{3+}/Zn^{2+} glass.

For the *S. aureus* model cultured with vancomycin-glass combinations, the results show that the Zn^{2+}-only glass at the 1/4 dilution combined with vancomycin had a significantly lower *S. aureus* growth than for vancomycin alone and for the Zn^{2+}-only glass alone (Figure 26). Therefore, the Zn^{2+}-only glass was shown to augment vancomycin to better suppress *S. aureus* growth in the CF airway infection model. This observed augmentation could be explained by the targeting of *S. aureus* through different mechanisms, as Zn^{2+} ions primarily act through ROS generation and bacterial glycolysis inhibition [79], [130] while vancomycin acts primarily through bacterial cell wall disruption [137].

For the Ga^{3+}-only glass, *S. aureus* growth was similar when cultured with and without vancomycin (Figure 26) and therefore we concluded that there was no augmentation of the antibiotic efficacy of vancomycin on *S. aureus* in the presence of the Ga^{3+}-only glass.

These findings suggest that in a monomicrobial CF-like airway microenvironment, gallium-releasing bioactive glass can augment tobramycin to suppress *P. aeruginosa* growth and zinc-releasing bioactive glass can augment vancomycin to suppress *S. aureus* growth.

4.5 Polymicrobial CF infections show complex and different bacterial growth responses to antibiotic-glass combinations compared to monomicrobial CF infections

P. aeruginosa and *S. aureus* growth in the polymicrobial CF airway co-infection model over 48 hours were assessed in the presence of tobramycin-glass combinations and vancomycin-glass combinations.

In the polymicrobial model, *P. aeruginosa* growth was significantly decreased by the Ga^{3+}-containing glasses, but largely unaffected by the Zn^{2+} glass (Figure 30; Figure 32). This was the same trend that was seen when *P. aeruginosa* was cultured in the monomicrobial model with tobramycin-glass combinations (Figure 24). Therefore, the results from the polymicrobial model suggest again that Ga^{3+} ions are able to suppress *P. aeruginosa* growth by mimicking Fe^{3+} ions in bacterial iron metabolism and/or through antibiofilm action [124], [127]. The results also again suggest that the Zn^{2+} ion concentration present in the Zn^{2+} bioactive glass extract was too low to have an antibacterial effect on *P. aeruginosa*.

Interestingly, the decrease in *P. aeruginosa* growth when cultured with the Ga^{3+}-containing glasses was much greater in the polymicrobial model (Figure 30; Figure 32) in comparison to the monomicrobial model (Figure 24). This is likely due to the innate competition between *P. aeruginosa* and *S. aureus* found in such polymicrobial infections [138]. A potential explanation for this finding is that due to this constant competition, any event that decreases the growth of one bacterium is magnified because the other bacterium is then able to grow more and therefore increasingly inhibit the other bacteria. Therefore, it is likely that when Ga^{3+} ions inhibited *P. aeruginosa* growth, *S. aureus* was

then able to grow more and therefore further inhibit *P. aeruginosa* growth. Coinciding with this theory, we see that *S. aureus* growth was increased in the polymicrobial model when the Ga^{3+}-containing glasses were added.

An initially surprising finding from the polymicrobial growth data was that *S. aureus* growth in the polymicrobial model was increased by up to 4-fold when cultured with the Ga^{3+}-containing glasses (Figure 30; Figure 32). This was initially surprising as in the monomicrobial model, *S. aureus* growth was significantly decreased by the same Ga^{3+}-only glass (Figure 26). However, this finding may be explained by considering the complex interplay and competition between *P. aeruginosa* and *S. aureus* in this polymicrobial environment. *P. aeruginosa* is widely known to outcompete *S. aureus* in polymicrobial infections through a variety of mechanisms [139], [140], [141]. Therefore, a possible explanation for this finding is that the addition of Ga^{3+} ions leads to the suppression of *P. aeruginosa* growth, which then decreases the *P. aeruginosa*-mediated suppression of *S. aureus* growth. Therefore, *S. aureus* growth is higher in these conditions where *P. aeruginosa* growth is inhibited in comparison to the no treatment control in which *P. aeruginosa* is free to grow and outcompete *S. aureus*. At first glance, this finding diverges from the earlier finding that *S. aureus* growth was decreased in the presence of the Ga^{3+}-only glass in a monomicrobial environment (Figure 26). But in the context of a polymicrobial environment, these findings suggest the anti-pseudomonal effects of the Ga^{3+}-containing glasses outweigh the anti-staphylococcal effects, and therefore inhibiting *P. aeruginosa* growth does more to increase *S. aureus* growth than the Ga^{3+} ions themselves do to decrease *S. aureus* growth.

The results also showed that *S. aureus* growth was not significantly decreased when cultured with the Zn^{2+}-only glass in the polymicrobial model (Figure 30; Figure 32). This finding diverged from the monomicrobial model in which *S. aureus* growth was decreased in the presence of the Zn^{2+}-only glass (Figure 26). Taking the competition between *P. aeruginosa* and *S. aureus* into account, it is possible that the inhibition by *P. aeruginosa* on *S. aureus* growth was far greater than the inhibition from the Zn^{2+} ions and therefore we don't observe a significant difference caused by the presence of the Zn^{2+}-only glass.

4.6 Effects of antibiotic-glass combinations on bacterial growth differ in the liquid phase compared to the hydrogel phase

P. aeruginosa and *S. aureus* growth in the liquid and hydrogel phases of the monomicrobial and polymicrobial CF airway infection models over 48 hours were assessed in the presence of the antibiotic-glass combinations. From this monomicrobial and polymicrobial data, we saw that trends in bacterial growth differed between the liquid phase and the hydrogel phase of the model.

For the two monomicrobial models cultured with antibiotic-glass combinations, the results showed that the antibiotics alone had a much greater inhibitory effect on their respective bacteria's growth in the liquid phase (Figure 25; Figure 27) compared to the hydrogel phase (Figure 24; Figure 26). Similarly, we saw that the antibiotic-glass combinations had a magnified inhibitory effect on bacterial growth in the liquid phase (Figure 25; Figure 27) compared to the hydrogel phase (Figure 24; Figure 26). A simple

explanation for this magnification of antibiotic-glass efficacy on the liquid phase could be that the antibiotic-glass combinations were added directly to the liquid phase of the model and therefore would be most efficacious on bacteria residing in the liquid phase. Furthermore, the treatment would be able to freely diffuse through the liquid phase, whereas its diffusion through the mucus-mimetic hydrogels may be more restricted, thereby reducing its impact on hydrogel phase growth. An additional explanation for this finding could be that the bacteria were able to form biofilms using the mucus-mimetic hydrogel layer as a substrate, and therefore in this biofilm form, the antibiotic-glass treatments were less effective against the bacteria compared to the liquid phase where bacteria would likely be in a planktonic state [24], [58].

For the polymicrobial models cultured with antibiotic-glass combinations, the results showed that *P. aeruginosa* growth in the liquid phase when cultured with both tobramycin-glass (Figure 31) and vancomycin-glass combinations (Figure 33) had similar growth trends compared to the hydrogel phase but magnified. This finding was similar to what we saw with the monomicrobial growth data. However, we found that *S. aureus* growth differed in the liquid phase compared to the hydrogel phase in a polymicrobial context. In both the polymicrobial models cultured with tobramycin-glass and vancomycin-glass, the results showed that *S. aureus* growth in the hydrogel phase was either unchanged or increased with the addition of the Ga^{3+}-containing glasses (Figure 30; Figure 32). In the liquid phase, however, we saw that *S. aureus* growth was decreased with the addition of the Ga^{3+}-containing glasses (Figure 31; Figure 33). This finding could once again be explained by the impaired diffusion of the treatment through the mucus layer and biofilm-induced resistance to the treatment which would therefore

impair the treatment's efficacy on hydrogel phase bacteria, while leaving liquid phase bacteria susceptible.

4.7 Bronchial epithelial cell viability is maintained in the presence of all effective antibiotic-glass combinations against *P. aeruginosa* in the CF model

16-HBE viability was assessed in the monomicrobial and polymicrobial CF airway infection models with the addition of the antibiotic-glass combinations. The *P. aeruginosa* monomicrobial model and the *P. aeruginosa* and *S. aureus* polymicrobial model were both cultured with tobramycin-glass combinations for 48 hours. The *S. aureus* monomicrobial model and the *P. aeruginosa* and *S. aureus* polymicrobial model were both cultured with vancomycin-glass combinations for 48 hours.

In the *P. aeruginosa* model (Figure 28) and the polymicrobial model (Figure 33), cell viability was maintained when 16 µg/ml tobramycin was added, but there was mass cell death when no tobramycin and no glass were added. The likely explanation for this is that bacteria overgrowth due to the lack of tobramycin led to cytotoxicity and mass cell death. Specifically, it appears that *P. aeruginosa* overgrowth led to cell death because (1) *P. aeruginosa* was the only bacteria present in the monomicrobial model and when it was uninhibited, mass cell death occurred (Figure 28), and (2) in the polymicrobial model, tobramycin resulted in mammalian cell survival (Figure 33) and tobramycin suppressed *P. aeruginosa* growth and not *S. aureus* growth (Figure 30).

Additionally in the models cultured with tobramycin-glass combinations, we see that mammalian cells survive when the models were cultured with the two Ga^{3+}-

containing glasses and mammalian cells die when the models were cultured with the Zn^{2+}-only glass (Figure 28; Figure 33). In line with this observation, we see that *P. aeruginosa* growth is significantly inhibited by the Ga^{3+}-containing glasses and not the Zn^{2+}-only glass in both the monomicrobial and polymicrobial models (Figure 24; Figure 30). Therefore, these results support the conclusion that 1, the Ga^{3+}-containing glasses are effective at suppressing *P. aeruginosa* growth and 2, mammalian cell death occurs in the airway infection model when *P. aeruginosa* growth is uninhibited.

P. aeruginosa can cause mammalian cell cytotoxicity through a number of potential mechanisms. *P. aeruginosa* possesses Type III secretion system (T3SS) protein complexes, needle-like apparatuses that allow *P. aeruginosa* to inject cytotoxins directly into host cells [142]. Through this T3SS mechanism, *P. aeruginosa* has been shown to modify host amyloid proteins, secreted by host cells as an innate immune mechanism, into cytotoxic prions [143], [144]. *P. aeruginosa*'s high motility and production of numerous virulence factors, including pyocyanin which generates ROS, contributes to its potential cytotoxicity [145], [146].

The cell viability data from the *S. aureus* monomicrobial model (Figure 29) and the polymicrobial model (Figure 34) cultured with vancomycin-glass combinations further support the theory that uninhibited *P. aeruginosa* growth results in mammalian cell death and also suggests that uninhibited *S. aureus* growth does not result in mammalian cell death. In the *S. aureus* monomicrobial model, when there is no vancomycin and no glass, we see that 16-HBE viability is greater than 90%, suggesting that *S. aureus* overgrowth does not cause significant cytotoxicity to the degree of *P. aeruginosa* overgrowth (Figure 29).

The lack of cytotoxicity from *S. aureus* overgrowth may be explained by the differences in the pathogenic mechanisms of *P. aeruginosa* and *S. aureus*. While *P. aeruginosa* colonization leads to ROS generation through pyocyanin synthesis and this leads to cytotoxicity, *S. aureus* does not produce ROS-generating metabolites [147]. Additionally, *S. aureus* is non-motile while *P. aeruginosa* is motile, and therefore *S. aureus* may have spread less quickly through the hydrogel phase and cell layer, leading to less cytotoxicity [119]. This difference in 16-HBE cytotoxicity also reflects clinical outcomes in which *P. aeruginosa* infections are associated with a higher mortality rate than *S. aureus* infections [148].

In the polymicrobial model containing both *P. aeruginosa* and *S. aureus*, mammalian cell death occurs in the groups with no glass and either 0 or 16 μg/ml vancomycin (Figure 34), suggesting that *P. aeruginosa* overgrowth, which is not inhibited by vancomycin (Figure 32), once again leads to mass 16-HBE death. When we add the glass extracts to the polymicrobial model at a dilution of 1/4 and 1/2, we see that mammalian cell viability is maintained (Figure 34), suggesting that all three glass extracts at a dilution of 1/4 and 1/2 sufficiently prevented *P. aeruginosa* overgrowth. Note that at a dilution of 1/32 and 1/16, the Zn^{2+} glass did not appear to prevent *P. aeruginosa* overgrowth because mass cell death did occur for these groups (Figure 33). This suggests that the Zn^{2+} glass is only able to prevent *P. aeruginosa* overgrowth at the lower dilutions and not at higher dilutions, while the Ga^{3+}-containing glasses prevent *P. aeruginosa* overgrowth even at the higher dilutions.

Overall, the cell viability data from the CF airway infection model cultured with antibiotic-glass combinations shows us that mammalian cell viability is successfully

maintained when cultured with antibiotic-glass combinations at high enough concentrations to inhibit bacterial growth.

CHAPTER 5. Conclusions

5.1 Limitations and Future Directions

To ensure that the developed *in vitro* airway infection model accurately represents key features of airway infections in CF, several validation strategies could be employed aiming to assess the biological relevance, reproducibility, and predictive capabilities of the model. Validating the microbial growth patterns, biofilm formation, and host cell responses observed in the model against data from CF patient samples would help to determine how well the *in vitro* environment replicates *in vivo* conditions. Additionally, incorporating measurable outputs such as transepithelial electrical resistance or inflammatory markers could help to determine the ability of the model to mimic host responses in real-world CF infection pathophysiology. To validate the reproducibility of the model, measures could be taken to demonstrate that the model produces consistent results across multiple experimental runs pertaining to cell viability, bacterial growth patterns, and treatment responses across different cell passages, hydrogel batches, and bacterial strains. Lastly, the model's predictive validity could be assessed by applying clinically used antibiotics and comparing the model's bacterial growth responses to established clinical outcomes. By incorporating these strategies, the model's credibility can be strengthened, supporting its potential utility in studying CF airway infections and evaluating novel therapeutic approaches.

There are a number of potential limitations associated with the airway infection model that was used to test the antibiotic-glass combinations in this project. While the mucus-mimetic hydrogels of the model are able to mimic the physical properties of the

CF and healthy mucus layer, these hydrogels lack several elements that contribute to the complexity of native airway mucus. Future work could look at incorporating some of these components such as DNA, lipids, and non-mucin proteins [12] into the mucus-mimetic layer of the model and assess how the addition of these components impacts antibiotic-glass efficacy. The airway infection model also lacks a host immune component. Future work could look at adding host immune cells to the model to explore how host immune cells interact with and impact the efficacy of antibiotic-glass combinations in a CF-like microenvironment.

In CF patients, microbial infections are typically chronic in nature as the impaired CF airway microenvironment creates a predisposition to persistent and recurring infections [28], [149]. In this project, the airway infection model was only cultured for a total of 48 hours with bacteria and therefore is limited in capturing this chronic nature of CF airway infection. While this time course may be sufficient to model bacterial growth in early and acute infections, the model is limited in predicting antibiotic-glass efficacy against bacteria in a more representative chronic infection context. Future work could focus on extending the time course of the model to better capture the long-term host-pathogen interactions and microbial adaptations found in chronic CF airway infections [150], [151].

Another key limitation of this work is a lack of certainty that the metal ions contained in the original bioactive glass formulations fully dissolved into the glass extract solutions that were used to prepare the antibiotic-glass combinations used in this thesis work. When preparing the bioactive glass extract solutions, a precipitate remained after 48 hours of dissolving the glasses in the shaking incubator. This precipitate could have

contained undissolved glass, and therefore not all of the metal ions contained in the glasses would have dissolved into the extract solution. To ensure the glass extracts are produced consistently, the dissolution time and temperature are clearly defined in the methods section. Before conducting future work with these antibiotic-glass combinations, it would be worthwhile to conduct a spectroscopy analysis on the bioactive glass extracts to confirm the presence of the Ga^{3+} and Zn^{2+} ions in the extract solutions, and that these metal ions are present in similar concentrations to that of the original glass formulations.

In hopes of advancing the work done in this project, future work could focus on optimizing the glass formulations in a number of ways. Firstly, the antibacterial ion concentrations could be changed or the type of ions used could be changed to better target specific CF pathogens. Secondly, ion composition could be altered to better tune the speed of ion release to more effectively treat CF infections or to ensure that the glasses are fully dissolved into solution. Fortunately, the highly tunable nature of borate bioactive glasses allows for extensive investigation into the efficacy of different glass compositions on treating CF infections [91].

Additionally, the efficacy of the antibiotic-glass combinations developed in this project could be investigated against other CF pathogens such as *H. influenzae*, *S maltophilia*, and *A. fumigatus* [4], [28]. The airway infection model created in this project also has the potential to easily be modified to model other mucosal bacterial infections such as in the GI tract, urogenital tract, etc. Therefore, the novel model and combination therapy created in this thesis project are highly adaptable and can be applied across a wide range of mucosal infection contexts.

5.2 Conclusions

In this thesis project, a novel combination therapy to treat bacterial airway infections in CF patients was developed using a combination of conventional antibiotics with metal ion-releasing bioactive glasses. The results of this research show that in a CF-like airway microenvironment, *P. aeruginosa* and *S. aureus* growth can be suppressed by the addition of metal ion-releasing bioactive glasses without compromising mammalian cell viability. It was shown that specific glass extracts can augment conventional antibiotics to better suppress bacterial growth in a monomicrobial CF airway infection model for both *P. aeruginosa* and *S. aureus*. The findings from the polymicrobial CF airway co-infection model containing both *P. aeruginosa* and *S. aureus* show increasingly complex and different responses to the antibiotic-glass combinations in comparison to the monomicrobial infection models. Importantly, mammalian cell viability was maintained in the presence of all effective antibiotic-glass combinations in the CF airway infection model while bacterial growth was simultaneously suppressed. These findings demonstrate the potential utility of such antibiotic-glass combinations as effective therapeutics for airway infections in CF patients and as a means of slowing the development of resistance to conventional antibiotics in CF pathogens.

References

[1] J. Guo, A. Garratt, and A. Hill, "Worldwide rates of diagnosis and effective treatment for cystic fibrosis," *J. Cyst. Fibros.*, vol. 21, no. 3, pp. 456–462, May 2022, doi: 10.1016/j.jcf.2022.01.009.

[2] J. J. LiPuma, "The Changing Microbial Epidemiology in Cystic Fibrosis," *Clin. Microbiol. Rev.*, vol. 23, no. 2, pp. 299–323, Apr. 2010, doi: 10.1128/CMR.00068-09.

[3] A. C. Blanchard and V. J. Waters, "Opportunistic Pathogens in Cystic Fibrosis: Epidemiology and Pathogenesis of Lung Infection," *J. Pediatr. Infect. Dis. Soc.*, vol. 11, no. Supplement_2, pp. S3–S12, Sep. 2022, doi: 10.1093/jpids/piac052.

[4] R. D. Junkins, C. McCormick, and T.-J. Lin, "The emerging potential of autophagy-based therapies in the treatment of cystic fibrosis lung infections," *Autophagy*, vol. 10, no. 3, pp. 538–547, Mar. 2014, doi: 10.4161/auto.27750.

[5] X. M. Bustamante-Marin and L. E. Ostrowski, "Cilia and Mucociliary Clearance," *Cold Spring Harb. Perspect. Biol.*, vol. 9, no. 4, p. a028241, Apr. 2017, doi: 10.1101/cshperspect.a028241.

[6] A. McShane *et al.*, "Mucus," *Curr. Biol.*, vol. 31, no. 15, pp. R938–R945, Aug. 2021, doi: 10.1016/j.cub.2021.06.093.

[7] L. J. Donoghue *et al.*, "BPIFB1 loss alters airway mucus properties and diminishes mucociliary clearance," *Am. J. Physiol.-Lung Cell. Mol. Physiol.*, vol. 325, no. 6, pp. L765–L775, Dec. 2023, doi: 10.1152/ajplung.00390.2022.

[8] J. V. Fahy and B. F. Dickey, "Airway Mucus Function and Dysfunction," *N. Engl. J. Med.*, vol. 363, no. 23, pp. 2233–2247, Dec. 2010, doi: 10.1056/NEJMra0910061.

[9] R. Bansil and B. S. Turner, "Mucin structure, aggregation, physiological functions and biomedical applications," *Curr. Opin. Colloid Interface Sci.*, vol. 11, no. 2, pp. 164–170, Jun. 2006, doi: 10.1016/j.cocis.2005.11.001.

[10] D. J. Thornton, K. Rousseau, and M. A. McGuckin, "Structure and Function of the Polymeric Mucins in Airways Mucus," *Annu. Rev. Physiol.*, vol. 70, no. Volume 70, 2008, pp. 459–486, Feb. 2008, doi: 10.1146/annurev.physiol.70.113006.100702.

[11] M. C. Rose and J. A. Voynow, "Respiratory tract mucin genes and mucin glycoproteins in health and disease," *Physiol. Rev.*, vol. 86, no. 1, pp. 245–278, Jan. 2006, doi: 10.1152/physrev.00010.2005.

[12] C. B. Morrison, M. R. Markovetz, and C. Ehre, “Mucus, mucins, and cystic fibrosis,” *Pediatr. Pulmonol.*, vol. 54, no. S3, pp. S84–S96, 2019, doi: 10.1002/ppul.24530.

[13] B. Button, S. F. Okada, C. B. Frederick, W. R. Thelin, and R. C. Boucher, “Mechanosensitive ATP Release Maintains Proper Mucus Hydration of Airways,” *Sci. Signal.*, vol. 6, no. 279, pp. ra46–ra46, Jun. 2013, doi: 10.1126/scisignal.2003755.

[14] R. C. Boucher, “Airway Surface Dehydration in Cystic Fibrosis: Pathogenesis and Therapy,” *Annu. Rev. Med.*, vol. 58, no. Volume 58, 2007, pp. 157–170, Feb. 2007, doi: 10.1146/annurev.med.58.071905.105316.

[15] M. R. Markovetz *et al.*, “Mucus and mucus flake composition and abundance reflect inflammatory and infection status in cystic fibrosis,” *J. Cyst. Fibros.*, vol. 21, no. 6, pp. 959–966, Nov. 2022, doi: 10.1016/j.jcf.2022.04.008.

[16] M. O. Henke and F. Ratjen, “Mucolytics in cystic fibrosis,” *Paediatr. Respir. Rev.*, vol. 8, no. 1, pp. 24–29, Mar. 2007, doi: 10.1016/j.prrv.2007.02.009.

[17] A. G. Henderson *et al.*, “Cystic fibrosis airway secretions exhibit mucin hyperconcentration and increased osmotic pressure,” *J. Clin. Invest.*, vol. 124, no. 7, pp. 3047–3060, Jul. 2014, doi: 10.1172/JCI73469.

[18] J. J. Wine, G. C. Hansson, P. König, N. S. Joo, A. Ermund, and M. Pieper, “Progress in understanding mucus abnormalities in cystic fibrosis airways,” *J. Cyst. Fibros.*, vol. 17, no. 2, Supplement, pp. S35–S39, Mar. 2018, doi: 10.1016/j.jcf.2017.09.003.

[19] N. Derichs, B.-J. Jin, Y. Song, W. E. Finkbeiner, and A. S. Verkman, “Hyperviscous airway periciliary and mucous liquid layers in cystic fibrosis measured by confocal fluorescence photobleaching,” *FASEB J.*, vol. 25, no. 7, pp. 2325–2332, 2011, doi: 10.1096/fj.10-179549.

[20] B. Button *et al.*, “A Periciliary Brush Promotes the Lung Health by Separating the Mucus Layer from Airway Epithelia,” *Science*, vol. 337, no. 6097, pp. 937–941, Aug. 2012, doi: 10.1126/science.1223012.

[21] B. Button *et al.*, “Roles of mucus adhesion and cohesion in cough clearance,” *Proc. Natl. Acad. Sci. U. S. A.*, vol. 115, no. 49, pp. 12501–12506, Dec. 2018, doi: 10.1073/pnas.1811787115.

[22] A. Balázs and M. A. Mall, “Mucus obstruction and inflammation in early cystic fibrosis lung disease: Emerging role of the IL-1 signaling pathway,” *Pediatr. Pulmonol.*, vol. 54, no. S3, pp. S5–S12, 2019, doi: 10.1002/ppul.24462.

[23] K. Kovach *et al.*, "Evolutionary adaptations of biofilms infecting cystic fibrosis lungs promote mechanical toughness by adjusting polysaccharide production," *Npj Biofilms Microbiomes*, vol. 3, no. 1, pp. 1–9, Jan. 2017, doi: 10.1038/s41522-016-0007-9.

[24] N. Høiby and O. Ciofu, "Pseudomonas aeruginosa biofilms in cystic fibrosis," *Future Microbiol.*, vol. 5, no. 11, pp. 1663–74, Nov. 2010, doi: 10.2217/fmb.10.125.

[25] M. Polívková, T. Hubáček, M. Staszek, V. Švorčík, and J. Siegel, "Antimicrobial Treatment of Polymeric Medical Devices by Silver Nanomaterials and Related Technology," *Int. J. Mol. Sci.*, vol. 18, no. 2, p. 419, Feb. 2017, doi: 10.3390/ijms18020419.

[26] L. Wang, C. Hu, and L. Shao, "The antimicrobial activity of nanoparticles: present situation and prospects for the future," *Int. J. Nanomedicine*, vol. 12, pp. 1227–1249, 2017, doi: 10.2147/IJN.S121956.

[27] I. W. Maina, N. N. Patel, and N. A. Cohen, "Understanding the Role of Biofilms and Superantigens in Chronic Rhinosinusitis," *Curr. Otorhinolaryngol. Rep.*, vol. 6, no. 3, pp. 253–262, Sep. 2018, doi: 10.1007/s40136-018-0212-6.

[28] E. Chiappini, G. Taccetti, and M. De Martino, "Bacterial Lung Infections in Cystic Fibrosis Patients: An Update," *Pediatr. Infect. Dis. J.*, vol. 33, no. 6, pp. 653–654, Jun. 2014, doi: 10.1097/INF.0000000000000347.

[29] "Patient Registry | Cystic Fibrosis Foundation." Accessed: Apr. 30, 2025. [Online]. Available: https://www.cff.org/medical-professionals/patient-registry

[30] J. Botelho, F. Grosso, and L. Peixe, "Antibiotic resistance in *Pseudomonas aeruginosa* – Mechanisms, epidemiology and evolution," *Drug Resist. Updat.*, vol. 44, p. 100640, May 2019, doi: 10.1016/j.drup.2019.07.002.

[31] J. C. Davies, "Pseudomonas aeruginosa in cystic fibrosis: pathogenesis and persistence," *Paediatr. Respir. Rev.*, vol. 3, no. 2, pp. 128–134, Jun. 2002, doi: 10.1016/s1526-0550(02)00003-3.

[32] R. Rosales-Reyes, S. Y. Vargas-Roldán, J. L. Lezana-Fernández, and J. I. Santos-Preciado, "*Pseudomonas Aeruginosa*: Genetic Adaptation, A Strategy for its Persistence in Cystic Fibrosis," *Arch. Med. Res.*, vol. 52, no. 4, pp. 357–361, May 2021, doi: 10.1016/j.arcmed.2020.12.004.

[33] M. I. Ahmed and S. Mukherjee, "Treatment for chronic methicillin-sensitive Staphylococcus aureus pulmonary infection in people with cystic fibrosis," *Cochrane Database Syst. Rev.*, vol. 2018, no. 7, p. CD011581, Jul. 2018, doi: 10.1002/14651858.CD011581.pub3.

[34] K. M. Craft, J. M. Nguyen, L. J. Berg, and S. D. Townsend, “Methicillin-resistant Staphylococcus aureus (MRSA): antibiotic-resistance and the biofilm phenotype,” *MedChemComm*, vol. 10, no. 8, pp. 1231–1241, Mar. 2019, doi: 10.1039/c9md00044e.

[35] M. N. Hurley and A. R. Smyth, “Staphylococcus aureus in cystic fibrosis: pivotal role or bit part actor?,” *Curr. Opin. Pulm. Med.*, vol. 24, no. 6, pp. 586–591, Nov. 2018, doi: 10.1097/MCP.0000000000000518.

[36] S. Lakhundi and K. Zhang, “Methicillin-Resistant Staphylococcus aureus: Molecular Characterization, Evolution, and Epidemiology,” *Clin. Microbiol. Rev.*, vol. 31, no. 4, pp. e00020-18, Sep. 2018, doi: 10.1128/CMR.00020-18.

[37] N. S. Harik, G. Com, X. Tang, M. Melguizo Castro, M. E. Stemper, and J. L. Carroll, “Clinical characteristics and epidemiology of methicillin-resistant *Staphylococcus aureus* (MRSA) in children with cystic fibrosis from a center with a high MRSA prevalence,” *Am. J. Infect. Control*, vol. 44, no. 4, pp. 409–415, Apr. 2016, doi: 10.1016/j.ajic.2015.10.015.

[38] S. Moreau-Marquis, B. A. Stanton, and G. A. O’Toole, “*Pseudomonas aeruginosa* biofilm formation in the cystic fibrosis airway,” *Pulm. Pharmacol. Ther.*, vol. 21, no. 4, pp. 595–599, Aug. 2008, doi: 10.1016/j.pupt.2007.12.001.

[39] S. J. Gabryszewski *et al.*, “Metabolic Adaptation in Methicillin-Resistant Staphylococcus aureus Pneumonia,” *Am. J. Respir. Cell Mol. Biol. Online*, vol. 61, no. 2, pp. 185–197, Aug. 2019, doi: 10.1165/rcmb.2018-0389OC.

[40] J. W. Costerton, P. S. Stewart, and E. P. Greenberg, “Bacterial biofilms: A common cause of persistent infections,” *Science*, vol. 284, no. 5418, pp. 1318–22, May 1999.

[41] C. Williams, R. Ranjendran, and G. Ramage, “Pathogenesis of Fungal Infections in Cystic Fibrosis,” *Curr. Fungal Infect. Rep.*, vol. 10, no. 4, pp. 163–169, Dec. 2016, doi: 10.1007/s12281-016-0268-z.

[42] G. Hong and N. Lechtzin, “Cystic fibrosis: We see fungus among us, but should we care?,” *J. Cyst. Fibros.*, vol. 18, no. 2, pp. 163–164, Mar. 2019, doi: 10.1016/j.jcf.2019.02.006.

[43] S. H. Chotirmall and N. G. McElvaney, “Fungi in the cystic fibrosis lung: Bystanders or pathogens?,” *Int. J. Biochem. Cell Biol.*, vol. 52, pp. 161–173, Jul. 2014, doi: 10.1016/j.biocel.2014.03.001.

[44] K. W. K. Tang, B. C. Millar, and J. E. Moore, “Antimicrobial Resistance (AMR),” *Br. J. Biomed. Sci.*, vol. 80, p. 11387, Jun. 2023, doi: 10.3389/bjbs.2023.11387.

[45] CDC, “Antimicrobial Resistance Facts and Stats,” Antimicrobial Resistance. Accessed: Jun. 25, 2025. [Online]. Available: https://www.cdc.gov/antimicrobial-resistance/data-research/facts-stats/index.html

[46] “Antimicrobial resistance.” Accessed: Jun. 25, 2025. [Online]. Available: https://www.who.int/news-room/fact-sheets/detail/antimicrobial-resistance

[47] M. J. Struelens, “The epidemiology of antimicrobial resistance in hospital acquired infections: problems and possible solutions,” *BMJ*, vol. 317, no. 7159, pp. 652–654, Sep. 1998, doi: 10.1136/bmj.317.7159.652.

[48] E. National Academies of Sciences, H. and M. Division, B. on P. H. and P. H. Practice, C. on the L.-T. H. and E. E. of A. R. in the U. States, G. H. Palmer, and G. J. Buckley, “The Health and Economic Burden of Resistance,” in *Combating Antimicrobial Resistance and Protecting the Miracle of Modern Medicine*, National Academies Press (US), 2021. Accessed: Jun. 25, 2025. [Online]. Available: https://www.ncbi.nlm.nih.gov/books/NBK577288/

[49] T. Pulingam *et al.*, “Antimicrobial resistance: Prevalence, economic burden, mechanisms of resistance and strategies to overcome,” *Eur. J. Pharm. Sci.*, vol. 170, p. 106103, Mar. 2022, doi: 10.1016/j.ejps.2021.106103.

[50] A. Vitiello *et al.*, “The Impact of Antimicrobial Resistance in Cystic Fibrosis,” *J. Clin. Med.*, vol. 13, no. 6, p. 1711, Mar. 2024, doi: 10.3390/jcm13061711.

[51] E. P. Perikleous, D. Gkentzi, A. Bertzouanis, E. Paraskakis, A. Sovtic, and S. Fouzas, “Antibiotic Resistance in Patients with Cystic Fibrosis: Past, Present, and Future,” *Antibiotics*, vol. 12, no. 2, Art. no. 2, Feb. 2023, doi: 10.3390/antibiotics12020217.

[52] G. Taccetti *et al.*, “Cystic Fibrosis: Recent Insights into Inhaled Antibiotic Treatment and Future Perspectives,” *Antibiotics*, vol. 10, no. 3, p. 338, Mar. 2021, doi: 10.3390/antibiotics10030338.

[53] F. Bugli *et al.*, “Antimicrobial peptides for tackling cystic fibrosis related bacterial infections: A review,” *Microbiol. Res.*, vol. 263, p. 127152, Oct. 2022, doi: 10.1016/j.micres.2022.127152.

[54] E. Peterson and P. Kaur, “Antibiotic Resistance Mechanisms in Bacteria: Relationships Between Resistance Determinants of Antibiotic Producers, Environmental Bacteria, and Clinical Pathogens,” *Front. Microbiol.*, vol. 9, p. 2928, Nov. 2018, doi: 10.3389/fmicb.2018.02928.

[55] M. J. Hajipour *et al.*, “Antibacterial properties of nanoparticles,” *Trends Biotechnol.*, vol. 30, no. 10, pp. 499–511, Oct. 2012, doi: 10.1016/j.tibtech.2012.06.004.

[56] A. H. A. M. van Hoek, D. Mevius, B. Guerra, P. Mullany, A. P. Roberts, and H. J. M. Aarts, “Acquired Antibiotic Resistance Genes: An Overview,” *Front. Microbiol.*, vol. 2, p. 203, Sep. 2011, doi: 10.3389/fmicb.2011.00203.

[57] G. Herrmann *et al.*, “Colistin-Tobramycin Combinations Are Superior to Monotherapy Concerning the Killing of Biofilm Pseudomonas aeruginosa,” *J. Infect. Dis.*, vol. 202, no. 10, pp. 1585–1592, Nov. 2010, doi: 10.1086/656788.

[58] I. Martin, V. Waters, and H. Grasemann, “Approaches to Targeting Bacterial Biofilms in Cystic Fibrosis Airways,” *Int. J. Mol. Sci.*, vol. 22, no. 4, p. 2155, Feb. 2021, doi: 10.3390/ijms22042155.

[59] B. W. Ramsey *et al.*, “Intermittent Administration of Inhaled Tobramycin in Patients with Cystic Fibrosis,” *N. Engl. J. Med.*, vol. 340, no. 1, pp. 23–30, Jan. 1999, doi: 10.1056/NEJM199901073400104.

[60] N. M. Fusco, K. A. Toussaint, and W. A. Prescott, “Antibiotic Management of Methicillin-Resistant Staphylococcus aureus–Associated Acute Pulmonary Exacerbations in Cystic Fibrosis,” *Ann. Pharmacother.*, vol. 49, no. 4, pp. 458–468, Apr. 2015, doi: 10.1177/1060028014567526.

[61] D. K. Lo, M. S. Muhlebach, and A. R. Smyth, “Interventions for the eradication of meticillin-resistant Staphylococcus aureus (MRSA) in people with cystic fibrosis,” *Cochrane Database Syst. Rev.*, vol. 2022, no. 12, p. CD009650, Dec. 2022, doi: 10.1002/14651858.CD009650.pub5.

[62] F. Lucca, M. Guarnieri, M. Ros, G. Muffato, R. Rigoli, and L. Da Dalt, “Antibiotic resistance evolution of Pseudomonas aeruginosa in cystic fibrosis patients (2010-2013),” *Clin. Respir. J.*, vol. 12, no. 7, pp. 2189–2196, 2018, doi: 10.1111/crj.12787.

[63] R. L. Gibson, J. L. Burns, and B. W. Ramsey, “Pathophysiology and management of pulmonary infections in cystic fibrosis,” *Am. J. Respir. Crit. Care Med.*, vol. 168, no. 8, pp. 918–51, Oct. 2003.

[64] G. Herrmann, E. Freitag, C. Deppisch, S. Heyder, U. Graepler-Mainka, and J. Riethmüller, “113 Inhalative meropenem–tobramycin–colistin combination improves lung function in chronic *Pseudomonas aeruginosa* colonization,” *J. Cyst. Fibros.*, vol. 14, p. S86, Jun. 2015, doi: 10.1016/S1569-1993(15)30290-3.

[65] A. A. Agyeman *et al.*, “Ceftolozane/tazobactam plus tobramycin against free-floating and biofilm bacteria of hypermutable *Pseudomonas aeruginosa* epidemic strains: Resistance mechanisms and synergistic activity,” *Int. J. Antimicrob. Agents*, vol. 62, no. 3, p. 106887, Sep. 2023, doi: 10.1016/j.ijantimicag.2023.106887.

[66] N. Cassir *et al.*, “Multi-target combination of antibiotics as salvage therapy for severe infection caused by pan-resistant *Burkholderia cenocepacia* following lung transplantation,” *Transplant. Rep.*, vol. 10, no. 1, p. 100170, Feb. 2025, doi: 10.1016/j.tpr.2024.100170.

[67] N. Alhajj, M. F. Z. R. Yahya, N. J. O’Reilly, and H. Cathcart, “Development and characterization of a spray-dried inhalable ternary combination for the treatment of *Pseudomonas aeruginosa* biofilm infection in cystic fibrosis,” *Eur. J. Pharm. Sci.*, vol. 192, p. 106654, Jan. 2024, doi: 10.1016/j.ejps.2023.106654.

[68] A. Aguilar-Colomer *et al.*, “Mucolytic and antibiotic combination therapy using silica-based nanocarriers to eradicate Escherichia coli biofilms,” *Nanoscale Adv.*, vol. 7, no. 11, pp. 3414–3425, doi: 10.1039/d5na00006h.

[69] S. L. Durfey *et al.*, “Combining Ivacaftor and Intensive Antibiotics Achieves Limited Clearance of Cystic Fibrosis Infections,” *mBio*, vol. 12, no. 6, pp. e03148-21, Dec. 2021, doi: 10.1128/mbio.03148-21.

[70] I. M. Balfour-Lynn and J. A. King, “CFTR modulator therapies – Effect on life expectancy in people with cystic fibrosis,” *Paediatr. Respir. Rev.*, vol. 42, pp. 3–8, Jun. 2022, doi: 10.1016/j.prrv.2020.05.002.

[71] R. V. E. Dagenais, V. C. Su, and B. S. Quon, “Real-World Safety of CFTR Modulators in the Treatment of Cystic Fibrosis: A Systematic Review,” *J. Clin. Med.*, vol. 10, no. 1, p. 23, Dec. 2020, doi: 10.3390/jcm10010023.

[72] A. Frei, A. D. Verderosa, A. G. Elliott, J. Zuegg, and M. A. T. Blaskovich, “Metals to combat antimicrobial resistance,” *Nat. Rev. Chem.*, vol. 7, no. 3, pp. 202–224, Mar. 2023, doi: 10.1038/s41570-023-00463-4.

[73] S.-L. Abram and K. M. Fromm, “Handling (Nano)Silver as Antimicrobial Agent: Therapeutic Window, Dissolution Dynamics, Detection Methods and Molecular Interactions,” *Chem. Weinh. Bergstr. Ger.*, vol. 26, no. 48, pp. 10948–10971, Aug. 2020, doi: 10.1002/chem.202002143.

[74] X. Wang *et al.*, “The synergistic antibacterial activity and mechanism of multicomponent metal ions-containing aqueous solutions against *Staphylococcus aureus*,” *J. Inorg. Biochem.*, vol. 163, pp. 214–220, Oct. 2016, doi: 10.1016/j.jinorgbio.2016.07.019.

[75] M. Dryden, “Reactive oxygen species: a novel antimicrobial,” *Int. J. Antimicrob. Agents*, vol. 51, no. 3, pp. 299–303, Mar. 2018, doi: 10.1016/j.ijantimicag.2017.08.029.

[76] M. Godoy-Gallardo *et al.*, “Antibacterial approaches in tissue engineering using metal ions and nanoparticles: From mechanisms to applications,” *Bioact. Mater.*, vol. 6, no. 12, pp. 4470–4490, Dec. 2021, doi: 10.1016/j.bioactmat.2021.04.033.

[77] A. Kessler, J. Hedberg, E. Blomberg, and I. Odnevall, "Reactive Oxygen Species Formed by Metal and Metal Oxide Nanoparticles in Physiological Media—A Review of Reactions of Importance to Nanotoxicity and Proposal for Categorization," *Nanomaterials*, vol. 12, no. 11, p. 1922, Jun. 2022, doi: 10.3390/nano12111922.

[78] N. Mutlu *et al.*, "Effect of Zn and Ga doping on bioactivity, degradation, and antibacterial properties of borate 1393-B3 bioactive glass," *Ceram. Int.*, vol. 48, no. 11, pp. 16404–16417, Jun. 2022, doi: 10.1016/j.ceramint.2022.02.192.

[79] Y. Xie, Y. He, P. L. Irwin, T. Jin, and X. Shi, "Antibacterial Activity and Mechanism of Action of Zinc Oxide Nanoparticles against Campylobacter jejuni," *Appl. Environ. Microbiol.*, vol. 77, no. 7, pp. 2325–2331, Apr. 2011, doi: 10.1128/AEM.02149-10.

[80] D. Li *et al.*, "Preparation of organic-inorganic composites with high antibacterial activity based on sepiolite, chitosan and zinc: The study of the active antibacterial sites of chitosan-zinc oxide structure," *Appl. Clay Sci.*, vol. 216, p. 106325, Jan. 2022, doi: 10.1016/j.clay.2021.106325.

[81] C. R. Chitambar, "Medical Applications and Toxicities of Gallium Compounds," *Int. J. Environ. Res. Public. Health*, vol. 7, no. 5, pp. 2337–2361, May 2010, doi: 10.3390/ijerph7052337.

[82] S. Wahab, A. Salman, Z. Khan, S. Khan, C. Krishnaraj, and S.-I. Yun, "Metallic Nanoparticles: A Promising Arsenal against Antimicrobial Resistance—Unraveling Mechanisms and Enhancing Medication Efficacy," *Int. J. Mol. Sci.*, vol. 24, no. 19, p. 14897, Oct. 2023, doi: 10.3390/ijms241914897.

[83] S. Shaikh *et al.*, "Mechanistic Insights into the Antimicrobial Actions of Metallic Nanoparticles and Their Implications for Multidrug Resistance," *Int. J. Mol. Sci.*, vol. 20, no. 10, 2019, doi: 10.3390/ijms20102468.

[84] D. Ege, K. Zheng, and A. R. Boccaccini, "Borate Bioactive Glasses (BBG): Bone Regeneration, Wound Healing Applications, and Future Directions," *ACS Appl. Bio Mater.*, vol. 5, no. 8, pp. 3608–3622, Aug. 2022, doi: 10.1021/acsabm.2c00384.

[85] V. R. dos Santos *et al.*, "Effect of Co, Cu, and Zn ions on the bioactivity and antibacterial properties of a borate bioactive glass," *J. Non-Cryst. Solids*, vol. 622, p. 122643, Dec. 2023, doi: 10.1016/j.jnoncrysol.2023.122643.

[86] A. Rahimnejad Yazdi, L. Torkan, W. Stone, and M. R. Towler, "The impact of gallium content on degradation, bioactivity, and antibacterial potency of zinc borate bioactive glass," *J. Biomed. Mater. Res. B Appl. Biomater.*, vol. 106, no. 1, pp. 367–376, 2018, doi: 10.1002/jbm.b.33856.

[87] K. O'Connell *et al.*, "Host responses to a strontium releasing high boron glass using a rabbit bilateral femoral defect model," *J. Biomed. Mater. Res. B Appl. Biomater.*, vol. 105, no. 7, pp. 1818–1827, 2017, doi: 10.1002/jbm.b.33694.

[88] H. Ding *et al.*, “A Novel Injectable Borate Bioactive Glass Cement as an Antibiotic Delivery Vehicle for Treating Osteomyelitis,” *PLoS ONE*, vol. 9, no. 1, pp. 1–9, Jan. 2014, doi: 10.1371/journal.pone.0085472.

[89] R. Borges *et al.*, “Bioactive Glasses as Carriers of Cancer-Targeted Drugs: Challenges and Opportunities in Bone Cancer Treatment,” *Materials*, vol. 15, no. 24, p. 9082, Dec. 2022, doi: 10.3390/ma15249082.

[90] S. Fakher and D. Westenberg, “Borate-based bioactive glasses properties: Clinical and biomedical applications,” *Ceram. Int.*, vol. 50, no. 24, Part A, pp. 52190–52204, Dec. 2024, doi: 10.1016/j.ceramint.2024.10.194.

[91] C. Wen *et al.*, “Effects of B2O3 on the structural evolution and biological behavior of borate bioactive glasses by sol-gel and melting methods,” *Ceram. Int.*, vol. 50, no. 22, Part C, pp. 47864–47875, Nov. 2024, doi: 10.1016/j.ceramint.2024.09.131.

[92] B. R. Grubb and A. Livraghi-Butrico, “Animal models of cystic fibrosis in the era of highly effective modulator therapies,” *Curr. Opin. Pharmacol.*, vol. 64, p. 102235, Jun. 2022, doi: 10.1016/j.coph.2022.102235.

[93] S. J. Bose, T. S. Scott-Ward, Z. Cai, and D. N. Sheppard, “Exploiting species differences to understand the CFTR Cl- channel,” *Biochem. Soc. Trans.*, vol. 43, no. 5, pp. 975–982, Oct. 2015, doi: 10.1042/BST20150129.

[94] D. C. Bouzek *et al.*, “Early Lung Disease Exhibits Bacteria-Dependent and -Independent Abnormalities in Cystic Fibrosis Pigs,” *Am. J. Respir. Crit. Care Med.*, vol. 204, no. 6, pp. 692–702, Sep. 2021, doi: 10.1164/rccm.202102-0451OC.

[95] D. A. Stoltz *et al.*, “Cystic Fibrosis Pigs Develop Lung Disease and Exhibit Defective Bacterial Eradication at Birth,” *Sci. Transl. Med.*, vol. 2, no. 29, p. 29ra31, Apr. 2010, doi: 10.1126/scitranslmed.3000928.

[96] X. Sun *et al.*, “Lung Phenotype of Juvenile and Adult Cystic Fibrosis Transmembrane Conductance Regulator–Knockout Ferrets,” *Am. J. Respir. Cell Mol. Biol.*, vol. 50, no. 3, pp. 502–512, Mar. 2014, doi: 10.1165/rcmb.2013-0261OC.

[97] X. Sun *et al.*, “Disease phenotype of a ferret *CFTR*-knockout model of cystic fibrosis,” *J. Clin. Invest.*, vol. 120, no. 9, pp. 3149–3160, Sep. 2010, doi: 10.1172/JCI43052.

[98] B. H. Rosen *et al.*, “Animal and Model Systems for Studying Cystic Fibrosis,” *J. Cyst. Fibros. Off. J. Eur. Cyst. Fibros. Soc.*, vol. 17, no. 2 Suppl, pp. S28–S34, Mar. 2018, doi: 10.1016/j.jcf.2017.09.001.

[99] R. Darrah *et al.*, “Cystic Fibrosis Mice Develop Spontaneous Chronic Bordetella Airway Infections,” *J. Infect. Pulm. Dis.*, vol. 3, no. 2, 2017, doi: 10.16966/2470-3176.128.

[100] A. Livraghi-Butrico *et al.*, "Mucus clearance, MyD88-dependent and MyD88-independent immunity modulate lung susceptibility to spontaneous bacterial infection and inflammation," *Mucosal Immunol.*, vol. 5, no. 4, pp. 397–408, Jul. 2012, doi: 10.1038/mi.2012.17.

[101] S. Pont and A.-B. Blanc-Potard, "Zebrafish Embryo Infection Model to Investigate Pseudomonas aeruginosa Interaction With Innate Immunity and Validate New Therapeutics," *Front. Cell. Infect. Microbiol.*, vol. 11, p. 745851, 2021, doi: 10.3389/fcimb.2021.745851.

[102] A. Lopez *et al.*, "Developing Tadpole Xenopus laevis as a Comparative Animal Model to Study Mycobacterium abscessus Pathogenicity," *Int. J. Mol. Sci.*, vol. 22, no. 2, p. 806, Jan. 2021, doi: 10.3390/ijms22020806.

[103] J. T. Fisher, Y. Zhang, and J. F. Engelhardt, "Comparative Biology of Cystic Fibrosis Animal Models," *Methods Mol. Biol. Clifton NJ*, vol. 742, pp. 311–334, 2011, doi: 10.1007/978-1-61779-120-8_19.

[104] G. A. O'Toole *et al.*, "Model Systems to Study the Chronic, Polymicrobial Infections in Cystic Fibrosis: Current Approaches and Exploring Future Directions," *mBio*, vol. 12, no. 5, pp. e01763-21, doi: 10.1128/mBio.01763-21.

[105] D. M. Cornforth, F. L. Diggle, J. A. Melvin, J. M. Bomberger, and M. Whiteley, "Quantitative Framework for Model Evaluation in Microbiology Research Using Pseudomonas aeruginosa and Cystic Fibrosis Infection as a Test Case," *mBio*, vol. 11, no. 1, p. 10.1128/mbio.03042-19, Jan. 2020, doi: 10.1128/mbio.03042-19.

[106] V. Bezzerri *et al.*, "Antibacterial and anti-inflammatory activity of a temporin B peptide analogue on an in vitro model of cystic fibrosis," *J. Pept. Sci.*, vol. 20, no. 10, pp. 822–830, 2014, doi: 10.1002/psc.2674.

[107] M. Hirsch *et al.*, "488 Chronic Pseudomonas aeruginosa infection in a cystic fibrosis in vitro model," *J. Cyst. Fibros.*, vol. 21, pp. S277–S277, 2022, doi: 10.1016/S1569-1993(22)01178-X.

[108] S. Kirchner, J. L. Fothergill, E. A. Wright, C. E. James, E. Mowat, and C. Winstanley, "Use of Artificial Sputum Medium to Test Antibiotic Efficacy Against Pseudomonas aeruginosa in Conditions More Relevant to the Cystic Fibrosis Lung," *J. Vis. Exp. JoVE*, no. 64, p. e3857, Jun. 2012, doi: 10.3791/3857.

[109] E. J. Baker, G. Allcott, A. Molloy, and J. A. G. Cox, "Cystic fibrosis sputum media induces an overall loss of antibiotic susceptibility in Mycobacterium abscessus," *Npj Antimicrob. Resist.*, vol. 2, no. 1, pp. 1–8, Nov. 2024, doi: 10.1038/s44259-024-00054-3.

[110] K. L. Palmer, L. M. Aye, and M. Whiteley, "Nutritional Cues Control Pseudomonas aeruginosa Multicellular Behavior in Cystic Fibrosis Sputum," *J. Bacteriol.*, vol. 189, no. 22, pp. 8079–8087, Nov. 2007, doi: 10.1128/jb.01138-07.

[111] O. W. Meldrum, G. E. Yakubov, M. R. Bonilla, O. Deshmukh, M. A. McGuckin, and M. J. Gidley, "Mucin gel assembly is controlled by a collective action of non-mucin proteins, disulfide bridges, Ca2+-mediated links, and hydrogen bonding," *Sci. Rep.*, vol. 8, no. 1, pp. 1–16, 2018, doi: 10.1038/s41598-018-24223-3.

[112] C. Werlang, G. Cárcarmo-Oyarce, and K. Ribbeck, "Engineering mucus to study and influence the microbiome," *Nat. Rev. Mater.*, vol. 4, no. 2, pp. 134–145, 2019, doi: 10.1038/s41578-018-0079-7.

[113] A. J. Huang, C. L. O'Brien, N. Dawe, A. Tahir, A. J. Scott, and B. M. Leung, "Characterization of an engineered mucus microenvironment for in vitro modeling of host–microbe interactions," *Sci. Rep.*, vol. 12, no. 1, pp. 5515–5515, 2022, doi: 10.1038/s41598-022-09198-6.

[114] C. L. O'Brien *et al.*, "Modeling Cystic Fibrosis Chronic Infection Using Engineered Mucus-like Hydrogels," *ACS Biomater. Sci. Eng.*, vol. 10, no. 10, pp. 6558–6568, Oct. 2024, doi: 10.1021/acsbiomaterials.4c01271.

[115] A. J. Huang, A. N. Clarke, N. Jafari, and B. M. Leung, "Characterization of Patterned Microbial Growth Dynamics in Aqueous Two-Phase Polymer Scaffolds," *ACS Biomater. Sci. Eng.*, vol. 7, no. 12, pp. 5506–5514, Dec. 2021, doi: 10.1021/acsbiomaterials.1c01130.

[116] H.-Y. Kim, "Statistical notes for clinical researchers: post-hoc multiple comparisons," *Restor. Dent. Endod.*, vol. 40, no. 2, pp. 172–176, May 2015, doi: 10.5395/rde.2015.40.2.172.

[117] J. Calvén, E. Ax, and M. Rådinger, "The Airway Epithelium—A Central Player in Asthma Pathogenesis," *Int. J. Mol. Sci.*, vol. 21, no. 23, Art. no. 23, Jan. 2020, doi: 10.3390/ijms21238907.

[118] E. Ruysseveldt, K. Martens, and B. Steelant, "Airway Basal Cells, Protectors of Epithelial Walls in Health and Respiratory Diseases," *Front. Allergy*, vol. 2, Nov. 2021, doi: 10.3389/falgy.2021.787128.

[119] C.-C. Liu and M.-H. Lin, "Hitchhiking motility of Staphylococcus aureus involves the interaction between its wall teichoic acids and lipopolysaccharide of Pseudomonas aeruginosa," *Front. Microbiol.*, vol. 13, Jan. 2023, doi: 10.3389/fmicb.2022.1068251.

[120] C. H. Goss *et al.*, "Gallium disrupts bacterial iron metabolism and has therapeutic effects in mice and humans with lung infections," *Sci. Transl. Med.*, vol. 10, no. 460, p. eaat7520, Sep. 2018, doi: 10.1126/scitranslmed.aat7520.

[121] A. G. Oglesby *et al.*, "The Influence of Iron on *Pseudomonas aeruginosa* Physiology," *J. Biol. Chem.*, vol. 283, no. 23, pp. 15558–15567, Jun. 2008, doi: 10.1074/jbc.M707840200.

[122] A. F. Konings *et al.*, “Pseudomonas aeruginosa Uses Multiple Pathways To Acquire Iron during Chronic Infection in Cystic Fibrosis Lungs,” *Infect. Immun.*, vol. 81, no. 8, pp. 2697–2704, Aug. 2013, doi: 10.1128/IAI.00418-13.

[123] C. R. Chitambar, “Gallium and its competing roles with iron in biological systems,” *Biochim. Biophys. Acta*, vol. 1863, no. 8, pp. 2044–2053, Aug. 2016, doi: 10.1016/j.bbamcr.2016.04.027.

[124] S.-R. Choi, M. A. Hassan, B. E. Britigan, and P. Narayanasamy, “Antimicrobial Activity of Gallium(III) Compounds: Pathogen-Dependent Targeting of Multiple Iron/Heme-Dependent Biological Processes,” *Curr. Issues Mol. Biol.*, vol. 46, no. 8, pp. 9149–9161, Aug. 2024, doi: 10.3390/cimb46080541.

[125] L. R. Bernstein, “Mechanisms of Therapeutic Activity for Gallium,” *Pharmacol. Rev.*, vol. 50, no. 4, pp. 665–682, Dec. 1998, doi: 10.1016/S0031-6997(24)01383-8.

[126] F. Runci, C. Bonchi, E. Frangipani, D. Visaggio, and P. Visca, “Acinetobacter baumannii Biofilm Formation in Human Serum and Disruption by Gallium,” *Antimicrob. Agents Chemother.*, vol. 61, no. 1, pp. e01563-16, Dec. 2016, doi: 10.1128/AAC.01563-16.

[127] J. Ma, S. Hou, M. B. Chan-Park, and H. Duan, “Antibiofilm Activity of Gallium(III) Complexed Anionic Polymers in Combination with Antibiotics,” *Macromol. Rapid Commun.*, vol. 42, no. 20, p. 2100255, 2021, doi: 10.1002/marc.202100255.

[128] C. R. Mendes *et al.*, “Antibacterial action and target mechanisms of zinc oxide nanoparticles against bacterial pathogens,” *Sci. Rep.*, vol. 12, no. 1, p. 2658, Feb. 2022, doi: 10.1038/s41598-022-06657-y.

[129] M. Moradi *et al.*, “In Vitro and In Vivo Antibacterial and Antibiofilm Activity of Zinc Sulfate (ZnSO4) and Carvacrol (CV) Alone and in Combination with Antibiotics Against Pseudomonas aeruginosa,” *Antibiotics*, vol. 14, no. 4, Art. no. 4, Apr. 2025, doi: 10.3390/antibiotics14040367.

[130] Z. D. Lila-Krasniqi, R. B. Halili, V. Hamza, and S. Krasniqi, “Evaluation of Antimicrobial Effectiveness of Dental Cement Materials on Growth of Different Bacterial Strains,” *Med. Sci. Monit. Basic Res.*, vol. 28, pp. e937893-1-e937893-6, Nov. 2022, doi: 10.12659/MSMBR.937893.

[131] W. Elkhatib and A. Noreddin, “In Vitro Antibiofilm Efficacies of Different Antibiotic Combinations with Zinc Sulfate against Pseudomonas aeruginosa Recovered from Hospitalized Patients with Urinary Tract Infection,” *Antibiot. Basel Switz.*, vol. 3, no. 1, pp. 64–84, Feb. 2014, doi: 10.3390/antibiotics3010064.

[132] M. R. Gonzalez, V. Ducret, S. Leoni, and K. Perron, "*Pseudomonas aeruginosa* zinc homeostasis: Key issues for an opportunistic pathogen," *Biochim. Biophys. Acta BBA - Gene Regul. Mech.*, vol. 1862, no. 7, pp. 722–733, Jul. 2019, doi: 10.1016/j.bbagrm.2018.01.018.

[133] S. Wang, J. Cheng, Y. Niu, P. Li, X. Zhang, and J. Lin, "Strategies for Zinc Uptake in Pseudomonas aeruginosa at the Host–Pathogen Interface," *Front. Microbiol.*, vol. 12, p. 741873, Sep. 2021, doi: 10.3389/fmicb.2021.741873.

[134] N. D. Hammer and E. P. Skaar, "Molecular mechanisms of Staphylococcus aureus iron acquisition," *Annu. Rev. Microbiol.*, vol. 65, p. 10.1146/annurev-micro-090110–102851, 2011, doi: 10.1146/annurev-micro-090110-102851.

[135] M. C. van Dijk, R. M. de Kruijff, and P.-L. Hagedoorn, "The Role of Iron in Staphylococcus aureus Infection and Human Disease: A Metal Tug of War at the Host—Microbe Interface," *Front. Cell Dev. Biol.*, vol. 10, Mar. 2022, doi: 10.3389/fcell.2022.857237.

[136] J. B. Bulitta *et al.*, "Two Mechanisms of Killing of Pseudomonas aeruginosa by Tobramycin Assessed at Multiple Inocula via Mechanism-Based Modeling," *Antimicrob. Agents Chemother.*, vol. 59, no. 4, pp. 2315–2327, Apr. 2015, doi: 10.1128/AAC.04099-14.

[137] M. A. Kohanski, D. J. Dwyer, and J. J. Collins, "How antibiotics kill bacteria: from targets to networks," *Nat. Rev. Microbiol.*, vol. 8, no. 6, pp. 423–435, Jun. 2010, doi: 10.1038/nrmicro2333.

[138] A. Hotterbeekx, S. Kumar-Singh, H. Goossens, and S. Malhotra-Kumar, "In vivo and In vitro Interactions between Pseudomonas aeruginosa and Staphylococcus spp.," *Front. Cell. Infect. Microbiol.*, vol. 7, p. 106, Apr. 2017, doi: 10.3389/fcimb.2017.00106.

[139] R. Shah *et al.*, "Pseudomonas aeruginosa kills Staphylococcus aureus in a polyphosphate-dependent manner," *mSphere*, vol. 9, no. 10, pp. e00686-24, doi: 10.1128/msphere.00686-24.

[140] G. Orazi, K. L. Ruoff, and G. A. O'Toole, "Pseudomonas aeruginosa Increases the Sensitivity of Biofilm-Grown Staphylococcus aureus to Membrane-Targeting Antiseptics and Antibiotics," *mBio*, vol. 10, no. 4, pp. e01501-19, Jul. 2019, doi: 10.1128/mBio.01501-19.

[141] L. M. Filkins *et al.*, "Coculture of Staphylococcus aureus with Pseudomonas aeruginosa Drives S. aureus towards Fermentative Metabolism and Reduced Viability in a Cystic Fibrosis Model," *J. Bacteriol.*, vol. 197, no. 14, pp. 2252–2264, Jul. 2015, doi: 10.1128/JB.00059-15.

[142] H. Selim, T. E. E. Radwan, and A. M. Reyad, “Regulation of T3SS synthesis, assembly and secretion in Pseudomonas aeruginosa,” *Arch. Microbiol.*, vol. 204, no. 8, pp. 1–10, Aug. 2022, doi: 10.1007/s00203-022-03068-5.

[143] S. Voth *et al.*, “Virulent Pseudomonas aeruginosa infection converts antimicrobial amyloids into cytotoxic prions,” *FASEB J.*, vol. 34, no. 7, pp. 9156–9179, 2020, doi: 10.1096/fj.202000051RRR.

[144] R. Balczon *et al.*, “Pseudomonas aeruginosa infection liberates transmissible, cytotoxic prion amyloids,” *FASEB J.*, vol. 31, no. 7, pp. 2785–2796, 2017, doi: 10.1096/fj.201601042RR.

[145] T. de Sousa *et al.*, “Study of Antimicrobial Resistance, Biofilm Formation, and Motility of Pseudomonas aeruginosa Derived from Urine Samples,” *Microorganisms*, vol. 11, no. 5, Art. no. 5, May 2023, doi: 10.3390/microorganisms11051345.

[146] A. Managò *et al.*, “Pseudomonas aeruginosa Pyocyanin Induces Neutrophil Death via Mitochondrial Reactive Oxygen Species and Mitochondrial Acid Sphingomyelinase,” *Antioxid. Redox Signal.*, vol. 22, no. 13, pp. 1097–1110, May 2015, doi: 10.1089/ars.2014.5979.

[147] L. Biswas and F. Götz, “Molecular Mechanisms of Staphylococcus and Pseudomonas Interactions in Cystic Fibrosis,” *Front. Cell. Infect. Microbiol.*, vol. 11, p. 824042, Jan. 2022, doi: 10.3389/fcimb.2021.824042.

[148] H. G. Ahlgren *et al.*, “Clinical outcomes associated with Staphylococcus aureus and Pseudomonas aeruginosa airway infections in adult cystic fibrosis patients,” *BMC Pulm. Med.*, vol. 15, no. 1, p. 67, Jun. 2015, doi: 10.1186/s12890-015-0062-7.

[149] A. Petrocheilou, A. Moudaki, and A. G. Kaditis, “Inflammation and Infection in Cystic Fibrosis: Update for the Clinician,” *Children*, vol. 9, no. 12, p. 1898, Dec. 2022, doi: 10.3390/children9121898.

[150] L. Camus, P. Briaud, F. Vandenesch, and K. Moreau, “How Bacterial Adaptation to Cystic Fibrosis Environment Shapes Interactions Between Pseudomonas aeruginosa and Staphylococcus aureus,” *Front. Microbiol.*, vol. 12, p. 617784, Mar. 2021, doi: 10.3389/fmicb.2021.617784.

[151] P. J. Planet, “Adaptation and Evolution of Pathogens in the Cystic Fibrosis Lung,” *J. Pediatr. Infect. Dis. Soc.*, vol. 11, no. Supplement_2, pp. S23–S31, Sep. 2022, doi: 10.1093/jpids/piac073.

Appendix A

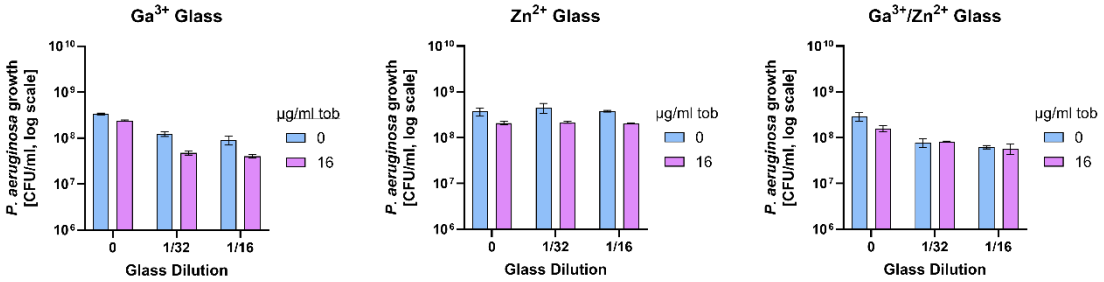

Figure 36: Concentration of *P. aeruginosa* (CFU/ml) in the hydrogel phase of the monomicrobial CF airway infection model with different tobramycin-glass combinations. The CF airway infection model, containing *P. aeruginosa*, was cultured with glass extracts containing Ga^{3+} and/or Zn^{2+} ions at two different dilutions (1/32, 1/16) with or without 16 µg/ml tobramycin for 48 hours. Mean ± SEM. N=3.

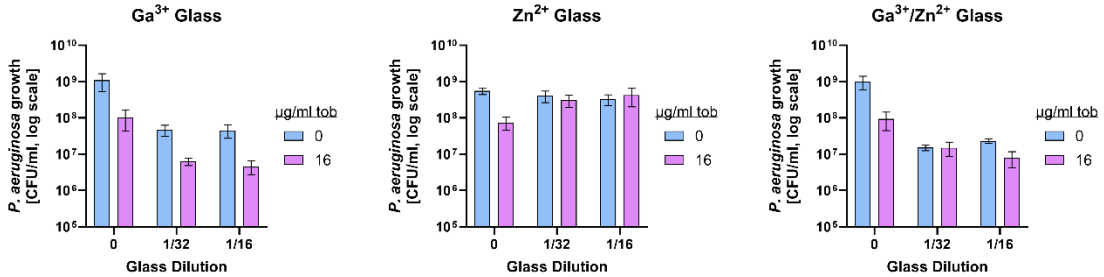

Figure 37: Concentration of *P. aeruginosa* (CFU/ml) in the liquid phase of the monomicrobial CF airway infection model with different tobramycin-glass combinations. The CF airway infection model, containing *P. aeruginosa*, was cultured with glass extracts containing Ga^{3+} and/or Zn^{2+} ions at two different dilutions (1/32, 1/16) with or without 16 µg/ml tobramycin for 48 hours. Mean ± SEM. N=3.

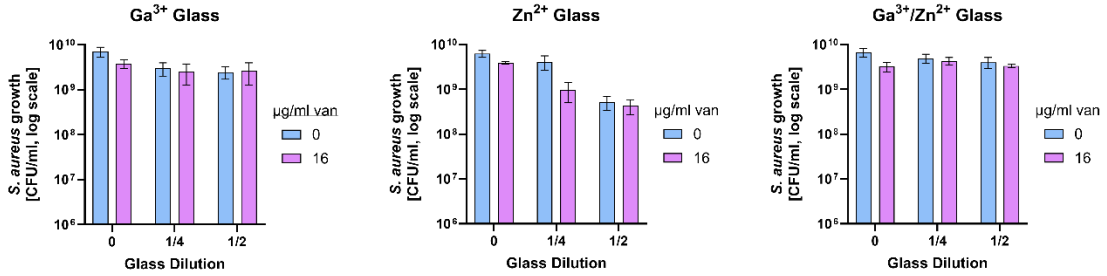

Figure 38: Concentration of *S. aureus* (CFU/ml) in the hydrogel phase of the monomicrobial CF airway infection model with different vancomycin-glass combinations. The CF airway infection model, containing *S. aureus*, was cultured with glass extracts containing Ga^{3+} and/or Zn^{2+} ions at two different dilutions (1/4, 1/2) with or without 16 µg/ml vancomycin for 48 hours. Mean ± SEM. N=3.

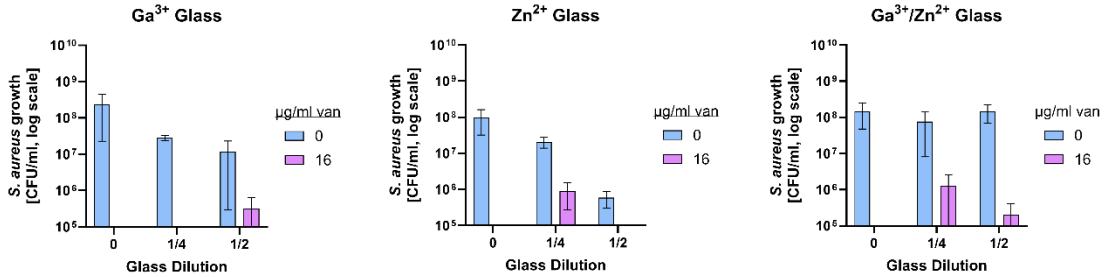

Figure 39: Concentration of *S. aureus* (CFU/ml) in the liquid phase of the monomicrobial CF airway infection model with different vancomycin-glass combinations. The CF airway infection model, containing *S. aureus*, was cultured with glass extracts containing Ga^{3+} and/or Zn^{2+} ions at two different dilutions (1/4, 1/2) with or without 16 µg/ml vancomycin for 48 hours. Mean ± SEM. N=3.

Appendix B

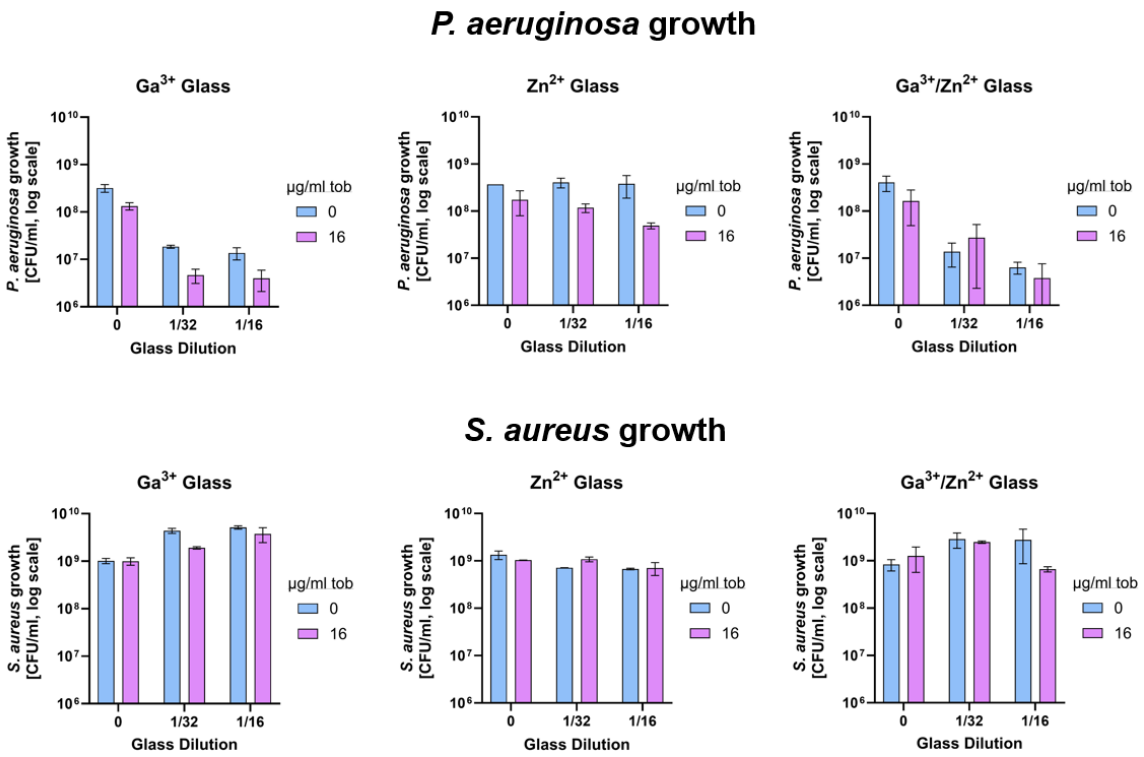

Figure 40: Concentration of *P. aeruginosa* and *S. aureus* (CFU/ml) in the hydrogel phase of the polymicrobial CF airway co-infection model with different tobramycin-glass combinations. The CF airway co-infection model, containing *P. aeruginosa* and *S. aureus*, was cultured with glass extracts containing Ga^{3+} and/or Zn^{2+} ions at two different dilutions (1/32, 1/16) with or without 16 µg/ml tobramycin for 48 hours. Mean ± SEM. N=2.

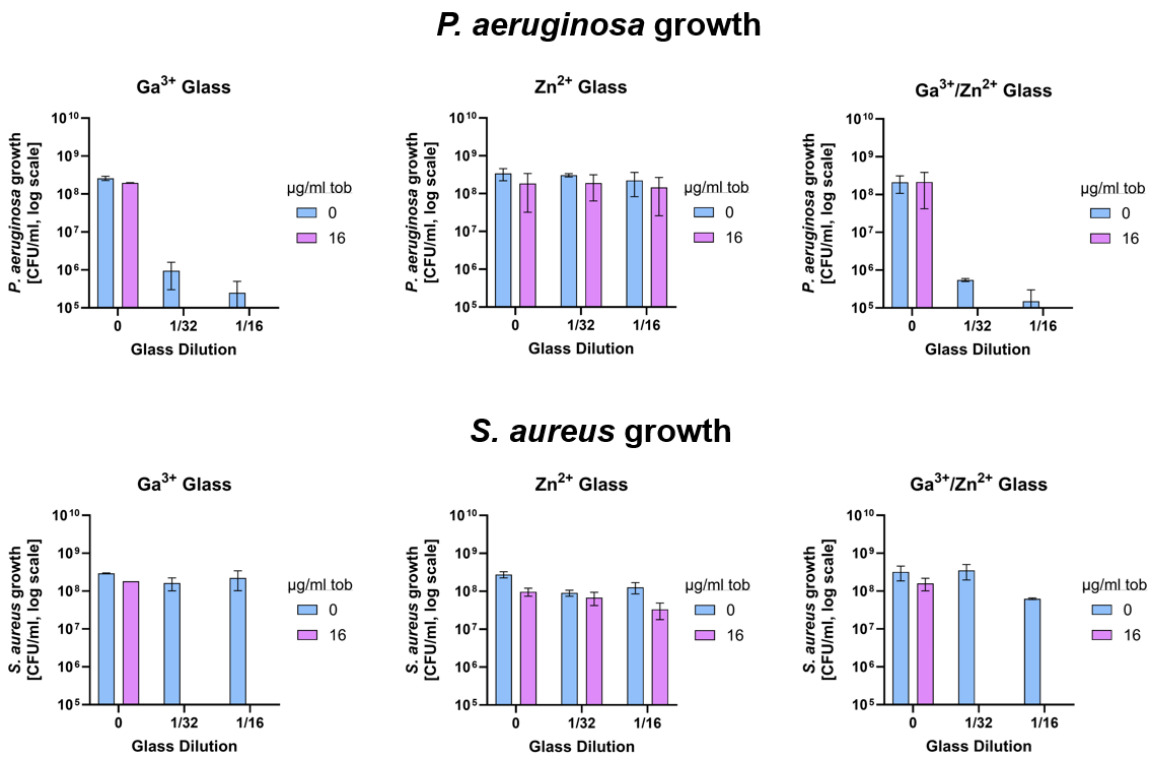

Figure 41: Concentration of *P. aeruginosa* and *S. aureus* (CFU/ml) in the liquid phase of the polymicrobial CF airway co-infection model with different tobramycin-glass combinations. The CF airway co-infection model, containing *P. aeruginosa* and *S. aureus*, was cultured with glass extracts containing Ga^{3+} and/or Zn^{2+} ions at two different dilutions (1/32, 1/16) with or without 16 µg/ml tobramycin for 48 hours. Mean ± SEM. N=2.

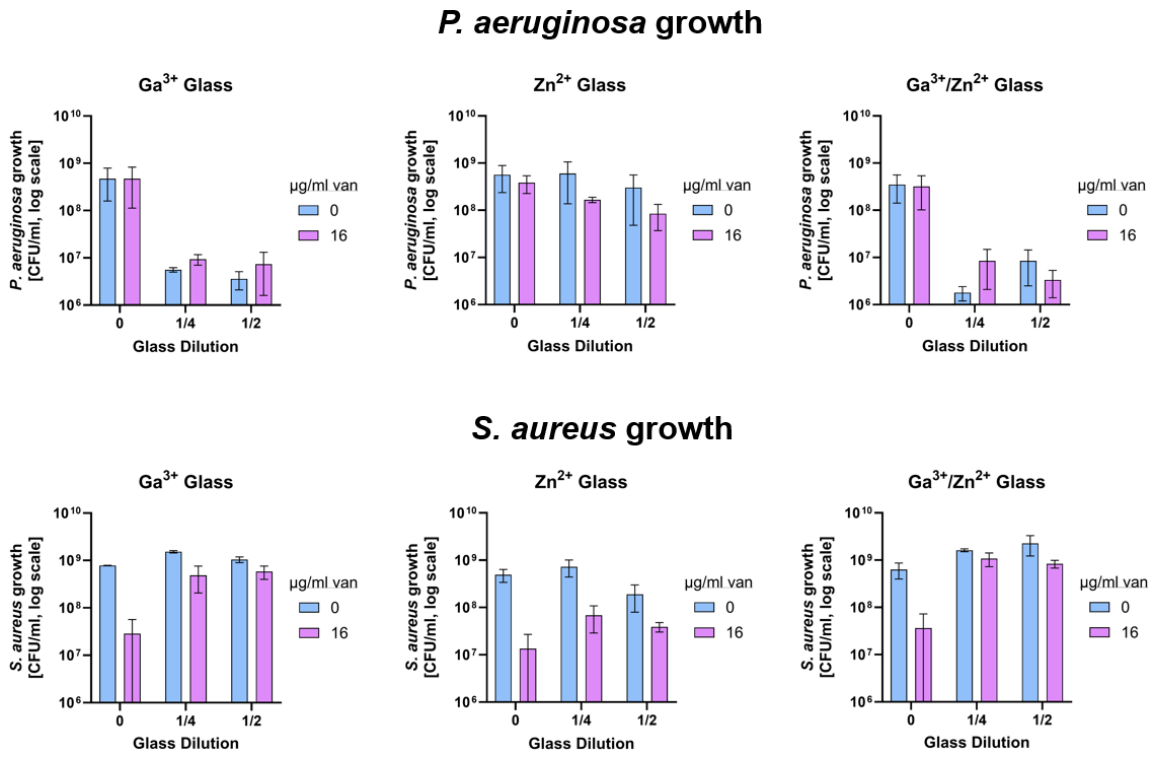

Figure 42: Concentration of *P. aeruginosa* and *S. aureus* (CFU/ml) in the hydrogel phase of the polymicrobial CF airway co-infection model with different vancomycin-glass combinations. The CF airway co-infection model, containing *P. aeruginosa* and *S. aureus*, was cultured with glass extracts containing Ga^{3+} and/or Zn^{2+} ions at two different dilutions (1/4, 1/2) with or without 16 µg/ml vancomycin for 48 hours. Mean ± SEM. N=2.

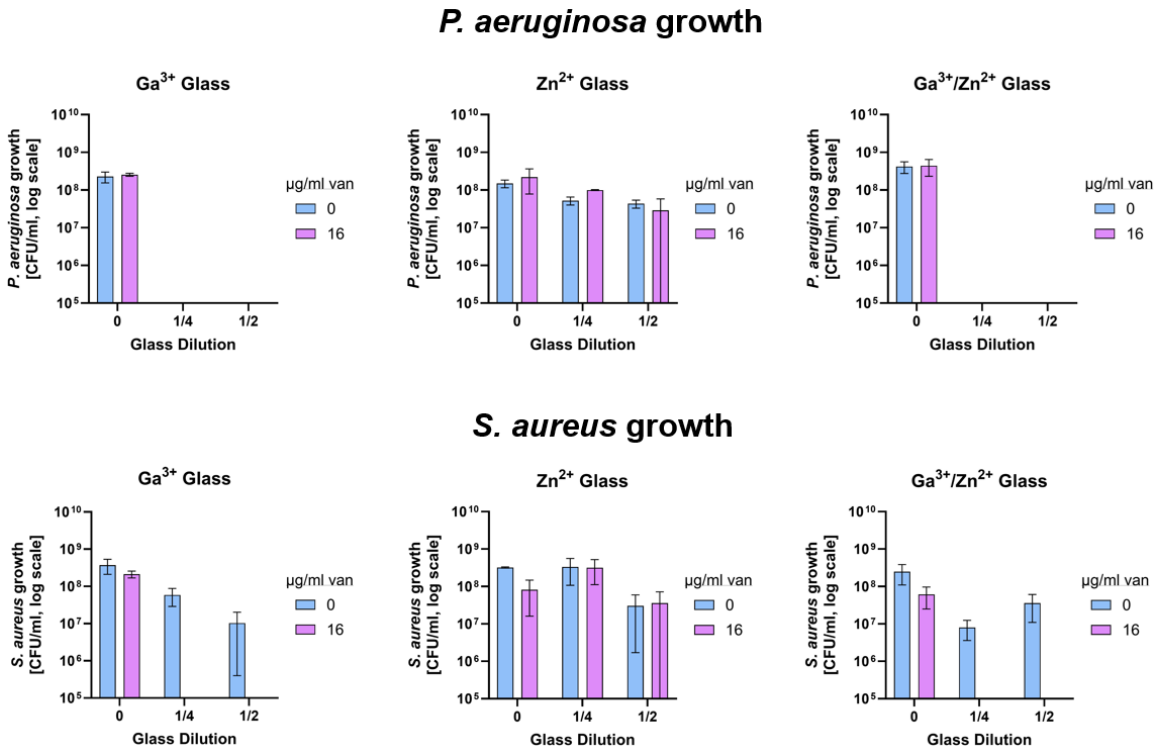

Figure 43: Concentration of *P. aeruginosa* and *S. aureus* (CFU/ml) in the liquid phase of the polymicrobial CF airway co-infection model with different vancomycin-glass combinations. The CF airway co-infection model, containing *P. aeruginosa* and *S. aureus*, was cultured with glass extracts containing Ga^{3+} and/or Zn^{2+} ions at two different dilutions (1/4, 1/2) with or without 16 µg/ml vancomycin for 48 hours. Mean ± SEM. N=2.